Deprotonation reactions from oxygen in the α-L-rhamnose radical cation

A quantum chemical simulation study of radiation induced damage using DFT and TDDFT methods

Siv Gundrosen Aalbergsjø

Thesis submitted for the degree of
Master of Physics

Biophysics and Medical Physics,
Department of Physics,
University of Oslo

August 16th 2010

© Siv Gundrosen Aalbergsjø

2010

Deprotonation reactions from oxygen in the α-L-rhamnose radical cation - A quantum chemical simulation study of radiation induced damage using DFT and TDDFT methods

Siv Gundrosen Aalbergsjø

http://www.duo.uio.no/

Printing: Reprosentralen, University of Oslo

‘

Law of compensation:

No calculation is ever a complete failure; It can always serve as a bad example.

-Anon-

Abstract

Damages from ionizing radiation to the sugar part of the DNA molecule may result in strand breaks. These are damages that can lead to mutations, cancer or cell death. Sugar damages in DNA can be studied experimentally by use of electron paramagnetic resonance (EPR) spectroscopy. In order to obtain a more complete understanding of the processes that occur immediately after irradiation, quantum chemical calculations are also more and more becoming an indispensable tool.

When carbohydrates in the condensed phase are oxidized by ionizing radiation, cation radicals and free electrons are generated. These products then partake in subsequent chemical reactions. In order to restore charge balance, the cations may send off a proton, deprotonate.

Deprotonation reactions from hydroxyl groups (leaving neutral oxygen-centered radicals) have been studied in the carbohydrate α-L-rhamnose ($C_3H_{12}O_5$). Rhamnose has four hydroxyl groups; all are possible positions for deprotonation reactions. The radiation-induced radicals in this sugar have been examined by EPR spectroscopy (Samskog and Lund 1980; Budzinski and Box 1985), but only one oxygen-centered radical was found, indicating that deprotonation selectively occurs from *one* of the four possible positions.

Theoretical quantum chemical calculations based on density functional theory (DFT) later confirmed (Pauwels *et al.* 2008) that the oxygen-centered radical in rhamnose is deprotonated at the O_4 position, yet no explanation was found for the observed selectivity.

In the present work, the electronic ground-state energy profiles for deprotonation from all four hydroxyl groups in rhamnose have been examined theoretically by means of DFT calculations. Both periodic boundary conditions, a two-layered cluster approach (ONIOM) and single molecule calculations have been used. Calculations of EPR properties of the obtained structures indicate that the periodic calculations are able to describe the experimentally observed radical. The energy profiles for the four different deprotonation reactions clearly indicate that deprotonation from O_4 is both thermodynamically and kinetically preferred.

Although these calculations would explain the observed preference for the O_4-centered radical, the calculated energy barrier for the deprotonation reaction is still much higher than the thermal energy available at the typically low temperature of the experiments (4 K and 77

K). Hence, in the electronic ground state, the deprotonation reaction would not be likely to occur.

One possible explanation is that excited states are involved in the radical formation. The deprotonation may well occur before the molecule relaxes into the electronic and vibrational ground states after the initial ionization event. In order to investigate the possible role of excited electronic states of the cation, the excited states of have been examined by time-dependent DFT (TDDFT).

The excited states were calculated throughout the deprotonation reactions and energy profiles were made. The attention has been focused on finding states with a lower energy barrier for the deprotonation reactions than the ground state and/or conical intersections with the ground state potential energy surface. So far, no such state has been found, but analyses still remain to be done.

In order to get a better understanding for the abilities and potential of the TDDFT method, benchmark calculations have also been performed on three small molecules (H_2O, CH_3 and CO^+) for which experimental data are available for comparisons.

Acknowledgements

First of all I would like to thank my supervisors Professors Einar Sagstuen and Eli Olaug Hole for their help and support these two years that I've spent at the Biophysics group. Thank you Einar for providing me with a theoretical thesis project where the applications of the methods I've been using, are within view, and in which I was allowed to see one of the interfaces between physics and chemistry. When I first started my university studies I found it hard to choose between these two subjects.

I would also like to thank Kjell Tage Øhman who discovered and helped me correct mistakes that caused me months of hair-tearing.

My project is part of a collaboration with the Center for Molecular Modeling (CMM) at Ghent University in Belgium. During the last year I spent two months in Ghent. I am grateful to the director for CMM, Prof. Dr. Michel Waroquier, for giving me these opportunities and for his hospitality. I was in particular welcomed and taken well care of by Drs. Ewald Pauwels and Hendrik De Cooman.

Ewald has been my unofficial supervisor and most important moral support for the last year. Most of the work presented in this thesis could not have been done, had it not been for him. Ewald taught me how to use the CP2K program, and provided me with working input files as well as starting geometries for the periodic calculations. It was also him who performed the linear interpolations of the optimized geometries needed for some of the analysis of the excited states. He helped me find new directions to move in, when the work I was doing proved to be a dead-end.

Thank you to both of you for the time you have spent on me, and especially to Ewald who twice travelled all the way to Oslo just to help me!

Finally I would like to thank friends and family who have been listening to my frustrations and helped me find entertaining distractions from my thesis. You know who you are.

Special thanks to the students at the Biophysics group; for company during long days at the study-hall, for Friday quizzes, for the movies we watched, for the TP and the GT. A very special one to the students at "Den kule lesesalen", off course.

Oslo, August 2010

Siv G. Aalbergsjø

Table of contents

1 Introduction 1
1.1 General motivation 1
1.2 Ionizing radiation 2
1.2.1 Effects of ionizing radiation on biological molecules 3
1.2.2 Interaction processes of ionizing radiation 5
1.3 EPR spectroscopy 9
1.4 α-L-rhamnose 10
1.5 Physics of molecular excited states 13
1.6 Object of this thesis 15
2 Quantum chemistry – Ground state calculations 17
2.1 Hartree-Fock theory 18
2.1.1 The basic Hartree-Fock method 18
2.1.2 Semiempirical methods 21
2.1.3 Beyond Hartree-Fock 21
2.2 Density functional theory 22
2.2.1 Kohn-Sham: Self-consistent field 22
2.2.2 The exchange-correlation functionals 24
2.2.3 Advantages and disadvantages of using DFT 25
2.3 Geometry optimizations 26
2.4 Influence from the surroundings 27
2.5 Basis sets 28
3 Excited state calculations and time-dependent DFT 31
3.1 How to describe an electronically excited state 31
3.2 Time-dependent DFT 33
3.2.1 Foundation 33
3.2.2 Applicability 34
3.2.3 TDDFT versus other excited state methods 36
3.2.4 Some applications to biomolecules 37
4 Methods used 39
4.1 Ground state calculations 39
4.1.1 Periodic calculations 39

4.1.2 Cluster- and single molecule calculations 40
4.1.3 Calculation of hyperfine coupling tensors 41
4.2 Excited state calculations 41
4.3 Basis sets 43
4.4 Functionals 44
4.5 Spin and charge analysis 44
5 Results and analyses 47
5.1 Ground state calculations on rhamnose 47
5.1.1 Periodic calculations using CP2K 48
5.1.2 Cluster and single molecule calculations using G03 56
5.2 Excited states 61
5.2.1 Test calculations on small molecules 61
5.2.2 TDDFT on rhamnose 66
6 Discussion and conclusions 73
6.1 Size of the model system 74
6.2 Ground state energy profiles for proton transfer reactions 76
6.3 Comparison of ground state calculations with literature 77
6.4 Desired properties of the calculated excited states 78
6.4.1 Excited states resulting from ionization 78
6.4.2 Reaction mediating states 81
6.5 Observed excited state properties 82
6.6 TDDFT benchmark calculations 84
6.7 Reliability of the calculations 85
6.8 Conclusive remarks 86
6.9 What now? 87
Bibliography 89
Appendix A: List of units 95
Appendix B: List of acronyms and abbreviations 97
Appendix C: Programs most used 99
Appendix D: Results 101
Appendix E: Animation 121

1 Introduction

1.1 General motivation

When *ionizing radiation* deposits energy by interactions with matter, positively (cationic-) and negatively (anionic-) charged products are formed. Such products are called *primary charged radicals*. These primary species are subsequently involved in various reactions; the most common are characterized by *electron*- and *proton transfers*, leading to neutral radicals. The newly formed species are sill highly reactive and will partake in chemical reactions that may lead to significant changes in the molecular structures.

If the radiation target is the DNA molecule, the molecular alterations that are induced might lead to biological consequences. Of special interest are changes created in the *sugar-phosphate backbone* of the molecule, as they can lead to irreparable damages to the DNA polymer. This is why an understanding of the basic physical- and chemical processes initiated by irradiation is important. One of the ambitions of radiation biophysics is to understand how the radiation deposits its energy in molecules of biological importance, how this leads to the formation of the very first (primary) radiation induced radicals and finally how these lead to chemical changes with biological consequences.

Part of the work of the electron paramagnetic resonance (EPR) laboratory at the Department of Physics in Oslo has been to investigate primary radiation damages to a variety of systems that act as model systems for the sugar-phosphate backbone of the DNA molecule. Most often these model systems are *carbohydrates* or derivatives of carbohydrates. EPR spectroscopy is a method for observing and identifying the (charged or neutral) radicals that are created during irradiation. This EPR-experimental research program has been complemented by advanced ground state *quantum chemistry modeling* to obtain a better *mechanistic* understanding of the processes.

By EPR spectroscopy, many different radicals are now known to be created upon irradiation DNA and DNA model systems. Still, the radical formation is highly *selective* given the large number of hypothetical products one could imagine and the much smaller number of actually observed products. This selectivity is in many respects unexplained, but experimental evidence implies that properties of the primary charged radicals occurring just after irradiation are crucial. At that point the inflicted molecules are in *excited states* which might influence

the electron- and proton transfer processes, thus playing an important role in deciding which neutral radicals are formed.

In order to promote the understanding of the mechanistics of the physical and chemical processes, several quantum chemical calculation methods have been developed over the last 50 years. These are both semiempirical and *ab initio* methods which can be used to calculate reaction pathways as well as electronic distribution in the ground- and excited states of molecules.

In the present work, modern quantum chemical methods, mainly *density functional theory* (DFT) and *time-dependent DFT* (TDDFT) have been used to study reactions that lead to the formation of a specific neutral *oxygen-centered* radical in the carbohydrate α-L-rhamnose. In this molecule, only one out of four possible oxygen-centered radicals has been observed experimentally.

The goal has been to understand the specificity by describing the reaction path from the primary cation radical that exists just after ionization, into the four different neutral oxygen-centered radicals. A subsidiary goal has been to learn how to use the recently developed TDDFT method to describe excited states for both isolated geometrical configurations of molecules and along reaction paths. There is still little experience with the use of this computational scheme. A large part of the present master project has been to perform calculations on test molecules at different levels of theory, whereupon the results have been compared with published experimental and theoretical data.

The rest of this chapter is devoted to describing some basic concepts and introduce the reader to terms and notations of the scientific language in this thesis. In the following chapters the essential methodologies are described in some more detail, followed by chapters describing and discussing the obtained results.

1.2 Ionizing radiation

The information presented here is mainly based on the textbooks by Attix, Henriksen and Henriksen and Hall and Giaccia (Attix 1986; Henriksen and Henriksen 1998; Hall and Giaccia 2006).

1.2.1 Effects of ionizing radiation on biological molecules

Ionizing radiation is radiation that is capable of creating ions when it interacts with matter. This is the case for fast charged particles such as *electrons*, *α-particles* and *heavier ions*, but also neutral particles such as *neutrons* can be ionizing. Electromagnetic radiation with energy above the ionization potential for molecules (a few eV) is also ionizing. This includes UV in the low energy end, but usually only *X-rays* and *γ-rays* are considered as electromagnetic ionizing radiation.

We are surrounded by ionizing radiation both from particles in cosmic radiation and from radioactive sources both inside and outside our own bodies. These natural sources have been present throughout time, and are weaker today than what they were when life appeared on this planet. Today ionizing radiation is also being used extensively for different practical purposes, especially in medicine and research. X-rays enable us to see things that are hidden behind an opaque surface and are therefore among other things, used for diagnostic purposes in hospitals. In cancer therapy the deadliness of large doses of ionizing radiation is exploited to kill cancer cells.

It is assumed that the prime target for radiation in living cells is the *DNA molecule*. The DNA molecule is built as a twisted ladder. The steps are made from *base pairs* that are hydrogen bound to each other and the backbone consists of *sugar-phosphate-chains* to which the bases are attached. There are four different bases present in the DNA molecule, adenine, cytosine, guanine and thymine. It is the ordering of these bases along the molecule that creates the genetic code. ***Figure 1*** shows a picture of a nucleotide which consists of a sugar molecule and a phosphate group with a guanine base attached, and ***Figure 2*** shows how these building blocks form the DNA helix. The hydrogen bonds between the bases (creating base pairs) hold the two intertwined sugar-phosphate backbone strings together; creating the helix structure. The hydrogen bond network is such that only adenine-thymine and guanine-cytosine pairs can be formed. This means that each of the two strand of the DNA hold all genetic information separately, as they are complementary to each other.

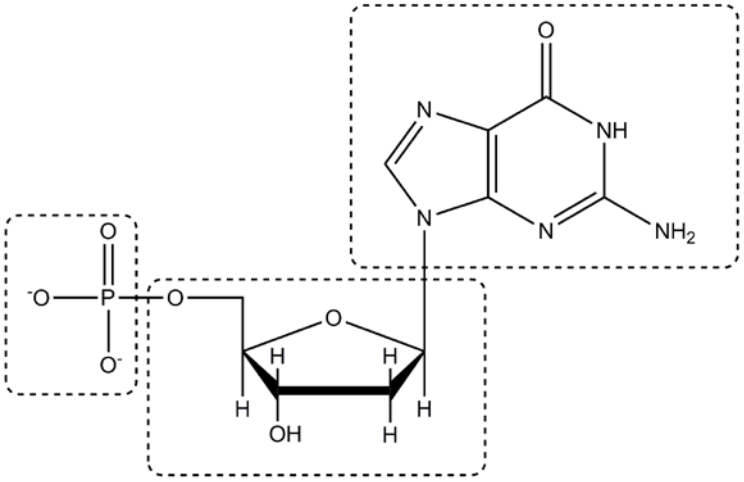

Figure 1: The deoxyribonucleotides are the building blocks of the DNA molecule. Here a nucleotide is shown with its three building blocks (from the left) the phosphate group, the deoxyribose and the nucleobase (guanine in this case).

Damages by ionizing radiation to DNA occur from *direct* and *indirect interactions* with the radiation. The direct damages are consequences of interaction of radiation with the DNA molecule itself, whereas the indirect damages are caused by chemical reactions between DNA and damaged molecules in the surroundings (mostly water). 40-50 % of all damages to DNA are consequences of direct interactions (Sagstuen and Hole 2009). *Strand breaks* are breaks in the sugar-phosphate backbone of the DNA, if two strand breaks occur close to each other; they are called *double strand breaks*. *Dimers* are damages where two bases above each other in the ladder are linked together, and *base damages* cover many different types of chemical changes in the bases.

There are several repair mechanisms in the cell, and these make sure that most of the damages that occur do not hurt the biology. The repair mechanisms are enabled by the fact that the two strands of the DNA are complementary. So if one strand is broken, it can be rebuilt by use of its “mirror image”. For this reason, double strand breaks are more difficult to repair than the other damages. The damages that are not repaired, or incorrectly repaired, can lead to serious biological effects such as cell death, mutation or cancer.

Ionization of the sugar (deoxyribose) part of the DNA molecule appears to be an essential starting point for several reaction routes which eventually lead to strand breaks which are especially difficult to repair (Sagstuen and Hole 2009). It is estimated that about 15 % of the direct damages to the DNA are to the deoxyribose part of the molecule (Close 1997).

It is desirable to know the exact processes that occur in DNA just after irradiation and to understand how these lead to damages that may or may not be repaired. Unfortunately the DNA molecule is so complex that it is not always feasible to study these processes at the

molecular level for the entire system. One is often restricted to study the building blocks of DNA separately, or even molecules that resemble the building blocks. Carbohydrates are often used for this purpose as they have many similarities with the (deoxy)ribose units of the sugar-phosphate chains in the DNA molecule. It has been shown that radiation damages both to the bases and to the phosphoribose backbone are essential for the formation of strand breaks in DNA (Bernhard and Close 2003).

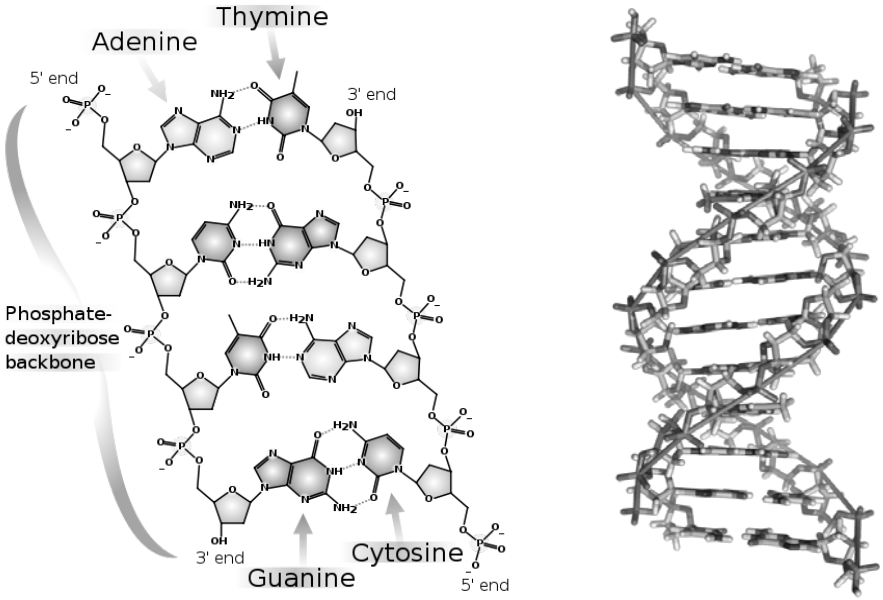

Figure 2: Illustrations (Wikipedia) of how two strings of nucleotides are connected by hydrogen bonds to form a double-helix structure of the DNA molecule. Adenine can only bind to thymine (two H-bonds) and guanine can only bind to cytosine (three H-bonds) and *vice versa*.

1.2.2 Interaction processes of ionizing radiation

Immediately after irradiation, the influenced molecules are in excited states. Some of them have been ionized by the radiation, others just excited. There are different kinds of excitations, as will be discussed in a later section (1.5); here the focus will be on *electronic excitations*.

The removal of an electron from a molecule will leave the molecule in an electronically excited state, see ***Figure 3***. The ionizing radiation creates excited *cation radicals* and *free electrons*. If the ejected electrons have sufficiently high energy, they will ionize the material further. If the electrons have low energy, they will meet up with other molecules and either re-establish charge balance in cation radicals, or create anion radicals (also in excited states). These cation- and anion radicals are called *primary radicals*. The

primary radicals will de-excite into their ground state by transferring energy either to vibrationally excited states or by emission of photons. The radicals will take part in chemical reactions with each other or with undamaged molecules giving rise to *secondary radicals*.

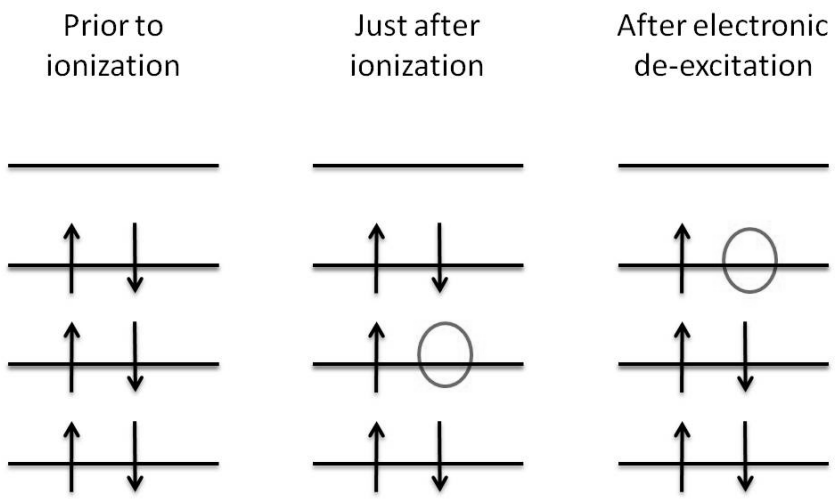

Figure 3: Simplified picture of an ionization process. The electrons occupy molecular orbitals (or energy states) indicated by horizontal lines where the higher lines have a higher energy. Initially each orbital contains two electrons with opposite spins. An electron is "knocked out" of the molecule leaving a hole in the electronic structure which is later moved upwards in the energy levels through de-excitation.

Ionizing radiation is divided into *directly ionizing* radiation and *indirectly ionizing* radiation. Directly ionizing radiation is charged particles which interact with the material through Coulombic interactions. Indirectly ionizing radiation is photons and neutrons, and they are called indirectly ionizing because they have relatively few interactions with the matter. In these interactions they transfer their energy to charged particles in the material which then go on to ionize further.

The interaction of radiation with matter is *stochastic*. There are many possible ways of interaction, and which one will occur in each incident is impossible to predict since it is governed by quantum mechanics. But because the radiation field consists of many particles and the number of incidents is large, the stochastic description is good.

For electromagnetic radiation the three most important types of interaction with matter are *Compton scattering, photoelectric effect* and *pair production*. These three processes have different regions of the photon energy spectrum in which they dominate, see ***Figure 4***. In biological tissue, the photoelectric effect dominates for photon energies below 100 keV, pair

production for energies above 10 MeV, and the Compton effect dominates between these values.

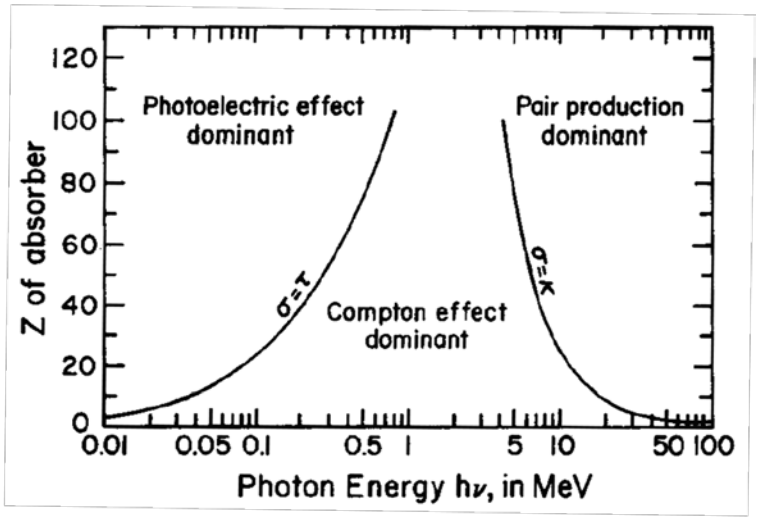

Figure 4: Relative importance of the three major types of X- and γ-ray interaction. The curves show the values of Z (effective atomic number) and E_γ (photon energy) for which two types of effects are equally important. (Evans 1955)

In a Compton scattering process, an incident photon hits an electron; this puts the electron in motion and creates a *scattered photon* with a lower energy than the incident photon (which has disappeared). ***Figure 5*** shows how the kinetic energy of the electron varies with the energy of the incoming photon. For low photon energies, most of the energy is transmitted to the scattered photon, but for higher photon energies, most of the energy is transferred to the electron. In the theoretical treatment of the Compton effect it is assumed that the electron is originally unbound, which is obviously not the case in matter. However the effect of the binding energy is most important for low energy radiation, and in this region it is the photoelectric effect that dominates.

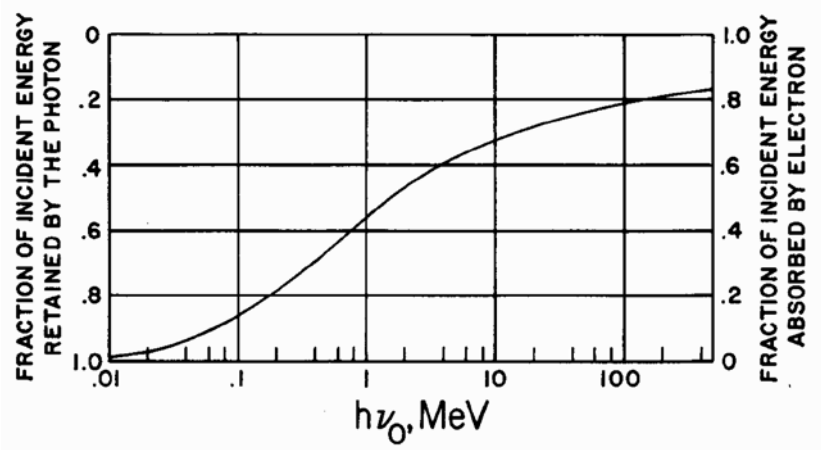

Figure 5: Mean fraction of the incident photon's energy given to the recoiling electron in Compton interactions. (Attix 1986)

In the photoelectric effect a molecule is excited or ionized through the absorption of a photon. In the case of ionization, the ejected electron is given a kinetic energy that corresponds to the difference in energy between the incoming photon energy and the binding energy of the electron:

$$E_{kinetic,electron} = h\nu - E_{binding,electron} - E_{kinetic,atom} \approx h\nu - E_{binding,electron}. \quad (1.1)$$

If the electron that is ejected in a photoelectric process is an inner shell electron, de-excitation of a less tightly bound electron will release energy. This energy can be released either as a photon (*characteristic X-ray*) or by ejection of loosely bound electrons (*Auger effect*). If the Auger effect comes into play, the molecule will be multiply charged. The creation of Auger electrons is more probable if the material has a low effective atomic number[1] (which is the case for biological tissue).

In a pair production process a photon interacts with the Coulomb field of an atomic nucleus or an electron, the photon disappears and a positron-electron pair is produced. This process can only occur if the photons have energy higher than $2m_e c^2 = 1.022 MeV$, if the process occurs in the vicinity of a nucleus, and $4m_e c^2$ in the vicinity of an atomic electron.

Whereas indirectly ionizing photons interact with matter sporadically, in events where large portions of the energy is lost, charged particles such as electrons (including those set into motion by incident photons) transfer some of their energy to almost every molecule they pass, leaving a trail of excited and ionized molecules behind them. For electrons, the three most important ways of interactions are *soft-collisions*, *hard-collisions* and *bremsstrahlung production*.

Soft-collisions are glancing collisions between electrons and molecules. They are numerous, and lead mainly to excitations, but can also result in ionization by ejection of valence electrons. Hard-collisions are processes where the electrons pass through the molecules. They are fewer, but the energy transferred to matter in these collisions is larger, and ionization is frequent. As for the photoelectric effect, the hard collisions lead to characteristic X-ray emission and/or Auger electrons whenever an inner shell electron is ejected. Bremsstrahlung production occurs when an electron passes near an atomic nucleus and X-ray photons are produced. Bremsstrahlung production is not significant in materials with low effective atomic number if the electron energy is below 10 MeV.

[1] The effective atomic number is the average atomic number in the molecule.

1.3 EPR spectroscopy

Electron paramagnetic resonance (EPR) spectroscopy is a method for observing and characterizing molecules containing one or more unpaired electrons. In molecules, the electrons organize in pairs, such that their spins cancel. This makes EPR spectroscopy impossible for most molecules. But in molecules containing an uneven number of electrons (radicals) and in a few other molecules (where not all of the electrons pair up), EPR measurements are possible[2]. This is why EPR is useful for investigating molecules exposed to ionizing radiation. For a more thorough description of the method than what is presented here Atherton's textbook (Atherton 1993) or other textbooks on the subject should be consulted.

The electron possesses a *magnetic moment* which aligns with the spin of the particle. This is what is being exploited in EPR spectroscopy. Through their magnetic moment, the electrons can interact with an external magnetic field. The electron is a spin ½ particle, which means that it has two eigenstates. These correspond to the component of the spin, along a chosen axis, being either +½ or -½ in units of $\hbar$. These states are denoted as *up* or *down*, α or β or (in the presence of a magnetic field) *parallel* or *anti-parallel* to the field. In these two states the magnetic moment will point in opposite directions, and the magnetic potential energy will be different in the presence of an outer magnetic field. This is known as the Zeeman effect. The magnetic potential energy of a single electron in a magnetic field is

$$E_{pot,mag}(\pm) = \pm\frac{1}{2} g_e \mu_B B_0 \tag{1.2}$$

where B_0 is the field strength of the external magnetic field, μ_B is the Bohr magneton and g_e is the *g*-factor which is 2.0023 for a free electron. In a sample containing many radicals, both energy levels will be occupied. However, since the spins that are oriented parallel to the magnetic field are higher in energy than the ones that are oriented anti-parallel, there will be more electrons with spin down than spin up. The difference in occupancy is determined by the *Boltzmann distribution*. Transitions between these two states can be induced by applying radiation with a frequency corresponding to the energy difference between the two states; this is known as the resonance condition:

$$h\nu = g_e \mu_B B_0 . \tag{1.3}$$

[2] Atoms or molecules with unpaired electrons exhibit a permanent magnetic moment and are called *paramagnetic*.

Because the occupancy of the two states differs, there will be a net absorption of radiation in the system; this is what creates the EPR signal.

The equations presented above are only valid for free electrons. In molecular systems, the electron magnetic moment will be affected by interaction both with the magnetic moment of nuclei (for those nuclei that possess a magnetic moment), the orbital angular momentum of the electron and the electronic environment of the molecule. The *g*-factor for an electron in a molecule will differ from the *g*-factor for a free electron, and might also depend on the *spatial orientation* of the magnetic field with respect to the molecular frame of reference. If this is the case, then it is referred to as the *g-tensor* which describes the variation in the *g*-factor with the magnetic field orientation.

The interaction of the electronic magnetic moment with that of the nuclei is called the *hyperfine coupling*. The hyperfine coupling causes a splitting of the EPR signal which is characteristic to the interacting nucleus. The hyperfine coupling may also be dependent of orientation and is hence described by the *hyperfine coupling tensor*.

The EPR spectrum is usually recorded keeping the frequency of the incoming radiation fixed and varying the magnetic field strength. This gives rise to an absorption signal when the resonance criterion is met. The different *g*-tensors for different molecular systems shift the resonance frequency from that in Eq. (1.3), and the hyperfine coupling tensor causes splitting of the signal. In this way it is possible to determine what kind of species that are present in the sample. By using *oriented crystal samples*, the different components of the *g*- and hyperfine coupling tensors can be determined, which makes it possible to attain even more information about the molecular structure.

Radicals are usually very reactive species; the reactions are driven by available thermal energy. When investigating radicals formed after irradiation, it is necessary to remove this energy by *cooling down* the sample, in order to observe the primary radicals. Liquid helium (T = 4.2 K) or nitrogen (T = 77 K) is used for this purpose.

1.4 α-L-rhamnose

α-L-rhamnose is a pyranose, a *carbohydrate* with a six-membered ring containing a ring oxygen. In its crystalline form it is monoclinic with a unit cell consisting of two asymmetrical units each consisting of a rhamnose molecule and a crystal water. The chemical structure of

rhamnose is shown in ***Figure 6***. The crystal structure has been determined by neutron diffraction (Takagi and Jeffrey 1978). The unit cell parameters are a = 7.901 Å, b = 7.922 Å, c = 6.670 Å and β = 95.52 °. The crystal structure is governed by extensive hydrogen bonding between the molecules. In particular there are two infinite hydrogen bond chains through the crystal, see ***Figure 7***, these follow the crystal axes.

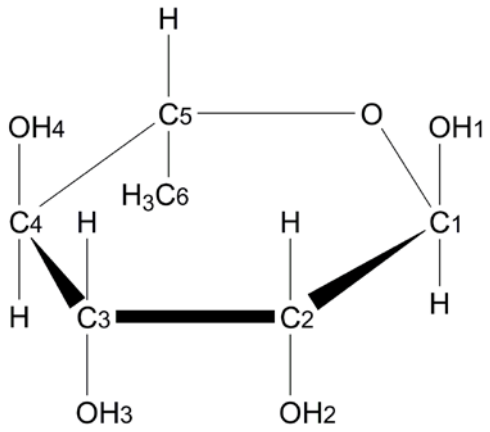

Figure 6: The structure of α-L-rhamnose with carbon atom and hydroxyl group numbering indicated.

Upon ionizing radiation, many different radical forms of rhamnose have been observed by single crystal EPR spectroscopy. Of special interest for the present work, is the observation of an *oxygen-centered* radical on O_4, see ***Figure 6***. This is the only observed oxygen-centered radical, and has been suggested to result from a primary radical cation through *deprotonation*[3] from the same oxygen. In a theoretical study using density functional theory (DFT) (Pauwels *et al.* 2006) all the possible oxygen centered radicals (see ***Figure 8***) were examined through calculation of EPR parameters (*g*- and hyperfine coupling tensors) and compared to experimental observations. Only structure d) in ***Figure 8*** was found to match with experiment.

[3] Deprotonation is the removal of a hydrogen atom nucleus.

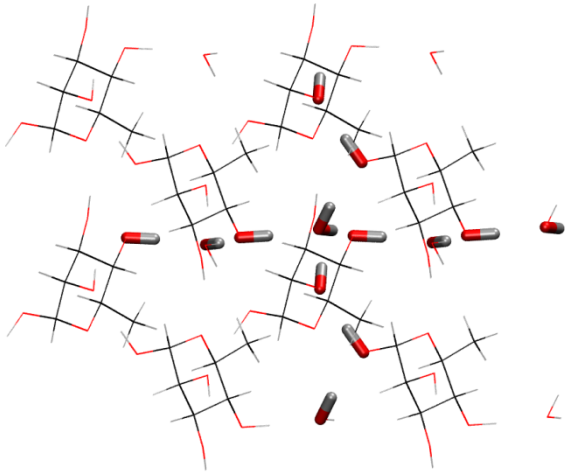

Figure 7: Hydrogen bond chains shown in a *<2a2b2c>* super cell of the crystal structure viewed down the a-axis, the b-axis is horizontal.

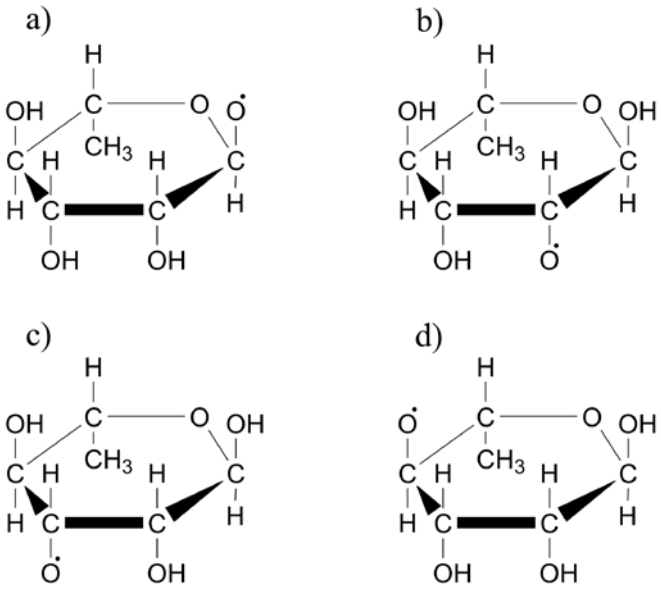

Figure 8: The four different radicals that might occur after deprotonation from a hydroxyl group in a rhamnose cation.

The oxygen centered radical has been measured by EPR techniques upon X-irradiation at temperatures of 77 K (Samskog and Lund 1980) and 4 K (Budzinski and Box 1985). Although these two observations reported different *g*- and hyperfine coupling tensors, a later DFT study has indicated that they are in fact representing the same radical, only differing in the electronic structure as a consequence of differing environments (Pauwels *et al.* 2008). In the same work it was suggested that the radical is formed upon a proton transfer reaction

along the infinite hydrogen bond chain in the *b*-direction of the crystal as a way of removing the excess charge from the cation, creating a neutral radical.

The calculations were performed using a periodic approach. Using a supercell that was doubled in length in the *b*-direction, the study showed a stable structure after three proton transfers along the chain. Using a cell that was tripled in the *b*-direction instead resulted in a stable structure after five proton transfers. This led the authors to suggest that in a real life crystal, the proton can move far away from the original cation position. The difference in EPR properties of the experimentally reported radicals is then explained as a result of reorientation of the waters and hydroxyl groups taking part in the proton transfer process, which might be possible at a temperature of 77 K, but not at 4 K.

In the same paper it is also pointed out that the energy barrier for the deprotonation reaction to take place is about 0.4 eV. This energy barrier is quite high, leading the authors to suggest that excited-state dynamics or tunneling might be involved in the reaction.

1.5 Physics of molecular excited states

For more detailed descriptions of the following phenomena, see for instance the textbook by Atkins and Friedman (Atkins and Friedman 2005).

The nuclei of the atoms in molecules move much slower than the electrons due to the difference in masses. This means that the calculation of molecular energies may be simplified by calculating the electronic energy while the nuclei are held fixed, and then adding the potential energy of the nuclei as a classical term. This is the *Born-Oppenheimer approximation* (BO approx). Under the BO approx. the electronic wave function will depend only parametrically on the nuclear coordinates, and a certain set of nuclear coordinates corresponds to a specific molecular energy. The molecular energy (excluding the kinetic energy of the nuclei) as a function of nuclear coordinates is called the *potential energy surface* (PES). Stable geometries correspond to *minima* and changing nuclear coordinates (as is what happens in a chemical reaction) corresponds to moving around on the surface.

Excited states in molecules arise from *rotational*, *vibrational* and *electronic excitations*. The energy gaps between the levels of excitation are ordered as:

$$\Delta E_{rot} < \Delta E_{vib} < \Delta \mathrm{E}_{elec} . \qquad (1.4)$$

In a crystal, the rotational degrees of freedom are all frozen. A molecule consisting of N_A atoms has $3N_A$-6 vibrational degrees of freedom. These vibrations can to a first approximation be described as harmonic vibrations in a vibrational coordinate[4]. There is an infinite number of electronically excited states which arise from moving one or more electrons from an electron orbital that is *occupied* in the ground state into one that is unoccupied (these are known as *virtual orbitals* and are higher in energy than the occupied orbitals).

In the electronically excited state, the alignment of the spins need not be the same as in the ground state. Ground state conformations of molecules containing an even number of electrons are usually singlet states (spin 0), but in the excited states, the spins might align differently so that the electron spins do not cancel and we may get *triplet* states (spin 1) or even higher. In radicals the ground state is usually a *doublet* state (spin ½), also here the excited states can contain higher spin.

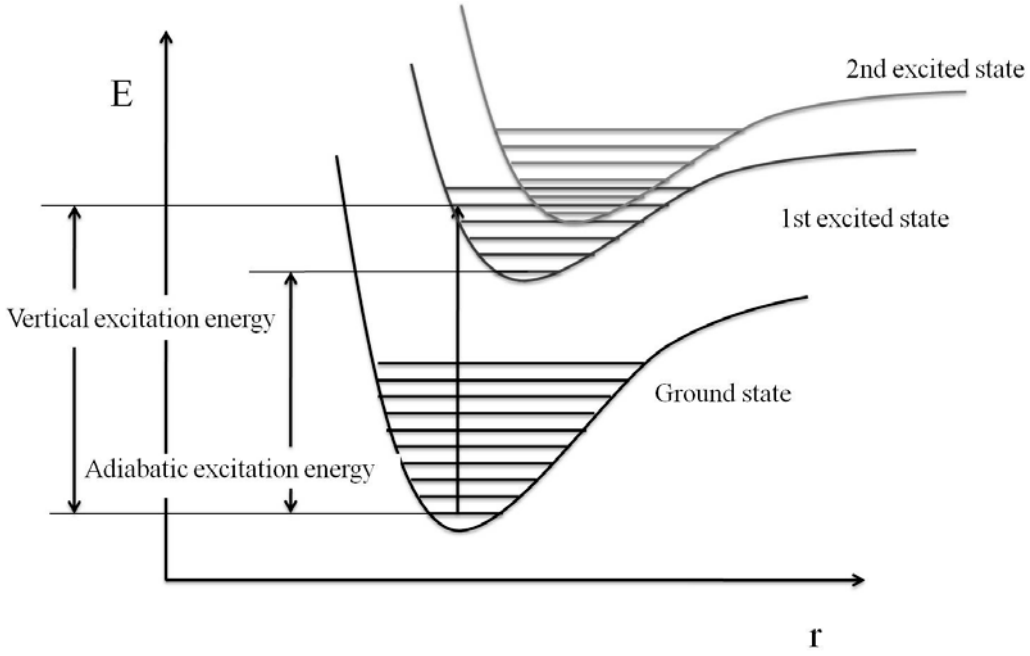

Figure 9: Excited state diagram that shows the PESs for three electronic states as a function of a vibrational coordinate. The vibrational states for each electronic state are drawn as horizontal lines. See the text below for further description.

Since the electron configuration is different in the electronically excited state, the Coulomb field from these electrons will change. This affects the shape of the PES. ***Figure 9*** illustrates how the PES for the different electronic states can be different. The excited states typically have their minimum at a larger bond distance than the ground state, because of more anti-bonding character of the electronic state. The vibrational levels for each electronic state are

[4] A vibrational coordinate is a linear combination of the coordinates of the nuclei in a molecule

drawn as horizontal lines. Drawn in the picture is an excitation due to the capture of a photon. The electronic excitation is assumed to happen without movement of the nuclei (because it is too fast). This means that the excitation does not occur to the vibrational ground state of the new electronic state, which is known as the *Franck-Condon principle*. The excitation is called *vertical* when there are no changes in nuclear coordinates. The energy difference between the vibrational ground states of the two electronic states is called the *adiabatic* excitation energy.

All excited states have a *finite life time*, this means that they have to de-excite eventually. The Franck-Condon principle is followed for *radiative* excitation and de-excitation, whereas *non-radiative* de-excitation involves nuclear motion, often transmission of energy into vibrational modes and then to surrounding molecules. This is possible because the vibrational levels of different electronically excited states overlap.

The larger the molecule is, the more closely spaced the electronic states will be.

1.6 Object of this thesis

The EPR laboratory at the Department of Physics, UiO, has initiated a research program investigating experimentally and theoretically radiation damages to carbohydrates. Carbohydrates are considered as plausible model systems for the sugar-phosphate chain of the DNA molecule.

Even though EPR spectroscopy is an excellent tool for analyzing radiation induced products, theoretical modeling can give insight as to why the observed products occur compared with a large number of other possible products. Early proton transfer processes in carbohydrates appear to be associated with high activation barriers, which points in the direction of pristine excited states playing an important part in the reactions. The excited states are difficult to examine experimentally, but can be modeled theoretically. These calculations are complex but lately they have been made possible through new methods.

In order to describe physics at the molecular level, quantum mechanics is needed. Many different approaches have been developed for this purpose, some of which are presented in chapters 2 and 3. By calculating the PESs of the different states, the behavior of the system can possibly be predicted and to some extent explained. In this thesis, density functional theory (DFT) and time-dependent density functional theory (TDDFT) have been applied to describe the ground state and the electronically excited states of the α-L-rhamnose cation radical.

The object of this thesis has been to examine the four possible sites for deprotonation from oxygen in the rhamnose cation radical, with the intention of understanding why only deprotonation from O_4 is observed. This is done by examining the profiles of the PES through each of the four deprotonations leading to each of the four different possible products (see also ***Figure 8***).

In addition, excited states of the system along the reaction paths have been calculated. This has been done to investigate the possibility of an electronically excited state being a mediator for the reactions. From the relatively large energy barrier for deprotonation found by Pauwels *et al.* (Pauwels *et al.* 2008) for the reaction, it seems that excited states (being vibrational or electronic in form) must play a part. It would be quite interesting to see if there is an electronically excited state with an energy profile for the proton transfer that does not have an energy barrier, or at least a smaller one than the ground state. If such a state exists for only one of the deprotonation reactions (the one from O_4), that might explain the selectivity observed in the radical formation.

In order to examine excited states, the TDDFT method was used. This is a relatively new computational method with the ability to treat quite large systems. There is still little experience with the use of TDDFT, and a large part of the work and even the motivation for starting this thesis project has been to learn how to employ the method. This has been done by comparing computational results at different levels of theory with each other and with data found in literature (both calculated and experimental).

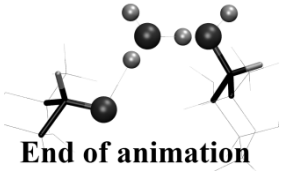

2 Quantum chemistry – Ground state calculations

Computational chemistry, or *quantum chemistry*, tries to use quantum mechanics to describe molecules. This is not an easy task, since the Schrödinger equation (SE) cannot be solved analytically for systems containing more than two charged particles. There are, however, numerous approaches for solving quantum mechanical problems for molecules using different approximations. Some of these will be briefly described here. For more detailed information, authoritative textbooks on the subject should be consulted, e.g. those of Pople and Beveridge, Cramer and Atkins and Friedman (Pople and Beveridge 1970; Cramer 2004; Atkins and Friedman 2005).

There are two major types of quantum mechanical computational methods, the *ab initio* methods and the *semiempirical methods*. In the *ab initio* methods the SE and a chosen model for the wave function is used along with only fundamental constants and information about which atoms are present. On the other hand, semiempirical methods rely on results from experiments through parameters included in the calculation approach.

As was mentioned in section 1.5, the Born-Oppenheimer approximation (BO approx) enables calculations of the electronic energy while the nuclei are held fixed. The electronic wave function will then depend parametrically on the nuclear coordinates, and the potential energy of the nuclei is added to the electronic energy as a classical term. Unfortunately, even this approximation does not make the problem solvable in most cases, and further approximations are needed.

According to quantum mechanics, a physical system is completely described by the wave function ψ, which is the solution to the SE. In practice one usually tries to solve the *time independent*, *non-relativistic* SE under the BO approx. This is what will be meant by the SE throughout the rest of this text, unless otherwise is stated. Throughout this chapter and the next, atomic units will be used, unless otherwise is specified. A list of the units is included in Appendix A.

2.1 Hartree-Fock theory

2.1.1 The basic Hartree-Fock method

In the *Hartree-Fock* (HF) method, the total wave function for the system is written as a *Slater determinant* of *spin orbitals* which again is comprised of *molecular orbitals* (MOs)

$$\Psi_{SD} = \frac{1}{\sqrt{N!}} \begin{vmatrix} \chi_1(1) & \chi_2(1) & \cdots & \chi_N(1) \\ \chi_1(2) & \chi_2(2) & \cdots & \chi_N(2) \\ \vdots & \vdots & \ddots & \vdots \\ \chi_1(N) & \chi_2(N) & \cdots & \chi_N(N) \end{vmatrix}, \tag{2.1}$$

where χ is a spin orbital, being a product of the MO, ψ, and the spin function, ξ, for the electron occupying that orbital.

$$\chi_i = \psi_i \xi_i \tag{2.2}$$

Writing the wave function as a Slater determinant makes sure that it is antisymmetric, as is required since electrons are fermions. All the MOs are orthogonal, and in closed shell systems, doubly occupied by electrons of different spins. Electrons have two possible spin states, referred to as α-spin and β-spin. There are more MOs than there are electrons, and the unoccupied orbitals are often referred to as *virtual orbitals*. The *occupied orbitals* are the ones that are lowest in energy. The highest occupied molecular orbital is called the HOMO and the lowest unoccupied orbital is referred to as the LUMO.

Under the BO approx. the Hamiltonian for a molecular system is

$$-\frac{1}{2}\sum_{i}^{electrons}\nabla_i^2 - \sum_{i}^{electrons}\sum_{A}^{nuclei}\frac{Z_A}{r_{iA}} + \sum_{i}^{electrons}\sum_{j>i}^{electrons}\frac{1}{r_{ij}}, \tag{2.3}$$

and when the wave function is approximated by a Slater determinant, the total energy is given by Eq. (2.4).

$$\begin{aligned} E &= 2\sum_{i}^{n} H_{ii} + \sum_{i}^{n}\sum_{j}^{n}(2J_{ij} - K_{ij}) \\ H_{ii} &= \int \psi_i^*(\mathbf{r}_1)(-\frac{1}{2}\nabla_1^2 - \sum_A \frac{Z_A}{r_{1A}})\psi_i(\mathbf{r}_1)d\mathbf{r}_1 \\ J_{ij} &= \iint \psi_i^*(\mathbf{r}_1)\psi_j^*(\mathbf{r}_2)\frac{1}{r_{12}}\psi_i(\mathbf{r}_1)\psi_j(\mathbf{r}_2)d\mathbf{r}_1 d\mathbf{r}_2 \\ K_{ij} &= \iint \psi_i^*(\mathbf{r}_1)\psi_j^*(\mathbf{r}_2)\frac{1}{r_{12}}\psi_j(\mathbf{r}_1)\psi_i(\mathbf{r}_2)d\mathbf{r}_1 d\mathbf{r}_2 \end{aligned} \tag{2.4}$$

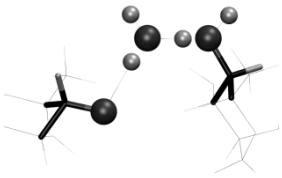

1 and 2 represent different electrons and *i* and *j* represent different orbitals and *n* is the number of occupied orbitals. *J* is called the Coulomb interaction, and *K* is the quantum mechanical exchange integral. As can be seen from Eq. (2.4) the energy for each MO is dependent of the shape of the other MOs. The best MOs are found by varying all the orbitals until the energy reaches a stable minimum. When this is achieved, the orbitals are said to be *self-consistent*.

In practice one starts out with a guess on the MOs, and these are used to calculate new and improved ones. When the change in energy from one iteration to the next is sufficiently small, the wave function has converged. This procedure is called the *self-consistent field* (SCF) procedure.

Finding the orbitals is a variational problem, and it turns out that the best MOs are eigenfunctions of the *Fock operator*

$$\hat{F}_i = -\frac{1}{2}\nabla_i^2 - \sum_A \frac{Z_A}{r_{iA}} + \sum_j (2\hat{J}_j - \hat{K}_j), \tag{2.5}$$

and the HF equations are the eigenvalue equations for the Fock operator, where the eigenvalues are the orbital energies

$$E_i = H_{ii} + \sum_j^n (2J_{ij} - K_{ij}). \tag{2.6}$$

The Fock operator only lets the electrons interact with an effective average of the other electrons in the system, and not directly with each other. This means that it does not give the exact energy of the system, and the energy that is calculated is often referred to as the HF-energy.

To simplify the calculations, the molecular orbitals are commonly written as linear combinations of *basis functions* ϕ,

$$\psi_i = \sum_\nu c_{\nu i}\phi_\nu. \tag{2.7}$$

Determining the molecular orbitals is then reduced to finding the set of coefficients, $c_{\nu i}$, which minimizes the HF energy. Inserting these basis functions for the orbitals and using a variational approach to find the coefficients leads to what is known as the *Roothaan equations* or the *secular equations*

$$\sum_{\nu}(F_{\mu\nu} - E_i S_{\mu\nu})c_{\nu i} = 0\,, \tag{2.8}$$

where the overlap integral

$$S_{\mu\nu} = \int \phi_\mu(1)\phi_\nu(1)d\mathbf{r}_1 \tag{2.9}$$

and

$$F_{\mu\nu} = H_{\mu\nu} + \sum_{\lambda\sigma} P_{\lambda\sigma}\left[(\mu\nu\,|\,\lambda\sigma) - \frac{1}{2}(\mu\sigma\,|\,\lambda\nu)\right]. \tag{2.10}$$

$H_{\mu\nu}$ is defined by

$$H_{\mu\nu} = \int \phi_\mu^*(\mathbf{r}_1)(-\frac{1}{2}\nabla_1^2 - \sum_A \frac{Z_A}{r_{1A}})\phi_\nu(\mathbf{r}_1)d\mathbf{r}_1\,, \tag{2.11}$$

P is known as the density matrix,

$$P_{\mu\nu} = 2\sum_i^{occ} c_{\mu i}^* c_{\nu i}\,. \tag{2.12}$$

and

$$(\mu\nu\,|\,\lambda\sigma) = \iint \phi_\mu(1)\phi_\nu(1)\frac{1}{r_{12}}\phi_\lambda(2)\phi_\sigma(2)dr_1 dr_2 \tag{2.13}$$

are *two-electron integrals*. There are N^4 such two-electron integrals to be evaluated (N is the number of basis functions). The implications of this on the choice of basis set (both in shape and size) will be discussed later on. For now, this means that the HF method scales as N^4 with respect to time, which is troublesome for large systems. It is therefore necessary to find a faster computational method for doing calculations on large systems.

HF theory as discussed above treats only doubly occupied orbitals and is called *restricted HF* (RHF). But there are ways of treating systems with one or more singly occupied orbitals such as radicals. In *restricted open-shell HF* (ROHF), the approach is about the same as for the closed-shell systems, but the fact that some of the orbitals are only singly occupied is taken into account when the calculations are performed. The alternative is *unrestricted HF* (UHF) which allows for the orbitals for the α- and β-spins to be different, giving twice as many MOs as RHF. UHF opens up for the possibility of spin polarization in the molecule, whereas ROHF does not. On the down side, UHF is vulnerable to *spin contamination*, which is to say that the resulting wave function is not an eigenfunction of the spin operator. ROHF does not have this deficiency.

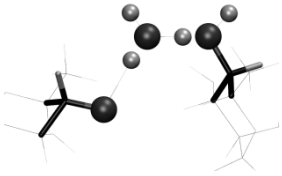

2.1.2 Semiempirical methods

Because of the very many integrals to calculate in the HF method, the calculations can take a lot of time for large systems. That is why the semiempirical methods were developed. What these have in common is that they do not calculate all integrals explicitly but either set them to zero (if they are likely to be very small) or assign them parametrically. The distinction between the methods is made by which integrals are calculated, which parameters are used and which basis set is used. These simplifications make the calculations much faster, but also less accurate for systems that do not closely resemble the systems they are calibrated for. Comparison of results is especially dangerous because errors might not cancel, but add to each other. The computational time for the Parameterized Model 3 (PM3) (Stewart 1989) which is a commonly used semiempirical method, scales as N^2 (Cramer 2004).

2.1.3 Beyond Hartree-Fock

Because the HF method does not take *electron correlation*, other than exchange, into account, the calculated energy will not be the correct energy for the system. There are different so-called *post Hartree-Fock methods* which have their basis in the HF method and manage to include some of this correlation. These methods are even slower than HF, and therefore not well suited for calculations on large systems. What the post-HF methods have in common is that they all start out with the HF wave function, and then improve upon that.

The *configuration interaction* (CI) method, writes the new wave function as a linear combination of Slater determinants with different occupation numbers in the molecular orbitals. In the HF determinant it is always the energetically lowest orbitals that are occupied. *Multiconfiguration SCF* (MCSCF) is similar to CI, but here the orbitals in the determinants with occupation numbers different from the HF occupation numbers, are re-optimized. In *Møller Plesset perturbation theory* (MP) the Fock operator is used as the non-interacting Hamiltonian. First order MP (MP1) returns the HF-energy, while going to higher orders (usually MP2 or MP4) improves upon this. In *coupled-cluster (CC) theory*, the new wave function is found by operation on the HF wave function with a “cluster operator”. This method is similar, but more robust than CI. While HF scales as N^4, CI with single and double excitations scales roughly as N^6, as do CC with single and double excitations, MP2 scales roughly as N^5 (Cramer 2004).

2.2 Density functional theory

Density functional theory (DFT) is another *ab initio* method, representing an alternative to HF theory. The rationale of the DFT method is to use the total *electron density* to predict the properties of a given system rather than the wave function. This means that in order to determine a specific property of the system at hand (e.g. a molecule) by DFT, it is necessary to know how this property depends on the electron density. In HF theory, all that is needed is the appropriate quantum mechanical operator.

In DFT all the electrons are treated as if they interact with each other and an *external potential*. This external potential may for instance be set up by the atomic nuclei in a molecule. DFT is built on two theorems by Hohenberg and Kohn, the *Existence theorem* and the *Variational theorem* (Hohenberg and Kohn 1964). The Existence theorem states that the external potential (and thereby the Hamiltonian) of the system is determined completely by the non-degenerate ground state electron density. In short this means that the ground state energy and all other electronic properties associated with the ground state, is uniquely determined by the electron density (which depends only on three spatial coordinates). The Variational theorem states that the electron density fulfils a principle of variation in the same way as the molecular orbitals in HF theory.

2.2.1 Kohn-Sham: Self-consistent field

The Existence theorem states that it is possible to do calculations on a molecule with the electron density as the starting point. It does not give any clues as to how this may be done. In practice, DFT calculations are performed by the so-called *Kohn-Sham (KS) method* (Kohn and Sham 1965). This method gives rise to equations that look quite similar to those of the HF method. The motivation behind the KS method is the realization that the Hamiltonian would look a lot simpler, had the system been one of non-interacting electrons. Therefore it starts with a fictitious system of non-interacting electrons with the same density as the real system (consisting of interacting electrons). The Hamiltonian for the real, interacting system can be divided into smaller parts, which gives an expression for the total energy of this form:

$$E[\rho(\mathbf{r})] = T_{ni}[\rho(\mathbf{r})] + V_{ne}[\rho(\mathbf{r})] + V_{ee}[\rho(\mathbf{r})] + \Delta T[\rho(\mathbf{r})] + \Delta V_{ee}[\rho(\mathbf{r})] \quad (2.14)$$

The energy is here expressed as a *functional* of the electron density ρ of the system (a functional is a function of one or more functions, as opposed to variables), hence the name Density Functional Theory. The first three terms represent the kinetic energy of the non-

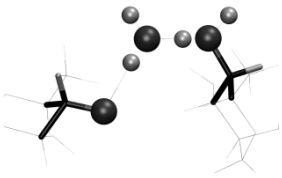

interacting electrons (the sum of the kinetic energy for each of the electrons), the classical electron-nuclear repulsion energy and the classical electron-electron repulsion energy. The fourth term contains the correction to the kinetic energy originating in the interaction between the electrons. The last term contains all corrections due to quantum mechanical exchange-, correlation- and classical self interaction energy. The two last terms are often replaced by a single term, $E_{xc}[\rho(\mathbf{r})]$, which is the sum of all corrections to the energy of the non-interacting system. This term is called the *exchange-correlation (XC) functional*, or just the functional. In this manner, all the difficult parts of the Hamiltonian are lumped together in one term. And by introducing the *KS orbitals* χ, which are electron orbitals resembling those of HF theory, Eq. (2.14) transforms to

$$\begin{aligned} E[\rho(\mathbf{r})] = \sum_i^n \left(\left\langle \chi_i \left| -\frac{1}{2}\nabla_i^2 \right| \chi_i \right\rangle - \left\langle \chi_i \left| \sum_A^{nuclei} \frac{Z_A}{|\mathbf{r}_i - \mathbf{r}_A|} \right| \chi_i \right\rangle \right) \\ + \sum_i^n \left\langle \chi_i \left| \frac{1}{2} \int \frac{\rho(\mathbf{r}')}{|\mathbf{r}_i - \mathbf{r}'|} d\mathbf{r}' \right| \chi_i \right\rangle + E_{xc}[\rho(\mathbf{r})], \end{aligned} \tag{2.15}$$

where *n* is now the number of electrons in the system. The connection between the KS orbitals and the electron density is

$$\rho = \sum_{i=1}^{n} \langle \chi_i \mid \chi_i \rangle . \tag{2.16}$$

Eq. (2.15) motivates the introduction of the *KS operator*, which is a one-electron operator (analogous to the Fock operator) defined by

$$h_i^{KS} = -\frac{1}{2}\nabla_i^2 - \sum_k^{nuclei} \frac{Z_k}{|\mathbf{r}_i - \mathbf{r}_k|} + \int \frac{\rho(\mathbf{r}')}{|\mathbf{r}_i - \mathbf{r}'|} d\mathbf{r}' + \frac{\delta E_{xc}}{\delta \rho} . \tag{2.17}$$

The KS method is formally similar to the HF method, but the KS operator replaces the Fock operator. The KS orbitals are expressed through basis functions in the same way as the molecular orbitals of HF theory. The orbital coefficients are optimized by solving the secular equations

$$\begin{aligned} \sum_\nu (K_{\mu\nu} - E_i S_{\mu\nu}) c_{\nu i} = 0 \\ K_{\mu\nu} = \left\langle \phi_\mu \left| -\frac{1}{2}\nabla^2 - \sum_A \frac{Z_A}{|\mathbf{r} - \mathbf{r}_A|} + \int \frac{\rho(\mathbf{r}`)}{|\mathbf{r} - \mathbf{r}`|} d\mathbf{r}` + \frac{\delta E_{xc}}{\delta \rho} \right| \phi_\nu \right\rangle , \end{aligned} \tag{2.18}$$

in an iterative SCF process. The electron density is then calculated from the orbitals that make up the solution to the secular equations.

Still missing is the XC functional, E_{xc}, and this is the heart of DFT's problems. It is also where there is a clear divide between DFT and the HF method. In the HF method it is assumed that the electrons do not interact directly with each other, but only with some kind of average of all the other electrons in the system. The Hamiltonian is approximated to the Fock operator, but the Fock operator problem is in turn solved exactly (with the exceptions of numerical problems and the problems of a limited basis set). DFT, on the other hand, employs an exact expression for the Hamiltonian, but in turn uses approximations for solving the problem. The approximation is the functional E_{xc}, which is unknown in its exact form. The challenge of the method is to create a functional which includes both exchange (the way HF theory does) and also electron correlation (which is not included in the HF method).

2.2.2 The exchange-correlation functionals

There are different ways of constructing an XC functional. Most functionals ignore the ΔT term in Eq. (2.14) - or include this in the other terms by adjusting parameters. The functional is expressed as an integral over the product of the electron density and energy density:

$$\begin{aligned} E_{xc}[\rho(\mathbf{r})] &= \int \rho(\mathbf{r})\varepsilon_{xc}[\rho(\mathbf{r})]d\mathbf{r} \\ &= \int \rho(\mathbf{r})\varepsilon_{x}[\rho(\mathbf{r})]d\mathbf{r} + \int \rho(\mathbf{r})\varepsilon_{c}[\rho(\mathbf{r})]d\mathbf{r} \end{aligned} \tag{2.19}$$

The electron density, ρ, is a density per volume, while the energy densities, ε, are densities per particle. Eq. (2.19) shows how the exchange and correlation energy densities are sometimes separated, but they can also be kept together in one term.

Except for maybe assuming a constant electron density, the *local density approximation* (LDA) is the simplest possible approximation to a functional. In this approximation, the energy density, ε_{xc}, at a given point, is only dependent on the electron density at this point. This makes it possible to find an analytic expression for ε_x by for instance using the expression for the energy density of a uniform electron gas. When it comes to ε_c, there is no simple analytical expression, even for a uniform electron gas. But there are functionals made from complicated expressions made from Monte Carlo calculations (Vosko *et al.* 1980).

It is possible to expand the LDA by including the possibility for the electron density to be independent of the electron spin. This is done by introducing an electron density which depends on whether the electrons have α-spin or β-spin. The *spin polarization function* is defined as

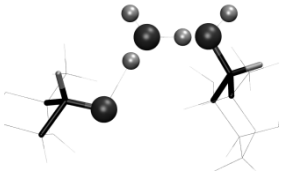

$$\zeta(\mathbf{r}) = \frac{\rho^{\alpha}(\mathbf{r}) - \rho^{\beta}(\mathbf{r})}{\rho(\mathbf{r})}, \tag{2.20}$$

and represents a kind of normalized spin density. This may be included in the expressions for ε_{xc}, and when it is used, the method is referred to as the local spin density approximation (LSDA).

A natural step beyond the LSDA is to let the energy density depend, not only on the electron density at the point of interest, but also on the electron density gradient at this point. This is called the *generalized gradient approximation* (GGA), and the energy density is then expressed as

$$\varepsilon_{x/c}^{GGA}[\rho(\mathbf{r})] = \varepsilon_{x/c}^{LSDA}[\rho(\mathbf{r})] + \Delta\varepsilon_{x/c}\left[\frac{|\nabla\rho(\mathbf{r})|}{\rho^{4/3}(\mathbf{r})}\right]. \tag{2.21}$$

Functionals denoted by ”B”, are GGA exchange functionals developed by Becke (Becke 1988) , these also contain an empirical parameter. The abbreviation ”LYP” denotes a GGA correlation functional developed by Lee, Yang and Parr (Lee *et al.* 1988). LYP is not a correction to the LDA, but calculates all the correlation energy and contains four empirical parameters adapted to the helium atom.

Rather than expanding the functional further by including the second derivative with respect to the density (these methods are called meta-GGA (MGGA)), or to include a dependency on the kinetic energy in the functional, HF exchange is often included. These functionals are referred to as *hybrid functionals*, because they mix HF and DFT exchange by using a set of parameters. A good example of a hybrid functional is B3LYP (Becke 1993):

$$E_{xc}^{B3LYP} = (1-a)E_x^{LSDA} + aE_x^{HF} + b\Delta E_x^{B} + (1-c)E_c^{LSDA} - cE_c^{LYP}. \tag{2.22}$$

B3LYP has three parameters, *a*, *b* and *c*, which are 0.20, 0.72 and 0.81 respectively. B3LYP is a quite robust functional, which is somewhat surprising since the parameters are actually not optimized for this functional, but for another similar hybrid functional. Even though the hybrid functionals include parameters, the methods are not referred to as semiempirical.

2.2.3 Advantages and disadvantages of using DFT

Time-wise, DFT scales as N^3 from the matrix diagonalization it takes to solve the secular equations, whereas HF scales as N^4 because of the two-electron integrals. This makes DFT

very advantageous when it comes to calculations on larger systems. Of course, including HF exchange in the functional makes DFT scale as N^4 as well, but it is still a lot faster than the HF based methods that include correlation.

Another advantage of DFT is its ability to treat systems where the total spin is different from zero without being exposed to spin contamination the way that UHF is.

In HF-based methods it is important to use basis functions where the two-electron integrals can be calculated efficiently. In DFT, on the other hand, these integrals do not appear, and the choice of basis functions need not depend on this property. The choice is freer to depend on other qualities of the functions without increasing the computational time. This is of course no longer the case if a hybrid functional (which includes HF- exchange) is used. With DFT the limit where expanding the basis set does not result in any significant improvements, is reached quicker than with HF. This reduces the necessary size of the basis set, and thereby the computational time for DFT calculations.

A great disadvantage of DFT is that there is no method for systematically improving the accuracy of the calculations in a similar manner as for the HF method. To improve upon a calculation, the functional may be swapped for a more advanced version (for instance going from LDA to GGA and MGGA), but in general this is not systematic once the hybrid functionals are included.

The KS method is also quite poor for describing systems that are not well described by a single Slater determinant, for instance systems containing a lot of non-dynamic correlation. This is partially corrected for by allowing different orbitals for α- and β-spin.

Another disadvantage of the DFT method is that it does not model weak interactions between molecules, and therefore often finds strange structures for instance for large bio-molecules. This is because the functionals do not include long distance interactions in the electron density. Van der Waals interactions, for instance, are very important for the geometrical structures of such large bio-molecules. Adding HF exchange to the functional improves on this weakness because HF is a non-local theory, as opposed to LDA and GGA, but the problem is not removed.

2.3 Geometry optimizations

Geometry optimizations are used to find stable geometrical conformations for molecules. A result of the BO approx. is that each set of nuclear coordinates, corresponds to a specific

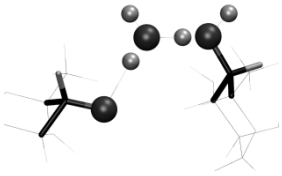

energy for the system. Calculations of the energy for a certain set of nuclear coordinates are called single point (SP) calculations. The potential energy surface (PES) describes the potential energy of the molecule as a function of its geometry (the kinetic energy of the nuclei is not included). A minimum on this surface corresponds to a stable geometry conformation. A PES will in general have several minima, all corresponding to stable geometries, but it is the global minimum that represents the equilibrium geometry of the molecule.

There are different methods for finding the minima on the PES. What they have in common is that they rely on calculating the energy of the system for different nuclear conformations and forces on the nuclei in terms of derivatives of the energy with respect to the nuclear coordinates. Because there are several minima on most PESs, the initial geometry (given to the computer by the user) is important in the geometry optimizations, since this is the point at which the computer will start its search. Which minimum is found, depends on the starting geometry, but also on the method for finding the electronic energy used.

2.4 Influence from the surroundings

Any system is influenced by its surroundings, also the orbitals in molecules. This means that when modeling a molecule (or larger system), the model will always be better if more detailed descriptions of the surroundings are included. Especially during geometry optimizations, the surroundings of the molecule will play an important part, since these will limit the available space and exert forces on the molecule.

In *single molecule (SM) calculations*, only the molecule of interest is modeled, completely without surroundings. This corresponds to a gas phase calculation, and is not a particularly good approximation if one is trying to model a solid or a liquid where there is a lot of interaction between the molecules. The SM model may be improved upon by adding one or more layers of molecules around the central molecule, this is called a *cluster calculation*. And even though the central molecule now has surroundings, the molecules around the edges do not. These molecules will then be modeled erroneously, and this error will to a small or large extent be transferred inwards in the model.

A cluster model gets better and better with larger cluster size, but of course the computational time goes up as well. To save time, when using a cluster model, it is possible to

model the different parts of the cluster, at different levels of theory[5], and even to freeze the coordinates in part of the system. This will lower the computational cost, but often also the quality of the results. As an alternative to a cluster model, there are models in which the single molecule is emerged into virtual surroundings either from discrete charges or a continuum.

Another way of modeling large systems is by using periodic calculations. In that case the molecules that are picked out fit into a box. When information from outside the box is needed, the information is collected from the other side of the box instead. In this way, a system of infinite size is simulated. In practice, the model will become better and better as the size of the initial box[6] increases, but the computational time will increase as well. When modeling a charged molecule, the total system will exhibit an infinite charge, which is counterbalanced by a uniformly distributed charge of the opposite sign. In these cases it is very clear that the size of the box is important to put a sufficient distance between the periodic images of the charged molecule.

2.5 Basis sets

The choice of *basis set* is one of the most important choices when doing a calculation. It is the collection of basis functions that will be used to approximate the molecular orbitals in HF theory, or the KS orbitals in DFT. The bigger the basis set, the more accurate the calculations will be, but they will also require a longer computational time. The construction of basis sets is done on two main criteria. First of all, one often desires a basis set where the functions resemble real atomic orbitals as much as possible. Secondly, one desires a basis set consisting of functions that are easy to do calculations on.

The first wish is granted by choosing so-called *Slater Type Orbitals* (STO). These are of the form

$$\phi(r,\theta,\varphi) \propto r^{n-1}e^{-\zeta r}Y_l^m(\theta,\varphi), \tag{2.23}$$

the same form as the eigenfunctions of the hydrogen atom. *n*, *l* and *m* are the quantum numbers for the orbitals, ζ is a constant which can be adapted and $Y_l^m(\theta,\phi)$ are the spherical harmonic functions. The STOs have no general analytic solution for the two-electron integrals that need to be calculated in the HF method, this makes them computationally expensive.

[5] By level of theory one means the computational method and basis set employed in the calculations.
[6] This box is referred to as a *supercell* in crystal calculations, since it may be larger than the unit cell of the crystal.

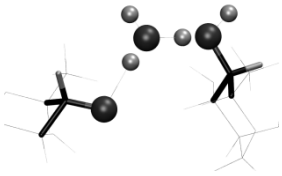

Another type of orbitals in common use, being less computationally expensive just because the two-electron integrals have general analytic solutions, is the *Gaussian Type Orbitals* (GTO). These are Gaussian functions of the form

$$\phi(x, y, z) \propto x^i y^j z^k e^{-\alpha(x^2+y^2+z^2)}, \tag{2.24}$$

where *i, j,* and *k* are positive integers which indirectly give the angular momentum of the orbital.

A common compromise between the STOs and the GTOs is to make specific linear combinations of GTOs designed to resemble the STOs. These basis functions are called *contracted basis functions*, while the GTOs that make them up are called *primitive functions*. The (mathematical) flexibility of the contracted basis sets is increased by adding several basis functions for each level (1s, 2s, $2p_x$, $2p_y$, $2p_z$, …). If all the primitive functions are used in a single contracted basis function, the set is called single-ζ. If the same set of primitives is used for two basis functions for each level, the set is called a double-ζ basis set, and so on. Using double- or triple-ζ basis sets does not increase the number of integrals to be calculated, but it gives more secular equations to be solved.

Even more (mathematical) flexibility can be added to the basis sets by including *polarization functions* and *diffuse functions*. Polarization functions are basis functions corresponding to higher angular momentum than the valence orbitals. An alternative is to introduce functions that are not centered on the atomic nuclei. Polarization functions are especially useful for achieving good geometries. Diffuse functions are used to represent electron density far away from the nuclei. They are made up of GTOs where α of Eq. (2.24) is up to a factor four lower than for the rest of the functions. Including polarization functions and/or diffuse functions rapidly increases the size of the basis set.

Two of the main classes of basis functions that are in common use are the Dunning sets and the Pople sets. The main difference between these are that the Pople sets use so-called *segmented contraction* whereas the Dunning sets use *general contraction*. A segmented contraction means that each primitive is only used in one contracted basis functions, and general contraction means that the all the contracted basis functions contain some of all the primitives, only with different weights.

The basis sets described above, are atom centered basis sets which simulate atomic orbitals. Off course, this is not the only possible kind of basis set. Maybe the most commonly used alternative is *plane waves*. The plane waves are of the form

$$\phi(\mathbf{r}) \propto e^{i\mathbf{k}\cdot\mathbf{r}}, \tag{2.25}$$

where the wave number **k** gives the wave length of the function. Plane waves are very useful for periodic calculations, but a large number of them are needed in order to model a function that changes quickly. This is for instance the case near the atomic nuclei where the electronic wave function changes rapidly.

When plane waves are used, they are sometimes used together with so-called *pseudopotentials*. This means that the inner electrons in the molecules are not modeled explicitly, but the potential from the nucleus is instead replaced by a total potential from the atomic core, acting on the outer electrons. The use of pseudopotentials will to a certain extent, but mostly in the core region, affect the shape of the molecular orbitals. The change is such that the orbitals do not change rapidly as they would without the pseudopotentials, thus removing some of the problems in using plane wave basis sets. Since it is mostly the core region that is affected by the pseudo-potentials, the chemical bonds will not be severely affected, and chemical properties of molecules may still be modeled in a good way.

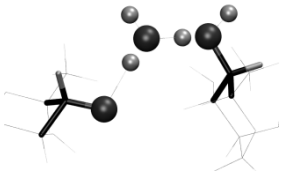

3 Excited state calculations and time-dependent DFT

A molecule that is not in its electronic ground state is said to be in an *excited state*. In the MO picture, this means that the electrons are not occupying the molecular orbitals with the lowest energy available; at least one electron is occupying an orbital of higher energy than the lowest lying one that is vacant. To describe these electronic states, one needs to go beyond simple HF and DFT, because both of these methods assume that the electrons are in the lowest available states.

By demanding a certain symmetry or spin multiplicity for the system (different from that of the ground state), both HF and DFT are able to describe the lowest excited state of this configuration. These are very restricted possibilities, especially for large molecules lacking symmetry. Therefore other, newer methods for calculating excited states have been developed. The natural extension of DFT into the realm of excited states is known as *time-dependent density functional theory* (TDDFT). TDDFT scales roughly as N^3 (Dreuw 2006), which makes it suitable for large systems.

3.1 How to describe an electronically excited state

Excitation energy

The excited states are higher in energy than the ground state, and the energy that separates them is called the *excitation energy*. Just as for the ground state, the excited state wave function, and thereby the energy, will depend on the nuclear conformation for the molecule. This means that the excited states have their own PES, different from that of the ground state. In general there is one PES per electronic configuration. It is also possible for the PESs for different states to cross each other, such that the energetic ordering of the states is different for different geometrical conformations of the nuclei. It is not even certain that the state which is the ground state for one conformation is so for another nuclear conformation. Also the stable geometrical conformations will differ for the different states. The point at which two PESs (of different electronic states in the same molecule) touch or even cross, is known as a *conical intersection*. At these intersections transition between the states is probable, and they therefore play an important role in *non-radiative* de-excitation processes.

Oscillator strength

The intensity of a *radiative transition* (involving the absorption or emission of a photon) in a molecule is proportional to the square of the *electric dipole transition moment*

$$\boldsymbol{\mu}_{fi} = < f \mid \hat{\boldsymbol{\mu}} \mid i >, \tag{3.1}$$

where *f* represents the final electronic state, *i* represents the initial state and $\hat{\boldsymbol{\mu}}$ is the electronic dipole moment operator. The oscillator strength for the transition from a state *n* into the ground state (denoted by *0*) is defined as

$$f_{n0} = \frac{2}{3}(E_n - E_0) \mid \mu_{n0} \mid^2, \tag{3.2}$$

where

$$\mid \mu_{n0} \mid^2 = < 0 \mid \hat{\mu}_x \mid n >^2 + < 0 \mid \hat{\mu}_y \mid n >^2 + < 0 \mid \hat{\mu}_z \mid n >^2. \tag{3.3}$$

The oscillator strength is a dimensionless quantity which is a measure for the radiative *transition probability* both from state *n* into *0* and the other way.

Radiative transitions are not the only way for a molecule to change its electronic configuration. De-excitation may occur through non-radiative transitions which involve transmission of energy into rotational and vibrational modes and then into the surrounding molecules.

Electronic configuration

In general the *electronic configuration* of an excited state will be a superposition of many excitations from occupied orbitals into virtual orbitals. This is especially the case in DFT, where the molecular orbitals are not physical or chemical quantities but rather mathematical aids.

It is customary to describe the electronic configuration in an excited state as a linear combination of states involving specific excitations in the molecular orbitals. The different terms in the sum may consist of *single-* or *double excitations* (or even higher numbers) where more than one electron is excited into a virtual orbital at the same time.

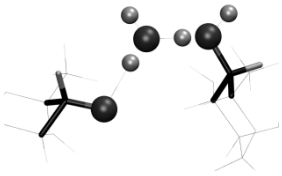

3.2 Time-dependent DFT

3.2.1 Foundation

TDDFT is a calculational method for determining the behavior of a system under the influence of time dependent electromagnetic fields. The most frequent kind of TDDFT in use is the *time-dependent density functional response theory* (TDDFRT) also known as *linear response TDDFT* (LR-TDDFT). The equations to solve in this method emerge from perturbing the system with an *oscillating electric field* and calculating the linear response of the system to this perturbation.

The polarizability of a molecule is its ability to respond to an electric field and acquire a dipole moment. The *dynamic polarizability* ($\alpha(\omega)$) is the response to an oscillating electric field with frequency ω. And the mean dynamic polarizability is given by

$$\alpha(\omega) = \sum_{n}{}' \frac{f_{n0}}{\omega_{no} - \omega}, \tag{3.4}$$

the prime on the summation indicates that $n = 0$ should not be included in the summation. f_{no} is the oscillator strength of the transition and ω_{n0} is defined by

$$\omega_{n0} = \frac{E_n - E_0}{\hbar}. \tag{3.5}$$

The dynamic polarizability is dependent on both the oscillator strengths and excitation energies of the excited states of the system. And if $\alpha(\omega)$ is known it is possible to derive the excitation energy and oscillator strength from this. Using LR-TDDFT the dynamic polarizability of the system is calculated by the use of the *density matrix* see Eq. (2.12) in section 2.1.1.

TDDFT is an excited state theory made to resemble ground state DFT. Its foundation is the *Runge Gross theorem* (Runge and Gross 1984), which is an analogue to the existence theorem of Hohenberg and Kohn for DFT. It states that the (now time dependent) charge density determines the external potential up to an additive *time dependent* function. This means that all spatial dependence is determined by the density. The wave function is then determined up to a time-dependent phase factor. This again means that the expectation value of any operator that does not contain a derivative or integral operator in time is uniquely determined by the

electron density. For an introduction to the formal theory of TDDFT see for instance (Casida 1995).

The exchange correlation functional is also time dependent in TDDFT. This functional is (as usual) not known. But in the limit of a slowly changing external potential, it is valid to replace the time-dependent functional with the time-*in*dependent functional evaluated at the current electron density (Casida 1995) . This is a local approximation in time, and it is called the *adiabatic local density approximation* (adiabatic approximation/ALDA)

$$v_{xc}(\rho t) \approx \frac{\delta E_{xc}[\rho_t]}{\delta \rho_t(\mathbf{r})}. \tag{3.6}$$

As can be seen from Eq.(3.6), time is taken into account by always using the current electron density, but there is no "memory" in the functional. The adiabatic approximation also works well beyond its domain of rigorous foundation (Casida 1995).

In linear response TDDFT using the adiabatic approximation, the excited states are described by a linear combination of *only* singly excited states. This would not be the case had the exact XC functional been used (Casida 2005). Being limited to use only single excitations somewhat reduces the applicability of the method, as will be mentioned later.

In TDDFT the excitation energies and oscillator strengths are calculated from the dynamic polarizability, and not from the wave function or electron density of the excited state, as would be intuitive. It is therefore not necessary to calculate each excited state by converging wave functions (one at a time) in order to find the excitation energies and oscillator strengths. Instead; it remains until after the excitation energies are calculated to decide which excited state is which in terms of electronic configuration. One advantage of this approach is that the entire energy spectrum is available at once, which is useful if the excitation energies and oscillator strengths can be used to determine whether a certain state is interesting or not. Since the calculation of the electronic configuration is time-consuming, the selection possibility may save a lot of computational time.

3.2.2 Applicability

For *valence excited states*[7], where the excitation energy is small compared to the ionization energy, TDDFT performs relatively well. The excitation energies have errors of about 0.2 – 0.8 eV. The shift in energy relative to experimental results is often systematic, so that it is

[7] Excited states involving outer (valence) electrons.

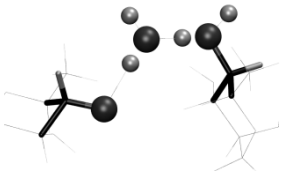

possible to compare the states to each other (Dreuw 2006). Even so, it is still necessary to used large basis sets including many virtual orbitals in order to achieve good accuracy (Dreuw and Head-Gordon 2005).

In general it can be said that TDDFT has difficulties in describing states with diffuse molecular orbitals. The errors can reach up to several eV for *Rydberg states*[8], valence states of molecules exhibiting *extended π-systems*[9], *doubly excited states* and *charge-transfer (CT) states*[10] (Dreuw and Head-Gordon 2005). These errors also affect the curvature of the PES.

Rydberg excited states are so high in energy, that the excited electron is barely bound. This means that the orbital this electron occupies, is very diffuse. These states are not described very well by TDDFT.

A CT state is a state in which the electron is excited into an orbital that does not overlap with the originally occupied orbital. Hence the excitation results in a transfer of electron density (and then also charge) from one area in the molecule to another. CT states are a particular problem for TDDFT; both the size of the excitation energy and the shape of the PES are unreliable. The excitation energies in the CT states are usually underestimated (Dreuw *et al.* 2003). Including non-local HF-exchange in the XC potential will reduce the long range problems in the PES. New functionals have been developed that split the Coulomb operator in two parts, so that more exact HF exchange can be included at long-range (Dreuw 2006). One such functional is CAM-B3LYP (Yanai *et al.* 2004) which is known to perform quite well for CT excited states (Dreuw and Head-Gordon 2005).

Since LR-TDDFT within ALDA only includes singly excited states, it cannot model doubly excited states. It also has problems modeling excited states of molecules with an open-shell ground state because many-electron excited states are required to describe these (Casida 2009). However it should be noted that this failure of TDDFT does not affect calculations of singly excited states of radicals (Kumar and Sevilla 2008; Ipatov *et al.* 2009).

As with ground state DFT, the choice of functional is crucial to achieve a viable result using TDDFT. Some of the problems described above require special functionals designed

[8] Singly excited states that have excitation energies close to the ionization potential.
[9] In π-systems the electrons occupy orbitals that are not centered on specific atoms but rather spread out along a chain of atoms.
[10] CT excited states result from excitations involving displacement of the charge from one part of the molecule to another.

especially for this type of problem. Including exact HF exchange is necessary in many cases using TDDFT. The B3LYP functional is found to perform quite well (Bauernschmitt and Ahlrichs 1996). It is later found that the PBE0 functional which will be introduced in section 4.4, is capable of handling vertical excitations into Rydberg states quite well, also in comparison to B3LYP and functionals designed to improve upon long-range problems in TDDFT (Adamo *et al.* 1999). The CAM-B3LYP functional is one of the functionals which is in quite wide use and performs well (Dreuw and Head-Gordon 2005). It was developed especially for TDDFT and the long range problematic in some excitations. In general it is a good idea to use several different functionals for the same calculations when using TDDFT, in order to get the full "true" picture, as the optimal functional depends on the type of excitation being modeled. This functional selectivity must be regarded as a strong disadvantage of the TDDFT method.

3.2.3 TDDFT versus other excited state methods

Some of the HF based methods which include correlation, described in the previous chapter (section 2.1.3), are also able to describe excited states. These methods are in use for that purpose, and yield more accurate results than TDDFT can offer. What the HF based methods have in common is that they can model many-electron excitations. This enables them to describe states that TDDFT is not immediately able to handle. But as was noted before, these methods are very time consuming, and are not suited for large molecules. The advanced HF based methods are not suited for treating systems larger than 10-20 atoms.

TDDFT is able to treat systems of up to 200 first row atoms (Dreuw and Head-Gordon 2005). For systems of this size, only two other *ab initio* methods may be applied; configuration interaction singles (CIS) and the random phase approximation (RPA) also known as time-dependent HF.

The CIS method uses the orbitals from the ground state HF solution. These orbitals are used to construct the wave function for the excited state as a linear combination of single excitations.

In the RPA the equations are obtained from linear response of the orbitals using time-dependent perturbation theory to first order. This method strongly resembles TDDFT, but does not include any correlation effects (since HF does not do so either). For excited states with excitation energy lower than ½ the ionization potential, TDDFT performs better than these two HF based methods (Bauernschmitt and Ahlrichs 1996).

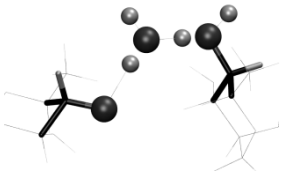

3.2.4 Some applications to biomolecules

None of the high level excited state-methods are applicable to large molecules such as DNA and DNA model systems. TDDFT is therefore a method which is increasing in use for excited state calculations on these large molecules; a few applications are presented here. Since TDDFT is well suited for examining excited states of cation radical with low excitation energy (Kumar and Sevilla 2008), the method is good for examining radiation damage, which corresponds to states where one electron is moved from an occupied orbital into the first unoccupied orbital.

Radicals on the sugar molecules in DNA can result in strand breaks (Kumar and Sevilla 2008). Several TDDFT studies have been performed that discuss how a radical stabilized on the nucleobase, can be transferred to the sugar via photo excitation (Adhikary *et al.* 2005; 2006; 2006; Kumar and Sevilla 2006; Adhikary *et al.* 2008). The smallest systems modeled were nucleosides (a nucleobase with an attached sugar), but also larger systems were included (nucleotides and systems including several bases). In these studies, the geometrical structure was optimized in the ground state where the radical cation is localized on the nucleobase; then vertical excitation energies were calculated.

It is pointed out (Adhikary *et al.* 2005) that the excitation energies and oscillator strengths found using a double-ζ basis set without diffuse functions do not change much (on average the excitation energies change 0.05 eV) upon going to a triple-ζ basis set including diffuse functions.

In the above mentioned studies it was found that excited states involving excitation from a low MO into the singly occupied MO (SOMO) of the radical corresponds to electron hole transference from the base to the sugar. This is expected to be followed by a deprotonation from the carbon atom with the lowest electron density. None of these studies modeled the deprotonation reactions; which would have been very time-consuming considering the size of the systems.

Mechanisms for non-radiative decay of adenine has also been studied by doing TDDFT calculations on geometries optimized with ground state DFT and CASSCF (Sobolewski and Domcke 2002). By investigation of the excited state energy profiles, conical intersections were found that might enable radiation-free de-excitation.

A study of a proton transfer process from –keto to –enol forms of guanine has been performed in order to decide whether this reaction might be facilitated by an excited state (Shukla and Leszczynski 2005). This was done by using TDDFT and the B3LYP functional to calculate barrier heights for the reaction. The barrier heights were in this case calculated by using vertical excitation energies with TDDFT on –keto, transition state and -enol geometries for the first excited state optimized the using CIS. The first excited singlet state of the system was not found to facilitate the transition, but the TDDFT results were found to be in good agreement with experimental data.

The efficiency of TDDFT to other numerical methods for excited state calculations has made it possible to perform dynamic simulations of excited states with this method. An implementation using local basis sets (Meng and Kaxiras 2008) scales linear with the number of electrons in the system, thus making dynamic simulations of larger molecules, such as biomolecules, possible.

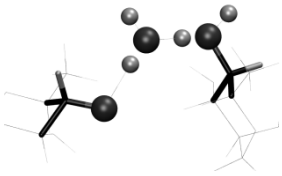

4 Methods used

The work presented in this thesis is DFT and TDDFT calculations on oxidized rhamnose. The calculations have been performed using two different computer programs; *CP2K* (the CP2K developers group 2009) and *Gaussian03* (G03) (Frisch *et al.* 2004). The calculational methods used in these two programs differ slightly, even though they are all DFT calculations. This means that the results cannot be expected to be identical, but if both programs (and the methods used in each of them) are performing well, then the results should be comparable. The term "level of theory" (LOT) is taken to mean the quantum chemical method and basis set used for the calculations, in the case of DFT and TDDFT the functional used is also part of the level of theory.

Unless otherwise is specified, the calculations on rhamnose have all been performed with a specified spin multiplicity of 2 (spin ½) and charge +1, this corresponds to the cation radical. And the unrestricted KS method has been used, meaning that α- and β electron orbitals are allowed to differ in their spatial distribution.

4.1 Ground state calculations

4.1.1 Periodic calculations

The periodic calculations on the ground state of rhamnose have been performed using CP2K and the Quickstep method (VandeVondele *et al.* 2005). All were performed using the hybrid *Gaussian and plane wave* scheme (GPW) (Lippert *et al.* 1997). This means that the KS orbitals have been expanded in a Gaussian basis set, whereas the electron density is expressed in a plane wave basis set. The GPW method also implies that pseudo-potentials are used to treat the core electrons and that only the valence electrons are modeled through the basis functions. The motivation behind this mix is that the electron-electron interaction energy calculations are more easily performed in a plane wave basis set, whereas the kinetic energy calculations and the calculations describing the interactions with the nuclei (in this case the atomic core) are more easily performed using the gaussian functions.

The starting geometry for the CP2K calculations was the experimentally determined structure for the intact crystal (Takagi and Jeffrey 1978). The geometry was then optimized for the radical cation. This optimized geometry was used as the first input for the *constrained*

geometry optimizations that were performed later. Successively, the previously attained wave functions were used for the next step in the calculation. Re-using wave functions like this saves computational time, but may also influence the results in that the new wave function will most likely resemble the starting wave function in character. The constrained geometry optimizations were bond elongations where one bond length in the molecular structure was constrained using a *harmonic restraint*. A restraint works in the fashion that a penalty function for the energy is imposed if the restrained coordinate changes from its nominal value. That the restraint is harmonic, means that it has the form of a classical spring. The restraint was placed on a bond length that was increased in steps of 0.1 Å, thus a scan of the PES was performed. Also here the wave functions attained in the previous step were used as input for the next step in the calculations. The geometry optimization method used is the LBFGS method (Byrd *et al.* 1995).

4.1.2 Cluster- and single molecule calculations

G03 was used for calculations on single molecules (SM) and clusters. Both single point (SP) calculations, constrained geometry optimizations and unconstrained geometry optimizations were made. In G03 the Berny algorithm for geometry optimizations (Peng and Schlegel 1993; Peng *et al.* 1996) is used. To produce PES profiles, two different approaches were employed. One was to make constrained geometry optimizations using the "ModRedundant" option. The other was to simply do SP calculations on the geometries achieved by just moving the hydrogen core away from the molecule in steps using the "Scan" option. The latter method was used when the constrained geometry optimizations resulted in geometries that did not correspond to the conformation that was to be investigated; for instance in some of the SM calculations the rhamnose molecule fell apart and formed three new molecules. Also here the bond elongations were performed in steps of 0.1 Å.

ONIOM

ONIOM (Svensson *et al.* 1996) is a method for speeding up the calculations on large clusters by not treating the entire cluster at the same LOT. This method lets the user specify different *layers* in the cluster; the central layer will usually be treated at the highest LOT, and the outer layers (farthest from the central molecule) only at a low LOT. For the work in this thesis, two-layered ONIOM was employed to perform geometry optimizations for clusters. Four different energies are calculated in the two-layered ONIOM scheme: The energy for the inner layer at

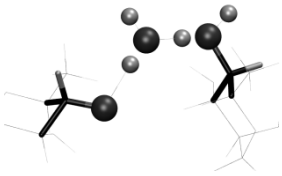

the high LOT, $E_{inner,high}$, the energy for the inner layer at the low LOT, $E_{inner,low}$, the energy for the entire system at the low LOT, $E_{cluster,low}$, and then the total energy, E_{ONIOM}, as a sum of these

$$E_{ONIOM} = E_{cluster,low} - \mathrm{E}_{inner,low} + E_{inner,high}. \quad (4.1)$$

In this way, the interactions between the molecules in the inner layer and the rest of the cluster are to some extent modeled. For the ONIOM calculations performed in this work, the semiempirical model PM3 (Stewart 1989) was applied for the low level calculations.

4.1.3 Calculation of hyperfine coupling tensors

The hyperfine coupling tensors associated with the deprotonated oxygen-centered radical resulting from the OH_4 deprotonation were calculated using G03. The stable geometries of the periodic calculations and the ONIOM cluster calculations were used. The hyperfine coupling tensor calculations were performed as B3LYP/6-311++G** single point calculations on the isolated neutral radical (22 atoms) only.

4.2 Excited state calculations

All the excited state calculations presented in this thesis are single point TDDFT calculations performed in G03. It would have been desirable to be able to use CP2K for excited state calculations on the geometries optimized in this program, but attempts to use TDDFT in this program resulted in convergence problems. Due to a quote found on the CP2K discussion group by one of the developers of the TDDFT code (Hutter 2009);

The TDDFT code has not been worked on for three years.
The performance is not very good and the oscillator strength calculation is missing.

attempts to circumvent the convergence problems were eventually abandoned. Rather than using CP2K to calculate the excited states, geometries from the CP2K geometry optimizations were used for SP calculations in the G03 program. This is not ideal since these geometries will not represent stable conformations in G03, but it is the best we can do for now.

The calculations on small molecules (H_2O, CH_3 and CO^+) were performed to see how different basis sets and functionals influence the results. Diffuse basis functions play a significant role in describing excited states, but the inclusion of these greatly increase the size

of the basis set and thereby the computational time. After these test calculations it was decided to use a double-ζ basis set including diffuse functions and polarization functions for the calculations on rhamnose.

Because the excited state calculations were performed as SP calculations (for each of the geometries in the bond elongation processes) separately, it was not trivial to follow the excited states from one geometry to the next. G03 numbers the states by excitation energy and they are relatively close to each other in energy. The program is not able to determine the spin multiplicity of the excited states and there is no symmetry present, so it is impossible to use any of these quantities to tell the different states apart. To solve this problem the bond elongation should be performed at sufficiently small steps so that the tracking of the excited states is made possible. This is computationally very expensive, and some time was saved by doing *linear interpolation* between two adjacent optimized geometries instead of making new geometry optimizations for all these points. The excited states were then calculated also for all these interpolation points.

For the first four steps in the deprotonation reaction 20 interpolated points were used between the steps, and after that only 10 interpolated points were used. ***Figure 10*** shows the result of the TDDFT calculations using interpolated geometries for one of the deprotonation processes. It was then possible to see clearly where the states might cross each other in energy. In order to determine whether the crossings were real, the electric-, magnetic- and velocity transition dipole moment to the ground state were used to tell the states apart, under the assumption that the transition dipole moment should be continuous.

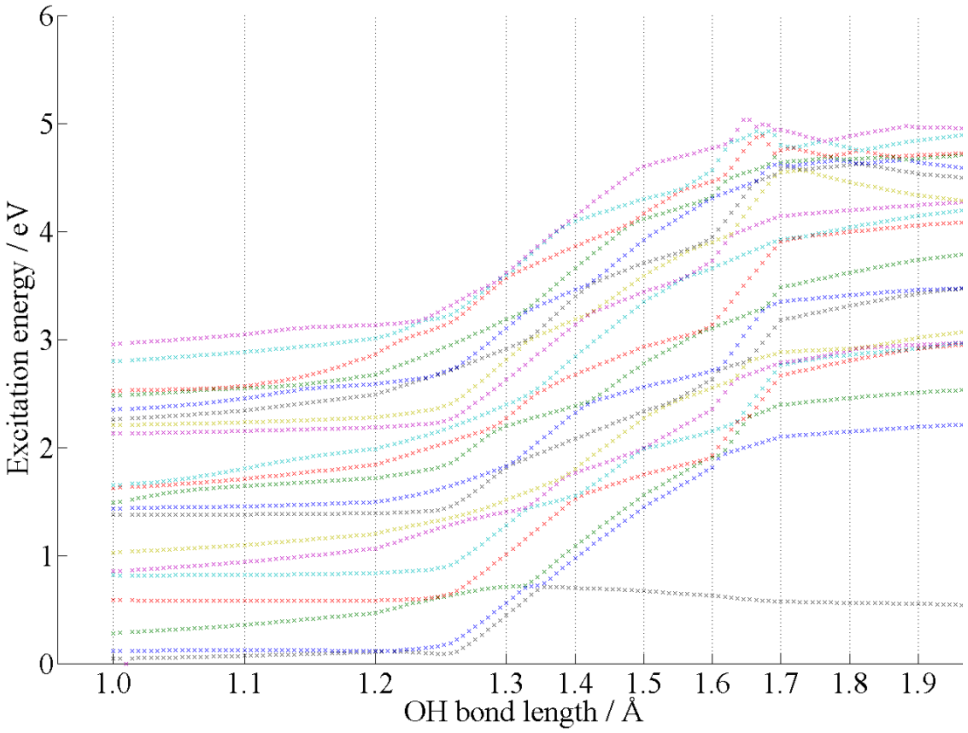

Figure 10: Vertical excitation energies for the first 20 excited states during the OH_4 deprotonation reaction for the rhamnose cation calculated in the single chain model. Geometries from optimizations in periodic code are at the positions of the vertical lines with interpolated points in between.

4.3 Basis sets

For the calculations using CP2K, a TZVP basis set (VandeVondele and Hutter 2007) was used with GTH pseudo-potentials (Goedecker *et al.* 1996; Hartwigsen *et al.* 1998; Krack 2005). The basis set is a Dunning set with triple-ζ valence and polarization functions. The electron density is expressed in a plane wave basis set, and the cutoff of 400 Ry corresponds to the highest frequency of this basis, giving a shortest wave length of about 2.3 Å.

For the calculations using G03, Pople basis sets have been used. The two most frequently used were 6-311G** (Krishnan *et al.* 1980) and 6-31++G** (Hehre *et al.* 1972; Hariharan and Pople 1973; Clark *et al.* 1983). Other basis sets that are used were 6-311G, 6-311++G, 6-311++G** and 6-31G**[11]. In the Pople sets, the first number (in this case 6) is the number of primitives used in the contracted core functions. The numbers after the hyphen indicates how many Gaussian functions are used in each valence function. This means that 6-311G has six

[11] For references, see those for 6-311G** and 6-31++G**.

primitive Gaussian functions for each core function, and one core function for each core orbital. There are three basis functions for each valence orbital (triple-ζ), one of these is a contraction of three Gaussian functions and the other two are scaled Gaussian functions. Stars in the designations of the Pople sets indicate the presence of polarization functions. One star means that there are added d-orbitals in addition to the p-orbitals that are already there, two stars means that p-orbitals are added on hydrogen and helium atoms as well. One or two plus signs indicate the presence of diffuse s- and p-functions. One plus sign indicates the presence of diffuse functions on heavy atoms, and two plus signs indicate the added presence of diffuse s-functions on hydrogen atoms. (Cramer 2004)

4.4 Functionals

A part of the work in this thesis has been to test the performance of different exchange-correlation functionals. The ones used are BLYP, B3LYP, PBE and PBE0. BLYP is a combination of the Becke's exchange functional (Becke 1988) and the correlation functional of Lee, Yang and Parr (Lee *et al.* 1988). B3LYP (Becke 1993) is a hybrid functional based on the exchange and correlation functionals that make up BLYP (see section 2.2.2). B3LYP includes HF exchange and is a quite robust functional despite the fact that the parameters used in this functional are in fact not optimized for B3LYP, but rather for a similar functional. PBE (Perdew *et al.* 1996; Perdew *et al.* 1997) is a GGA functional proposed by Perdew, Burke and Ernzerhof. The PBE0 (Adamo and Barone 1999) functional is a hybrid functional based on PBE, including exact HF exchange. This hybrid functional does not include empirical parameters.

4.5 Spin and charge analysis

Charge and spin will not necessarily be distributed evenly in molecules. Some atoms attract electrons more efficiently than others (have a higher electronegativity) and can create polarization of the molecule; this is the origin of hydrogen bonds between molecules. Especially ions and radicals are exposed to this since all the molecular orbitals cannot be doubly occupied. Consequently there is a need for a method to determine the spin- and charge distribution of molecules.

The electron density and spin density functions provide three-dimensional information about the distributions. Nevertheless, in many situations it is convenient to have some notion of the net charge and the net spin on a certain atom, this analysis is known as *population*

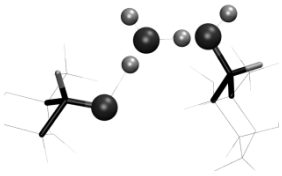

analysis. In the present work, Mulliken population analysis (Mulliken 1955) has been used, among other things to determine whether it is a proton transfer or a hydrogen transfer process that is being studied. In a Mulliken analysis, the number of electrons "belonging" to a certain nucleus is calculated from the atomic orbitals centered on that nucleus contributing to the occupied molecular orbitals.

It would have been very interesting to be able to describe the charge distribution of the excited states as well as that of the ground state. This could have contributed to the understanding of the mechanisms for the deprotonation reactions, but in the present work, such a method has not been found.

5 Results and analyses

This chapter consists mainly of three parts. The first part presents the results of the ground state calculations on the rhamnose cation radical. The calculations are mainly focused on establishing energy profiles for four different deprotonation reactions from the cation. The deprotonations in question are those from the four hydroxyl groups in the molecule (see ***Figure 11*** for numbering scheme). These deprotonation reactions are the main focus of this thesis. The second part of this chapter contains benchmark calculations using TDDFT on three small molecules (H_2O, CH_3 and CO^+) where the performance of different functionals and basis sets is tested. The third section contains TDDFT calculations of the excited states of rhamnose in the deprotonation reactions mentioned above.

5.1 Ground state calculations on rhamnose

Ground state calculations were performed in order to describe the possible deprotonation routes from each of the four hydroxyl groups (OH_1, OH_2, OH_3 and OH_4) in the rhamnose cation (see ***Figure 11***). The calculations were performed as partially constrained geometry optimizations, in which specific constraints were placed on the bond lengths of the original OH groups only. The calculations were performed at (roughly) three different system sizes, where the most accurate description was expected to be obtained from the largest system. The smallest system was a single molecule, the intermediate system was a multi-molecular cluster consisting of altogether 294 atoms, and the largest system was a supercell containing 416 atoms used for the periodic calculations.

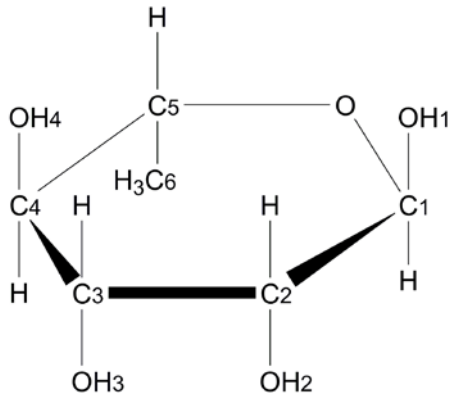

Figure 11: The structure of α-L-rhamnose with carbon atom and hydroxyl group numbering indicated. This figure is identical to ***Figure 6***, repeated here for convenience.

5.1.1 Periodic calculations using CP2K

The periodic calculations for the rhamnose crystal were performed using CP2K within the GPW approach. The periodic supercell used consisted of the crystalline unit cell doubled in every direction (with axis lengths thus being 15.802 Å, 15.844 Å and 13.340 Å). This supercell contains 16 rhamnose molecules and 16 water molecules, altogether 416 atoms. The functional used was BLYP, and the basis set was TZVP-GTH with a cutoff at 400 Ry.

The crystal structure geometry was optimized without constraints for both the intact structure (charge 0, spin 0) and with one cation (charge 1, spin ½). These geometries will be referred to as the intact geometry and the cation geometry. The energies of the cation structure at these two geometries are given in ***Table 1***. The difference between the energies is a measure of the kinetic energy available if the cation is left in its ground state just after ionization; there will be an energy excess of 0.01 eV available for moving around on the PES (energetically allowed movement of the nuclei).

Table 1: Energies of the cation (charge 1, spin ½) structure for two optimized geometries[a].

Geometry	Energy /Hartree	Energy / eV
Intact geometry	-2214.285407	-
Cation geometry	-2214.285882	-
Energy difference	-0.000475	-0.01

[a] Intact geometry refers to the geometry found by geometry optimization of the intact structure, cation geometry corresponds to the geometry found by geometry optimization of the cation structure.

In addition to full geometry optimizations of the crystal structure (both for the intact structure and the cation), partially constrained geometry optimizations were performed on the cation structure. This in order to model the deprotonation reactions from each of the four hydroxyl groups separately, starting from the fully optimized cation geometry. The constrained coordinate was that of the OH bond distance of the original hydroxyl group in focus. The imposed constraint was a harmonic restraint. The bond elongations were performed in steps of 0.1 Å from 1.0 Å to 2.0 Å, with constrained geometry optimizations in each point. The resulting energy profiles are shown in ***Figure 12***.

For three of the deprotonation reactions (1, 2 and 4), a local drop in energy was observed as the bond distance increased beyond about 1.7 Å. For all three of them, new *unconstrained* geometry optimizations were subsequently performed, starting from the point lowest in these local minima. This led to modified minimum-energy geometries, represented in ***Figure 12*** as single diamonds. The proton did not return to its original position when the constraint was removed in any of these three cases. In Appendix D, tables showing the energies plotted in ***Figure 12*** are presented.

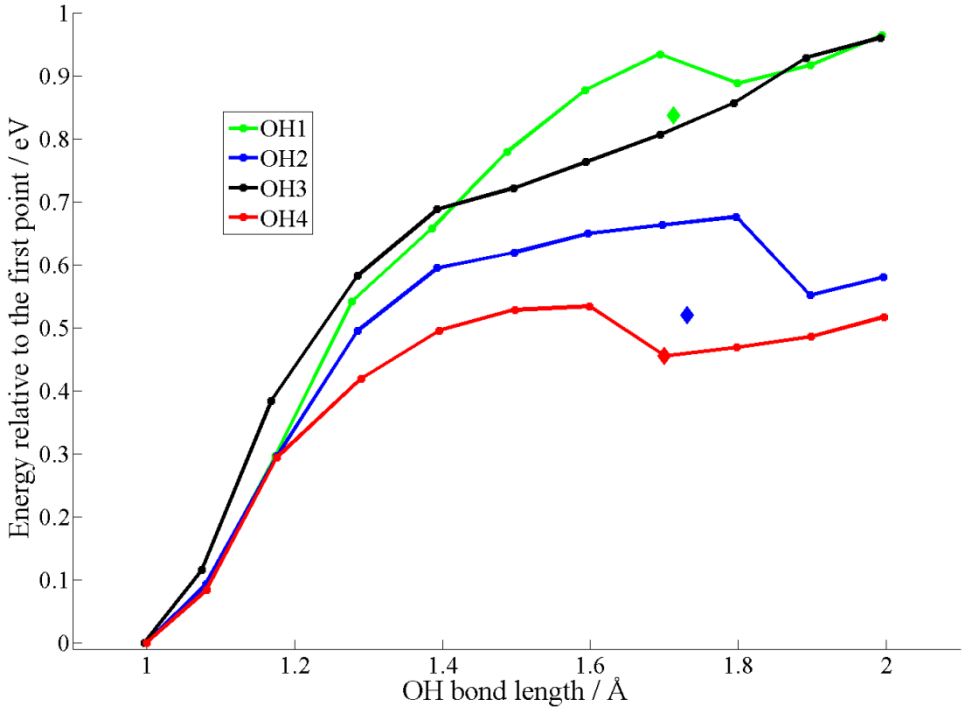

Figure 12: Ground state energy profiles for all four routes for deprotonation from hydroxyl groups in the rhamnose cation. The profiles are computed using CP2K and geometry optimizations constrained by imposing harmonic restraints on the OH bond length of the original hydroxyl groups. The calculated points are shown as dots, and the lines represent linear interpolations between these points. The diamonds represent geometries optimized without constraints starting from the lowest point in the local minimum beyond 1.7 Å for each curve.

Cation deprotonation at OH_1

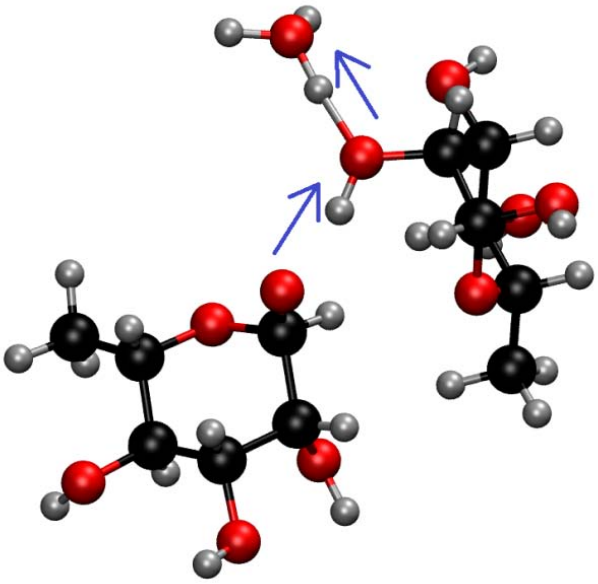

Figure 13: Unconstrained optimized structure for the OH_1 deprotonation process at an OH_1 bond length of 1.7 Å. Two proton transfers have taken place, indicated by arrows.

For the OH_1 deprotonation process, the proton is pushed towards the oxygen of the OH_2 group on a neighboring rhamnose molecule, see ***Figure 13***. Once the proton is approaching the oxygen atom, the proton originally bonded to the oxygen of this hydroxyl group starts moving towards the oxygen of the next water molecule in the hydrogen bond chain. And as this proton attaches to the oxygen in the water molecule, there is a concomitant drop in the potential energy of the molecule (see ***Figure 12***).

When the constraint on the OH-bond is removed, the geometry converges to that shown in ***Figure 13***. As illustrated in the figure, the process consists of a two-proton transfer; only the first proton transfer was imposed by constraints in the geometry optimizations. The energy barrier for this two-proton transfer reaction was calculated to be 0.93 eV. Upon re-optimization from the local minimum structure without constraints, a structure was found with an energy 0.84 eV higher than the starting point for the deprotonation reaction, as can be seen from ***Figure 12***.

Cation deprotonation at OH_2

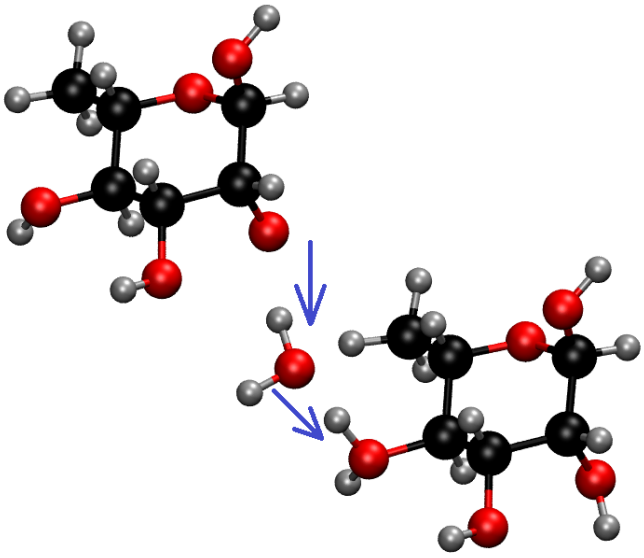

Figure 14: Unconstrained optimized structure for the OH_2 deprotonation process at an OH_2 bond length of 1.7 Å. Two proton transfers have taken place, indicated by arrows.

For the OH_2 deprotonation reaction, the proton is pushed towards the oxygen atom of the water molecule to which it is hydrogen bonded. As the proton approaches the oxygen atom, one of the protons in the water molecule starts moving towards the oxygen atom of the OH_4 hydroxyl group of the next rhamnose molecule in the hydrogen bond chain, see ***Figure 14***. And as this proton attaches to the oxygen of the hydroxyl group, there is a concomitant drop in the potential energy of the molecule (see ***Figure 12***).

As the constraint on the OH-bond is removed, the geometry converges to that shown in ***Figure 14***. The figure shows that the process consists of a two-proton transfer, while only the first proton transfer was imposed by constraints in the geometry optimizations. The energy barrier for this reaction is 0.68 eV and the re-optimized local minimum structure is 0.52 eV higher than the starting point for the deprotonation reaction, see ***Figure 12***.

Cation deprotonation at OH_3

For the OH_3 deprotonation reaction, the proton is hydrogen bonded to the ring oxygen of the adjacent rhamnose molecule in the crystal. The ring oxygen does not have a proton to eject further. As the proton is moved towards the ring oxygen, there is a monotonic raise in energy. The bond between the ring oxygen and C_1 of the receiving molecule breaks and the proton[12] of the OH_1 hydroxyl group of this molecule starts moving towards its hydrogen bonded neighbor. A schematic view of this reaction is shown in ***Figure 15***.

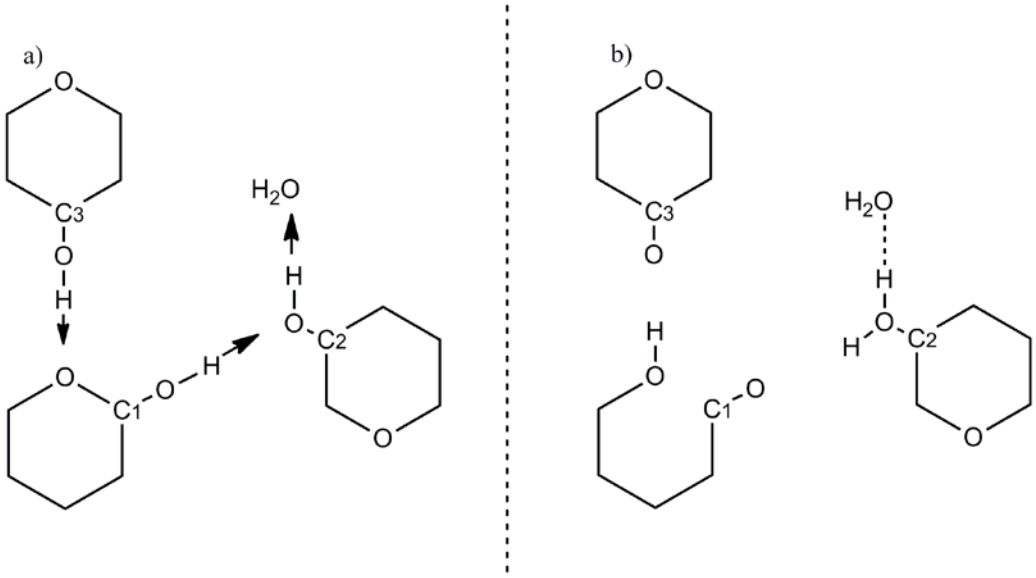

Figure 15: Schematic view of the OH_3 deprotonation reaction. a) The starting point (before deprotonation). The arrows indicate the proton transfer directions. b) The molecular structures after constrained geometry optimization. The configuration shown is not stable, and the reaction is reversed when the constraints on the optimization are removed. See also ***Figure 16***.

An attempt was made to see if the completion of this proton transfer might cause a reduction in the potential energy also for this deprotonation reaction by applying constraints both on the OH bond distance and by forcing the ring open by constraint. But while this led to a stable structure in the presence of the constraints (shown in ***Figure 16***), the reaction was reversed when the constraints were removed. The calculations therefore do not indicate any possibility for deprotonation of the cation from the OH_3 group.

[12] It is difficult to see from the charge analysis whether it is a proton that moves or a hydrogen atom.

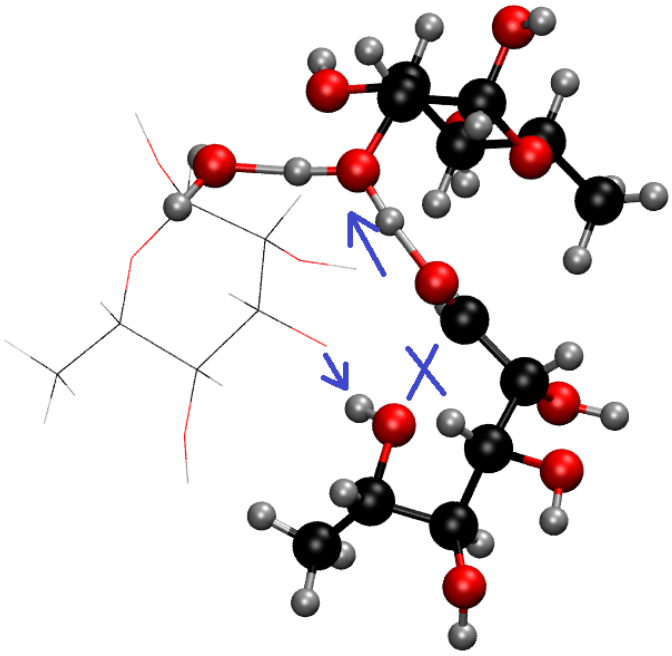

Figure 16: The unstable structure for the OH_3 deprotonation process, as schematically depicted in ***Figure 15b***. The original proton-donating molecule is shown by sticks only.

Cation deprotonation at OH_4

For the OH_4 deprotonation reaction, the proton is pushed towards the oxygen of the adjacent water molecule. As the proton approaches this water, one of the water protons starts moving towards the oxygen atom of the OH_4 group of the next rhamnose molecule in the hydrogen bond chain, see ***Figure 17***.

As can be seen from ***Figure 12***, the energy exhibits a local minimum at about 1.7 Å. This corresponds to a conformation where the original rhamnose proton has moved on to the water molecule, and one of the water protons has been transferred from the water molecule to the neighboring rhamnose molecule. Also in this case only the first of these proton transfers was constrained in the calculation.

Re-optimization from this geometry without constraints resulted in no noticeable change in geometry. This implies that the two proton transfer starting from the OH_4 group of the cation leads to a stable conformation. The unconstrained optimization was attempted first by using the wave functions from the constrained optimizations as the initial guess (as was done for all the other reactions). When this did not result in any significant change in the geometry, new wave functions produced by the computer program were used in a second attempt; this did not result in a changed geometry either. The stable structure is depicted in ***Figure 17***.

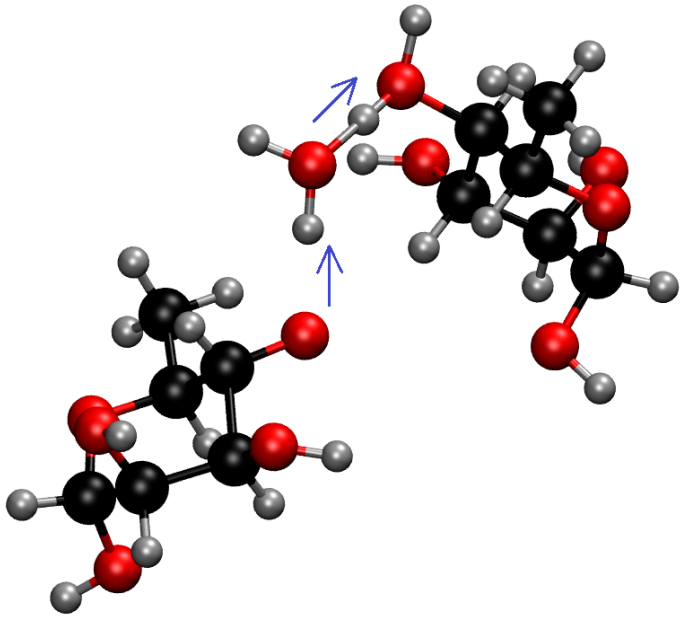

Figure 17: Re-optimized structure following the deprotonation from OH_4 of the rhamnose cation. Two proton transfers have taken place as indicated by arrows.

The energy of this stable structure is 0.46 eV above the energy of the starting point for the reaction, and to reach this structure, there is a barrier of 0.53 eV. Pauwels and co-workers (Pauwels *et al.* 2008) have performed similar calculations, using a different computer program (CPMD). In that work, the stable geometry did not occur after only two proton transfers, but rather after three transfers. Therefore, in the present work attempts were made to "push" the next proton in the chain towards its hydrogen bonding partner (this time on a water molecule) by adding a new constraint. However this did not lead to a stable structure once the constraints were removed.

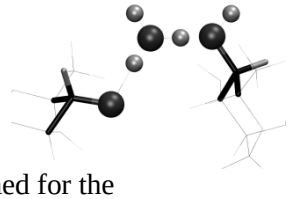

Table 2: Calculated hyperfine coupling tensors for the isolated OH_4-deprotonated rhamnose cation structures (22 atoms). Hyperfine coupling tensor calculations were performed for the optimized structures obtained in the periodic calculations (a) and in the ONIOM-cluster approach (b). For comparison, corresponding results from a previous computational study of the same deprotonation process (c) (Pauwels *et al.* 2008) and the experimental values found by Pauwels *et al.* to be relevant for comparison (d) (Samskog and Lund 1980) are given.

a: Results from periodically optimized geometry in the present study

			Eigenvectors		
Atom	A_{iso}	A_{aniso}	a*	b	c
H_2	34.30	-2.48	0.7388	-0.4884	-0.4643
		-0.34	0.3408	-0.3236	0.8827
		2.82	0.5813	0.8104	0.0727
H_3	-4.43	-9.75	-0.2187	0.1811	0.9588
		-0.73	0.9093	0.3943	0.1330
		10.49	-0.3540	0.9010	-0.2509
H_4	73.16	-5.96	0.3792	0.8336	-0.4017
		-3.67	-0.1960	0.4967	0.8455
		9.63	0.9043	-0.2419	0.3517
HO_3	-3.10	-5.30	-0.5563	0.8194	0.1379
		0.75	0.8027	0.4870	0.3442
		4.54	-0.2149	-0.3022	0.9287

b: Results from cluster-optimized geometry in the present study

			Eigenvectors		
Atom	A_{iso}	A_{iso}	a*	b	c
H_2	39.00	-2.82	0.6964	-0.5420	-0.4703
		-0.29	0.4141	-0.2317	0.8802
		3.10	0.5861	0.8078	-0.0632
H_3	-8.62	-10.78	-0.1290	0.2866	0.9493
		-1.44	0.9074	0.4202	-0.0035
		12.22	-0.3999	0.8610	-0.3142
H_4	62.20	-5.39	0.3874	0.8025	-0.4537
		-3.86	-0.1653	0.5446	0.8222
		9.24	0.9070	-0.2435	0.3437
HO_3	-0.57	-5.43	-0.4940	0.8523	0.1721
		0.20	0.8678	0.4710	0.1585
		5.24	-0.0540	-0.2276	0.9723

c: Theoretical results of Pauwels et al (RO4 radical)

			Eigenvectors		
	A_{iso}	A_{aniso}	a*	b	c
H_2	50.4	-3.5	0.692	-0.528	-0.492
		-0.3	0.579	-0.001	0.851
		3.8	-0.431	0.849	-0.305
H_3	-1.7	-10.3	-0.160	0.150	0.976
		-0.3	0.943	0.316	0.106
		10.6	-0.293	0.937	-0.192
H_4	87.1	-5.9	0.443	0.881	0.163
		-4.6	-0.209	-0.075	0.975
		10.5	0.872	-0.466	0.151
HO_3	-4.0	-6.6	-0.460	0.865	0.202
		0.9	0.881	0.474	-0.024
		5.7	0.116	-0.167	0.979

d: Experimental results from Samskog and Lund

	A_{iso}
H_2	39
H_3	
H_4	112
HO_3	

Hyperfine coupling tensors were calculated for the freely optimized deprotonated radical structure (isolated radical with no environment present) by a SP calculation in G03. ***Table 2*** holds a summary of the results and the relevant experimental data and theoretical results found in the literature. A comparison of the calculated hyperfine couplings with the experimental results indicates that the description of the OH_4 deprotonation process in the present work provides a realistic description of the experimentally observed radicals.

Summary

Figure 12 implies that deprotonation reactions from the hydroxyl groups OH_1, OH_2 and OH_4 of the rhamnose cation may lead to stable conformations, whereas only the deprotonation from OH_4 has been observed experimentally (Samskog and Lund 1980; Budzinski and Box 1985). The OH_4-deprotonated structure yields calculated EPR parameters in fair agreement with the experimental data of Samskog and Lund as well as the previous calculational data by Pauwels and co-workers.

The energy barriers associated with the deprotonation reactions are fairly high (0.53 – 0.93 eV). For this reason, the reactions are not expected to occur at the very low temperatures at which deprotonation from OH_4 experimentally observed (as low as 4 K). On the other hand, energetically the calculations show a clear preference for the OH_4 reaction as compared to the other two. ***Table 3*** shows the calculated relative abundances of the different products at the temperatures used in the experiments and at room temperature. According to these data, the experimental observation of only the OH_4 deprotonation product easily can be understood.

Table 3: Expected relative abundances of the radicals resulting from the different deprotonation reactions based on relative energies at the freely optimized points for the deprotonated structures.

Temperature /K	**4**	**77**	**300**
OH_4/OH_1	-	10^{25}	10^{7}
OH_4/OH_2	10^{82}	10^{04}	10^{1}

5.1.2 Cluster and single molecule calculations using G03

Due to the large size of the supercell in the periodic calculations, and also to the problems with computing excited states in CP2K, several attempts have been made to reproduce the results from the CP2K ground state calculations using Gaussian03 single molecule- and cluster calculations.

Single molecule calculations

The SM calculations were all performed on the B3LYP/6-31++G** LOT. The calculations were performed with and without geometry optimizations. The bond elongations were performed with step lengths of 0.1 Å. None of these calculations led to any reliable results: Geometry optimization of just a single rhamnose cation radical led to ring opening by a rupture of the C_4-C_5 bond.

Performing constrained geometry optimizations for the four OH bond elongations from the ring-opened structure resulted in just uphill energy profiles for OH_1 and OH_4. For OH_2 and OH_3 the proton jumped sideways to the oxygen of the adjacent hydroxyl group (the OH_2 and OH_3 groups are adjacent), see ***Figure 18***. In an attempt to circumvent this problem the $C_3C_2O_{C2}H_{OC2}$ dihedral angle was frozen for the OH_2 case and the analogue (opposite) was done for the OH_3 case. This simply resulted in a complete destruction of the ring structure with the release of a water molecule, see ***Figure 19***.

After these attempts, energy profiles with bond elongations from the molecular geometry in the experimentally observed crystal structure, with imposed spin and charge (cation radical), were performed. All these calculations resulted in uphill energy profiles. The charge analysis indicated that it is actually a hydrogen atom that is transferred, not a proton.

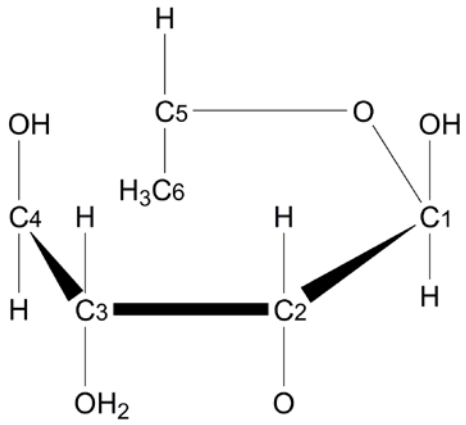

Figure 18: Result of bond elongation with constraint placed only on the OH_2 bond distance for a rhamnose cation radical.

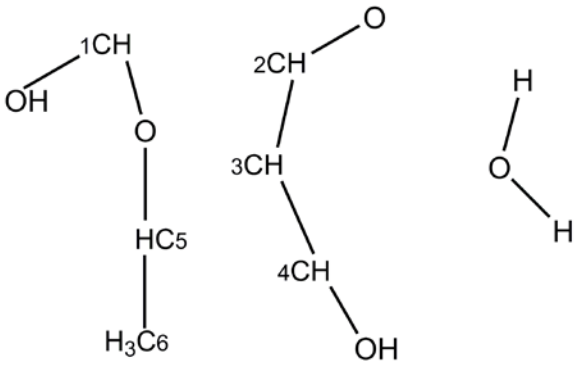

Figure 19: Result of bond elongation with constraint on the OH_2 bond distance and the $C_3C_2O_{C2}H_{OC2}$ dihedral angle for a rhamnose cation radical.

It is not considered surprising that the single molecule calculations do not reproduce the results from the periodic calculations since no proton acceptors are present. Also, the

considerable movements of the molecule during the SM geometry optimizations indicate that the surroundings ought to be included for stability purposes. It was decided to investigate whether it was possible to reproduce the results from CP2K using a cluster model. This calculation was made for the most interesting deprotonation reaction, OH_4, only.

Cluster calculation

In deciding on the size and shape of the cluster, two main issues were considered. The cluster should include all three molecules directly involved in the deprotonation reaction; these molecules will be referred to as the central molecules. In the case of the OH_4 deprotonation from the cation radical, this meant rhamnose-water-rhamnose as in see ***Figure 17***. The three molecules alone add up to 49 atoms. It was also desirable to include all molecules that are hydrogen bonded to the central molecules in the crystal structure. The cluster size then became 294 atoms.

This cluster is shown in ***Figure 20*** with the central atoms highlighted. The size of this cluster is so large that it was decided to treat all molecules not directly involved in the deprotonation reaction at the PM3 level, whereas the central molecules were treated at the B3LYP/6-311G** LOT using ONIOM. The geometry optimization was started from the last point in the CP2K scan (after two proton transfers, with an OH bond length of 2 Å). All the molecules in the outer PM3 layer were held fixed, while the three inner molecules were allowed to relax freely. This resulted in the geometry shown in ***Figure 20***.

As a result of the ONIOM geometry optimization, the protons moved slightly back towards their original crystal positions, and the structure stabilized with three protons on the water oxygen. The original OH bond distance is reduced from 2.0 Å to 1.5 Å. From this geometry a relaxed scan of the PES was then performed by imposing a constraint on the OH bond distance of the original fourth hydroxyl group. This bond length was reduced in steps of 0.1 Å in six steps. The resulting energy profile is shown in ***Figure 22***.

Also these calculations show an energy barrier for the deprotonation reaction. However, in this case the energy barrier is 0.02 eV, which is negligible in comparison to the barriers resulting from the CP2K calculations. A closer inspection of the structure before and after the initial ONIOM geometry optimization reveals that there is a considerable amount of movement also of heavier atoms, see ***Figure 21***. This is most likely due to the fact that the hydrogen bonds between the three central molecules and the environment are not well represented at the PM3 level, making the calculation behave more like a gas phase calculation

rather than that of a solid state structure. ***Figure 21*** also shows that the "bridge" on which the positive charge moves, is "flattened out". This might be, at least part of, the reason why the energy barrier is lower in the cluster calculations.

Hyperfine coupling tensors were calculated for the deprotonated neutral radical (isolated, without any environment included, 22 atoms) at the B3LYP/6-311++G** LOT for the geometry optimized without constraints in the cluster. These results are given in ***Table 2***. It appears from the data in ***Table 2*** that; these results do not agree well with neither the relevant experimental data and theoretical results found in literature, nor with the results obtained from calculations using the periodic optimization (section 5.1.1).

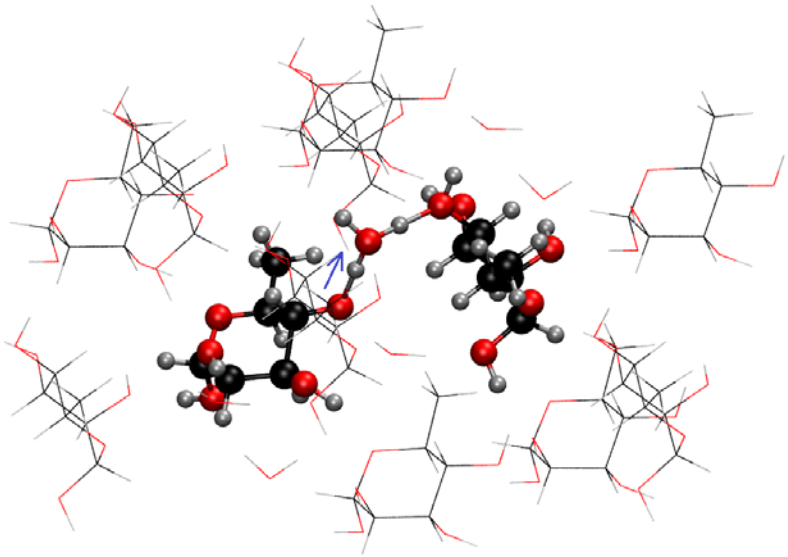

Figure 20: The molecular cluster used to describe the OH_4 deprotonation reaction using G03 for the (ONIOM) optimization and PES scan. The structure shown is the G03 optimized structure where only one proton transfer has taken place, indicated by an arrow. The molecules treated at the PM3 level are shown as sticks; these are held fixed during the geometry optimizations.

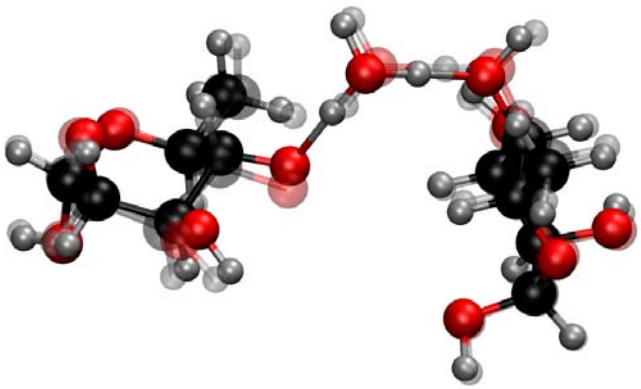

Figure 21: Changes in geometry as a result of the geometry optimization using G03 for the three central molecules. The surrounding PM3 layer is not shown in this figure as it is kept fixed in space. The starting point of the optimization, being the last point of the CP2K scan, is shown as a ghost.

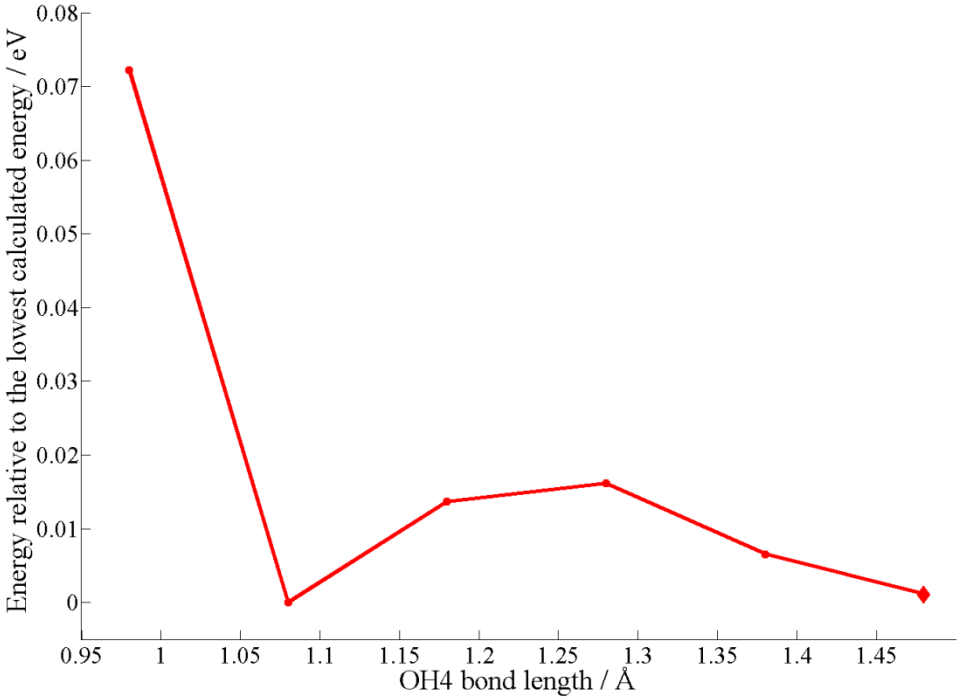

Figure 22: Ground state energy profile for the deprotonation from the OH_4 group of the rhamnose cation. Energies are calculated using the cluster shown in Figure 20 with G03 and ONIOM in a two-layered cluster. The calculated points are shown as dots, and the line represents linear interpolations between these points. The diamond (the last point) represents the geometry optimized without constraint, starting from the last point in the corresponding calculation performed in the periodic code.

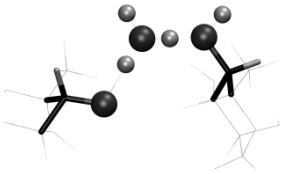

5.2 Excited states

5.2.1 Test calculations on small molecules

TDDFT calculations on H_2O, CH_3 and CO^+ were performed with the purpose of examining how the choices of basis set and functional affect the results. All calculations presented in this chapter used Gaussian03. For all three molecules a geometry optimization was first performed using B3LYP/6-311G**, and subsequently TDDFT calculations were performed as SP calculations at these optimized geometries. For H_2O, a geometry optimization was also performed using PBE/6-311++G** with the intention of checking the effect of slightly differing geometries for the TDDFT calculations. The resulting geometries are shown in ***Table 4***.

Table 4: Optimized geometries using the G-311G** basis set in G03, the functional used is given in parentheses.

Molecule	Bond distance / Å	Bond angle / degrees	Dihedral angle / degrees
H_2O (B3LYP)	0.96176	103.82084	-
H_2O (PBE)	0.96996	104.19528	-
CH_3 (B3LYP)	1.08063	120.01110	0.00078
CO^+ (B3LYP)	1.11047	-	-

The functionals and basis sets used for the TDDFT calculations were B3LYP, BLYP, PBE and PBE0 and 6-311G, 6-311G**, 6-311++G, 6-311++G** and 6-31++G**, respectively. The results of the calculations presented in this section are compared to the results reported by Hirata and Head-Gordon (Hirata and Head-Gordon 1999) where both experimental and calculated results are given.

H_2O

For H_2O the first five singlet excited states were calculated, in two different series. The first series used B3LYP and all different basis sets, and for the second series, all functionals were used together with the 6-311++G** and 6-31++G** basis sets. Both series were made using the B3LYP/6-311G** geometry. In addition a SP PBE/6-311++G** calculation of the excited states using the PBE/6-311G** optimized geometry was made for comparison. All results are tabulated ***Table 16***, ***Table 17*** and ***Table 18*** in Appendix D.

It appears that one of the excited states of the H_2O molecule has zero oscillator strength. This state is marked with grey shading in ***Table 5*** and ***Table 6***. ***Table 5*** shows a summary of the results where a comparison of the different basis sets using B3LYP is made. The second and third excited states are very close in energy, and their ordering changes when going from the simplest basis set 6-311G to any of the other (larger) sets. The presence of diffuse functions in the basis sets also lead to changes in the fifth excited state. In general, the excitation energies are lowered by 0.5-1 eV when diffuse functions are added to the basis sets. Adding polarization functions to the basis set leads to a relatively smaller increase in the excitation energies. Reducing the basis from triple- to double-ζ valence does not affect the excitation energies by more than 0.1 eV.

Table 5: Excitation energies (in eV) for the first five singlet excited states of H_2O. B3LYP and different basis sets were used in SP calculations on the B3LYP/6-311G** optimized geometry. The numbers marked in grey correspond to states with zero oscillator strength. The calculations were performed using G03.

6-311G	6-311G**	6-311++G	6-311++G**	6-31++G**
7.10	7.35	6.69	6.88	6.83
9.13	9.24	8.34	8.42	8.36
9.13	9.68	8.61	9.06	9.02
11.28	11.61	10.24	10.58	10.54
13.66	13.59	10.95	11.08	11.17

A comparison of the excitation energies calculated on the two different geometries (PBE/6-311G** and B3LYP/6-311G**) results in the same excited states with more or less identical excitation energies. These results are included in ***Table 6*** and are also presented in more detail in Appendix D.

Table 6 shows the changes in excitation energies with functionals, and also how these energies compare to excitation energies presented by Hirata and Head-Gordon (Hirata and Head-Gordon 1999). In comparison to the experimental values, it appears that PBE0 performs better than the other functionals. It is also apparent from the table that the TDDFT results deviate from the experimental values by roughly 1 eV.

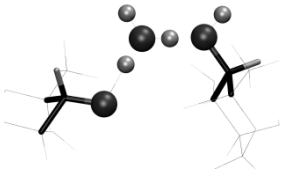

Table 6: Excitation energies (in eV) for the first five singlet excited states of H_2O. Results from using different functionals are compared to reported values (including experimental values). The numbers marked in grey correspond to states with zero oscillator strength.

PBE [c]	BLYP [a]	B3LYP [a]	PBE [a]	PBE0 [a]	BLYP [b]	B3LYP [b]	EXP [b]
6.36	6.25	6.88	6.40	7.14	6.18	6.83	7.4
7.82	7.66	8.42	7.85	8.70	7.26	8.18	9.1
8.52	8.39	9.06	8.56	9.36	8.04	8.84	9.7
9.95	9.79	10.58	10.00	10.90	7.67	8.69	10.0
10.59	10.48	11.08	10.65	11.34	8.31	9.08	10.17

[a] Basis set used was 6-311++G**, and the geometry was found using B3LYP/6-311G**. The calculations were performed using G03.
[b] Results from (Hirata and Head-Gordon 1999), where the basis set 6-311(2+,2+)G** was used for the calculated values.
[c] Basis set used was 6-311++G**, and the geometry was found using PBE/6-311G**. The calculations were performed using G03.

CH_3

For CH_3, TDDFT calculations of the first ten excited states were performed. The large numbers of excited states were calculated since many of the first excited states had zero oscillator strengths, and were therefore assumed not to be comparable with experimental observations. What will later be referred to as the first two excited states for CH_3 are actually the first two states with oscillator strength different from zero. For the B3LYP functional, all basis sets were used, and a summary of the results are presented in ***Table 7***. Then, calculations were performed using all functionals with the two basis sets 6-311++G** and 6-31++G**; a summary of these results is given in ***Table 8***. More extensive results, including those states that have zero oscillator strengths, can be found in ***Table 19*** and ***Table 20*** in Appendix D.

The choice of basis set severely affected the results for CH_3, both with respect to the values of the excitation energies and oscillator strengths and which states appeared, as can be seen from ***Table 7***. The presence of polarization functions changed the results marginally, the difference in energy being of the order of 0.1 eV. Diffuse functions, on the other hand, changed the results considerably. The energies of the states were lowered with as much as 1 eV when the diffuse functions were present; and the numbering of the excited states changed because new states (involving the diffuse functions) appeared. The oscillator strengths were also affected by the presence of the diffuse functions. Comparing basis sets with double- and triple- ζ valence, the change in energy for the excited states is of the order of 0.1 eV.

Table 7: Excitation energies (in eV) of the first two excited states of CH_3 with oscillator strengths different from zero. B3LYP and different basis sets were used in SP calculations on the B3LYP/6-311G** geometry. The calculations were performed using G03.

6-311G	**6-311++G**	**6-311G****	**6-311++G****	**6-31++G****
6.34	5.26	6.37	5.25	5.19
11.07	8.76	10.98	8.73	9.00

For CH_3 it is not clear which functional performs better relative to experimental values. ***Table 8*** shows that PBE0 gives the better result for the first excited state, but is farthest off for the second state. Since all the functionals overestimate the energy for the second excited state, this may be due to the fact that what is labeled as the second state in ***Table 7*** and ***Table 8*** is not the second calculated state, but in fact the ninth excited state. It is possible that there is a lower lying excited state that should have been picked instead, but was ignored because of its small oscillator strength. This suspicion is backed by the differences in the calculated energies in this work and in the work of Hirata and Head-Gordon.

Table 8: Excitation energies (in eV) of the first two excited states of the CH_3 radical. Results from using different functionals are compared to reported values (including experimental values).

BLYP [a]	**B3LYP [a]**	**PBE [a]**	**PBE0 [a]**	**BLYP [b]**	**B3LYP [b]**	**EXP [b]**
4.79	5.25	5.00	5.54	4.66	5.16	5.73
8.23	8.73	8.43	8.98	5.53	6.17	7.44

[a] Basis set used was 6-311++G**, the two states are the first and the ninth excited states. These are the first two states with oscillator strengths different from zero. The geometry was found using B3LYP/6-311G**. The calculations were performed using G03.

[b] Results from (Hirata and Head-Gordon 1999) , where the basis set 6-311(2+,2+)G** is used for the calculated values.

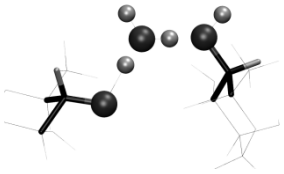

CO^+

The first five excited states of CO^+ were calculated using TDDFT. The first two states turned out to be nearly degenerate and are regarded as one state; and what is really the third excited state is referred to as the second state. This re-numbering of states simplifies the comparison of the results with those of Hirata and Head-Gordon, who do not speak of degenerate states. For the B3LYP functional, all basis sets were used, and a summary of the results are presented in ***Table 9***. Then calculations were performed using all functionals with the two basis sets 6-311++G** and 6-31++G**. A summary of these is to be found in ***Table 10***. More extensive results are given in ***Table 21*** and ***Table 22*** in Appendix D.

For this molecule, the presence of polarization functions in the basis sets had a larger effect on the energies than did the diffuse functions, see ***Table 9*** for details. The polarization functions lowered the excitation energies by some tenths of an eV, and also lowered the oscillator strengths for the first excited state. The list of the excited states still contained the same states in the same order when diffuse functions were added to the basis set, and the energies changed by less than 0.1 eV. The oscillator strengths remained the same with and without diffuse functions. In the case of CO^+, the difference between double- and triple-ζ valence was smaller than for CH_3.

Table 9: Excitation energies (in eV) of the first two excited states of the CO^+ cation radical. B3LYP and different basis sets were used in SP calculations on the B3LYP/6-311G** geometry. The first excited state is actually the first and the second which are nearly degenerate. The calculations were performed using G03.

6-311G	**6-311++G**	**6-311G****	**6-311++G****	**6-31++G****
3.69	3.68	3.38	3.38	3.35
5.52	5.53	5.62	5.64	5.56

When it comes to the performance of the different functionals, it seems that B3LYP is the best choice in the case of CO^+. ***Table 10*** shows that all the functionals overestimated the excitation energy of the first excited state, but B3LYP was closer to the experimental values than PBE and PBE0, and is also quite close for the second excited state. Also in the case of CO^+ it appears that the theoretical calculations of the excitation energies can be off with about 1 eV.

Table 10: Excitation energies (in eV) of the two first excited states of the CO^+ cation radical. Results from using different functionals are compared to reported values (including experimental values).

BLYP [a]	B3LYP [a]	PBE [a]	PBE0 [a]	BLYP [b]	B3LYP [b]	EXP [b]
3.14	3.38	3.43	3.81	3.50	3.76	2.26
5.08	5.63	5.38	6.02	5.11	5.79	5.82

[a] Basis set used was 6-311++G**. The first excited states are the two first calculated states as they are nearly degenerate, the second state is really the third calculated excited state. The geometry was found using B3LYP/6-311G**. The calculations were performed using G03.

[b] Results from (Hirata and Head-Gordon 1999) , where the basis set 6-311(2+,2+)G** was used.

Summary

All in all it is apparent that the results from the TDDFT calculations can miss the experimental values by up to about 1 eV. This difference is much larger than the variations that appear from changing the basis set and functionals. It is thus difficult to pick one functional that should perform better than the others based on these results. When it comes to basis sets, it is apparent that both diffuse and polarization functions are important in describing the excited states. Reducing from triple- to double-ζ results in energy changes of about 0.1 eV, which is a small change compared to the differences between experimental and calculated values for the excitation energies.

5.2.2 TDDFT on rhamnose

Because of difficulties using TDDFT in CP2K, all the excited state calculations were performed in G03. The excited state calculations were all performed as SP calculations on geometries optimized for the ground states. The goal was to see how the excited states behaved throughout the different deprotonation reactions. Geometries from all four CP2K scans and also from the cluster scan in G03 were used in the calculations. Only the three reactions that led to stable structures (OH_1, OH_2 and OH_4) were examined by TDDFT.

TDDFT calculations are quite time demanding, therefore it was necessary to choose just a few molecules to be included in the calculations. The systems that will be referred to as single chains contain the three molecules directly involved in the deprotonation process (49 atoms) and there is one such model for each reaction see ***Figure 23***. The system that will be

referred to as the star shaped model combines the three single chains (101 atoms), see ***Figure 24***.

All the excited state calculations on rhamnose have been performed using the basis set 6-31++G**. At this point, analysis to link the different excited states of the different geometries together has only been performed for the OH_4 deprotonation reaction on the CP2K geometries using the B3LYP basis set. This is due to the problems mentioned in section 4.2 making the analysis time consuming. Plots of the energies of the excited states *versus* bond length for all sets of calculations are shown in Appendix D, but the states corresponding do different geometries are not linked in those plots.

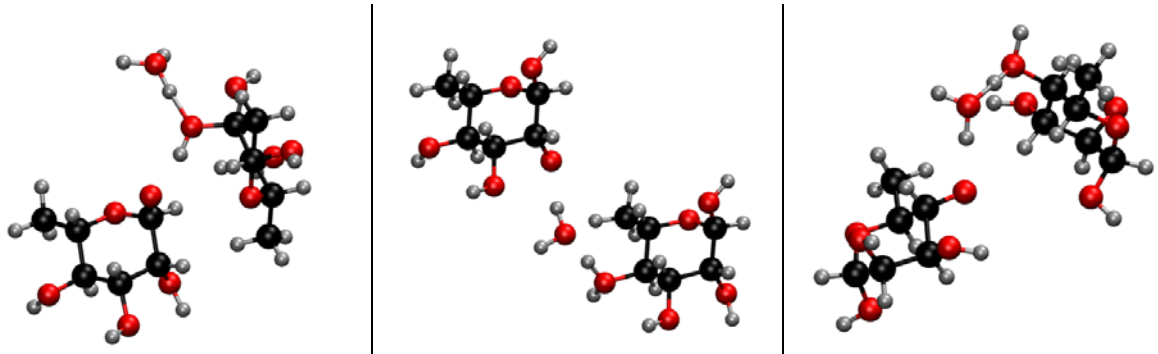

Figure 23: Single chain models for a) OH_1 reaction b) OH_2 reaction and c) OH_4 reaction. All models comprise of two rhamnose molecules and a water molecule (49 atoms).

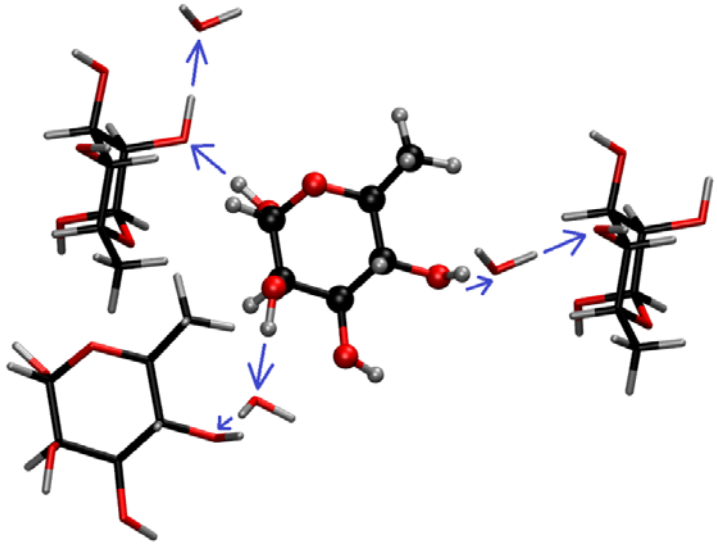

Figure 24: Star shaped model. This model consists of four rhamnose molecules and three water molecules (101 atoms). These are all the molecules directly involved in the three deprotonation reactions (OH_1, OH_2 and OH_4).

All the observed excited states for all the systems presented in this chapter and in Appendix D are states in which an electron is excited from a β-orbital into the first virtual β-orbital, the β-LUMO. For all the excited state plots presented here and in the appendix, examination of the oscillator strengths have been performed in order to see whether one or more states stand out as a possible mediator for the proton transfer process. No state was found in which the oscillator strength was small for the un-deprotonated structure and large for the deprotonated structure without the deprotonation also including a drastic increase in the energy of the excited state.

Charge and spin analyses have not been performed for the excited states, but for the OH_4 deprotonation an attempt was made to study the orbitals involved in the excitations in order to describe how the spin and charge localization changes both upon excitation and through the deprotonation reaction. This analysis revealed that the molecular orbitals is a very unreliable tool for this type of investigation. From one step in the deprotonation reaction to the next, the involved orbitals had often changed severely, including into linear combinations of each other. This is most likely due to the fact that the orbitals used in DFT calculations are not real molecular orbitals but KS orbitals that are mainly mathematical aids in the calculations.

Single chain models

OH_4

For the OH_4 deprotonation, excited states were calculated on two different sets of geometries. The first set consisted of eleven geometries from the deprotonation reaction calculated in CP2K. The second set consisted of six geometries from the deprotonation reaction calculated in the G03 cluster. For the CP2K geometries, three different functionals (PBE, BLYP and B3LYP) were used, and the results were compared. For the BLYP and PBE functionals, convergence was not reached for the first five steps in the deprotonation reaction. As a consequence, B3LYP was chosen as the functional to be used for the rest of the calculations, since this converged in all steps except for one (the first). For the G03 geometries only B3LYP was used.

Figure 25 and ***Figure 26*** show plots of how the first nine excited states behave through the deprotonation reaction for the CP2K geometries in the case of the B3LYP functional. What is different in the two figures is that ***Figure 25*** shows the ground state energy calculated in G03 at the same time as the excited states were calculated, while in ***Figure 26*** the ground state

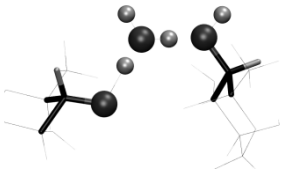

energy from CP2K is used as the base. The reason for this use of two plots is that the ground state energy calculated in G03 is guaranteed to be unphysical because none of the interactions with the environment are taken into account. The first point on the curves is missing, because the excited states did not converge in this point.

In the plots, one excited state stands out in its resemblance to the ground state, whereas all the other excited states remove themselves from the ground state through the deprotonation reaction (the excitation energies increase). Even the first excited state has an energy barrier for the deprotonation that is higher than that of the ground state energy. This implies that none of these excited states aid the proton transfer processes.

For the TDDFT calculations on the CP2K geometries all three functionals (BLYP, B3LYP and PBE) indicated the presence of a first excited state that was similar to the ground state, and that all the other states increased in excitation energy through the deprotonation reaction. The plots indicating this are given in Appendix D (***Figure 34***, ***Figure 35*** and ***Figure 36***). Still, more analysis (linking the different states together) has to be performed of the results from all three functionals in order to compare the results properly.

Comparing the results from the CP2K geometries with the results of the calculations performed on the G03 geometries is difficult as the ground state energy profiles are very different. But in the last two points of the reaction path from the G03 geometries (1.38 and 1.48 Å) the emergence of a first excited state that is a lot closer to the ground state is visible to the trained and optimistic eye also in these calculations. The plot of the excited states for the G03 geometries is shown in the Appendix D, ***Figure 38***.

<u>OH_1 and OH_2</u>

Distinct differences are apparent when comparing the excited state energies for OH_1 and OH_2 (given in Appendix D for the interested reader) with those of OH_4. For the OH_4 there is a clear two-fold grouping of the states after deprotonation has occurred; the ground state and first excited state, and the all the other states. For OH_1 this was not at all the case; all the states are spread out evenly. For OH_2 a similar pattern as for OH_4 was observed, but with the second excited state in the middle forming its own group. What this grouping of the states means for the chemistry of the system is difficult to say.

Other than what is mentioned above, more analysis is necessary before it is possible to discuss these results any further. The calculations on the OH_1 and OH_2 deprotonation reactions were all performed using B3LYP.

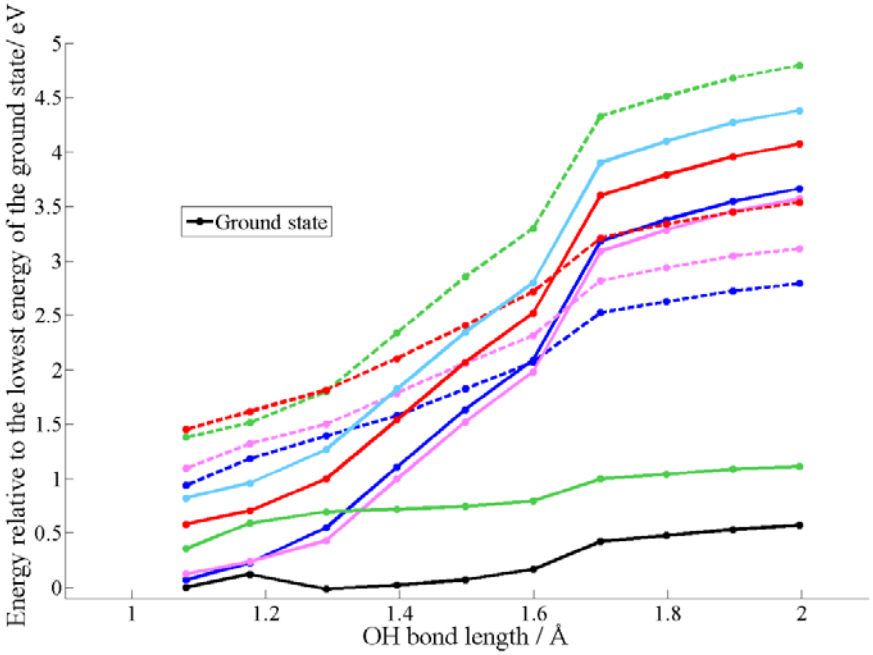

Figure 25: First nine excited states followed through the OH_4 bond elongation. Excited state calculations were performed in G03 on geometries from optimizations in CP2K. The excitation energy is added to the ground state energy from the G03 SP calculations. A table of excitation energies can be found (***Table 23***) in Appendix D. The excitation energies calculated at optimized geometries are shown as dots, and the lines represent linear interpolations between these points.

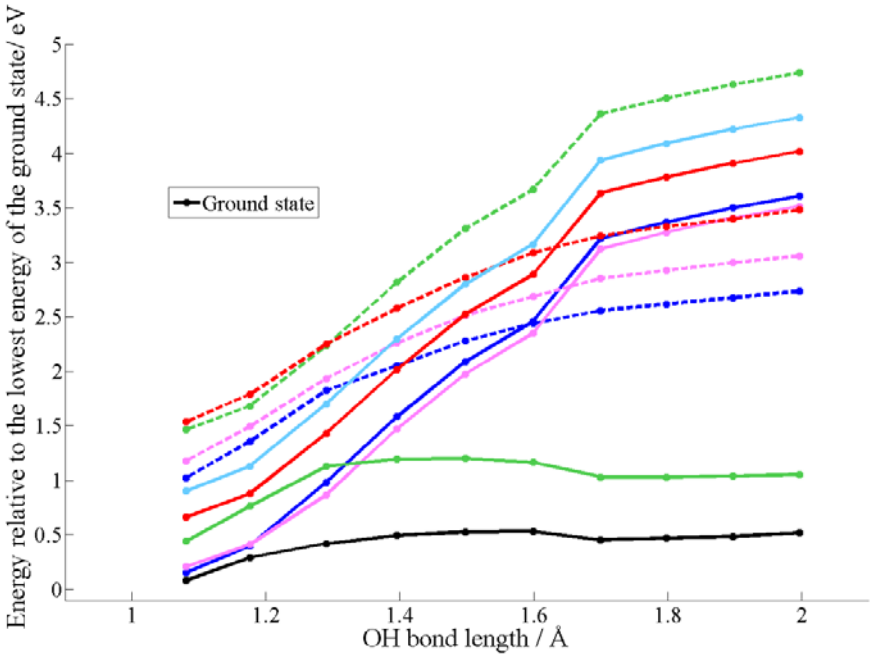

Figure 26: First nine excited states followed through the OH_4 bond elongation. Excited state calculations were performed in G03 on geometries from optimizations in CP2K. The excitation energy is added to the ground state energy from the CP2K calculations. A table of excitation energies can be found (***Table 23***) in Appendix D. The excitation energies calculated at optimized geometries are shown as dots, and the lines represent linear interpolations between these points.

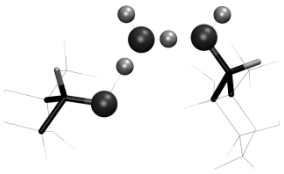

Star shaped model

For the star shaped model, excited state calculations were performed on all three deprotonation reactions using the CP2K geometries. These calculations were all performed with the B3LYP functional. However, a full analysis in which all excited states were completely followed during the bond elongations proved too expensive from a computational point of view, to fit within the time frame of this thesis. As such, preliminary results are presented in a rough form in Appendix D. A strikingly similar pattern can be recognized with respect to the single chain models, only now the excited states are a lot closer to each other and a bit lower in energy. This is as expected since the molecular system is larger. The first excited states that stand out in the OH_4 and OH_2 deprotonation reactions also seem to be present in the star shaped model. A full analysis would be necessary to verify this.

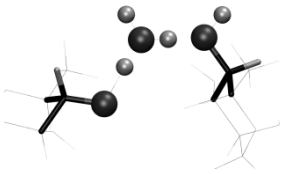

6 Discussion and conclusions

Quantum chemistry is a research field which enables prediction of the electron configurations of molecular systems. Comparison of theoretical calculations and experimental data may support or invalidate the interpretations of the experimental data, with respect to specific physical properties of the molecule. However, due to the complexity of mulitiatom-multielectron systems, such calculations have been hampered with much uncertainty, as all calculational methods are based on various approximations.

The approximations start already at the Born-Oppenheimer approximation, which is the starting point for almost all quantum chemical approaches. The introduction of the Fock operator is the major approximation in all HF based theories and many attempts have been made to improve the accuracy using the HF-framework. DFT inherently should be better suited in this respect, but the unknown XC potential introduces approximations to this method. In addition, there are the approximations associated with the limited basis sets, the limited size of the model systems as well as numerical issues, since the problems cannot be solved analytically.

In spite of the uncertainties involved, quantum chemistry calculations have over the years become an indispensable tool for experimentalist as well as theoreticians. Experimentalists may find additional evidences for accepting or rejecting proposed models, by performing new, specifically designed experiments. Theoreticians have been able to model previously not understood structures and processes and make predictions for experimental verification. Conscious and careful use of these calculational methods has become a cornerstone in modern physical-, chemical- and biological research. For this reason, the scientific community continuously strives for improvements of the theoretical methods. Still, it is essential to remember that only experiment can tell us something indisputable about nature, and experimental data should always be the point of reference.

For the work on rhamnose in this thesis, the only experimental observations with which the results obtained can be compared are the observation of the radical centered on O_4. The calculated hyperfine tensors for the OH_4 deprotonated rhamnose cation may be compared to both theoretical and experimental results for the O_4-centered radical in the literature. The present hyperfine coupling tensor calculations on the periodically optimized geometry are in good agreement with the theoretical results presented by Pauwels and co-workers (Pauwels *et al.* 2008), and comparable (though not quite as close) to the experimental results attained at

77 K (Samskog and Lund 1980). *g*-tensor calculations were, due to time constraints, not made in the present work.

There is a peculiar disagreement between the two sets of experimental data for the O_4 deprotonated rhamnose cation reported in the literature. The results by Budzinski and Box (Budzinski and Box 1985) were obtained at 4 K and deviate significantly from those obtained by Samskog and Lund (Samskog and Lund 1980) at 77 K. Pauwels and co-workers have discussed this situation, and here it is only suggested (in agreement with Pauwels *et al.*) that the Budzinski and Box results describe a radical structure for which the EPR parameters cannot be modeled by a single molecule, as is done in the present work. Consequently, comparisons with experimental data are limited to those presented by Samskog and Lund, for the present work.

The calculations using the cluster-optimized geometry are not in a similarly good agreement with the literature data as those for the periodically optimized structures. Base on these quite preliminary hyperfine coupling tensor data it is concluded that apparently the periodically optimized structure represents a better approximation to the real radical structure as produced and characterized experimentally.

6.1 Size of the model system

It is important to realize that calculations made at different levels of theory may provide different results due to different approximations being involved. It is hence important to compare calculations performed at the same levels of theory, as well as within the same model systems and computer programs.

The SM calculations on the rhamnose cation radical were performed at the B3LYP/6-31++G** LOT using G03. The cluster calculations were performed at the ONIOM(PM3:B3LYP/6-311G**) LOT using G03. Finally, the periodic calculations were performed at the GPW BLYP/TZVP-GTH LOT using CP2K. This variation in both LOT, model system and computer program makes direct comparison of the results difficult.

Within the framework of this thesis, there was no room for repeating any of the calculations at different levels of theory. Thus since the different sets of calculations gave quite different results there is no way of deciding strictly to what extent the LOT is decisive for the results, and to what extent the differences arise from the different model systems and computer programs. Still, with the information at hand, an attempt has been made to decide how the size of the model system affects the results.

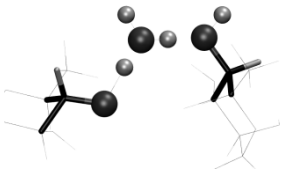

The geometry optimization of the cation radical structure in the SM calculations resulted in large changes in the molecular geometry (including ring-opening). Similar large geometrical changes were not observed in the periodic calculations, but were to some extent in the cluster calculations. In the cluster calculations the interactions with the surroundings were modeled at the PM3 level. The importance of the surrounding molecules is expected due to the extensive hydrogen bonding in the crystal structure.

Also other interactions than the hydrogen bonds in the crystal seem to be important, as ***Figure 21*** in section 5.1.2 shows that not only the hydrogen- and oxygen atoms in the molecules, but also the carbon atoms move significantly when going from a periodic optimization scheme to the cluster scheme. It appears that the PM3 method is not able to model these intermolecular interactions good enough to fully maintain the crystal structure. Although it is not definite whether the periodical calculation yield a more correct structure, these calculations are expected to include the chemical interactions with the surroundings in a better way. It should be noted that in ***Figure 21*** the two geometries displayed correspond to different OH bond lengths. A more relevant comparison might have been to display the CP2K geometry corresponding to a bond length closer to the one achieved with the cluster in G03, but these data are currently not available.

For the TDDFT calculations on rhamnose in this work, two different model systems have been tested, referred to as the single chain models and the star shaped model. In principle, only the star shaped model can be reliably employed for direct comparisons of the three different deprotonation reactions, as only this model is the same for all reaction processes. However, it was found from a preliminary analysis, that the results from the two models are very similar. None of these models include any surroundings other than those molecules directly involved in the proton transfer processes.

Attempts were made to create a model system consisting of the star shaped model (101 atoms) with all hydrogen bonding partners of the central atoms included (but with the neighboring rhamnose molecules reduced to water molecules). The size of this new cluster was 194 atoms, which turned out to be too computer expensive and were for calculations, and was therefore abandoned.

6.2 Ground state energy profiles for proton transfer reactions

When comparing the calculated energy profiles for the bond elongations in the three different model systems (SM, periodical and cluster), it is important to note that they were achieved using different approaches.

In the SM approach two different schemes were employed. First the radical cation structure was optimized starting from the experimental crystal structure. This was done prior to examination of the PES using constrained geometry optimizations with the constraint placed on the OH bond length in question. The bond length was increased in steps of 0.1 Å. In the other scheme the geometry from the experimentally observed crystal structure was used as is, and the PES was examined without performing any geometry optimizations, only constrained bond elongations. Both types of calculations suggest that proton abstraction into empty space (that is, without any proton acceptor available) will not occur easily from any of the oxygen positions in the rhamnose cation as the energy profiles for these reactions were just uphill.

In the periodic approach the radical cation geometry was also optimized from the experimental crystal structure prior to performing constrained geometry optimizations with successively longer bond lengths, to examine the PES. This resulted in energy profiles showing local minima after deprotonation for the OH_1, OH_2 and OH_4 reactions but only an uphill energy profile for OH_3 (***Figure 12***).

In the cluster approach calculations were only performed for the OH_4 deprotonation reaction. No optimization of the cation from the initial crystal structure was performed. Rather, the geometry optimization of the radical cation structure was started from the last point in the CP2K bond elongation process for the OH_4 reaction, where the bond distance was 2 Å. This resulted in a stable structure (within this approach this means hat the proton stabilized after only one proton transfer), and the PES profile was attained from transferring the proton back to its original position using constrained geometry optimizations.

Since wave functions were successively re-used in the proton transfer reaction calculations, the starting point of the optimizations might affect the results. This is because the spin and charge is more easily localized by the programs when the proton is removed from its original position, resulting in wave functions that are of a different nature in the two first approaches as compared to the cluster approach.

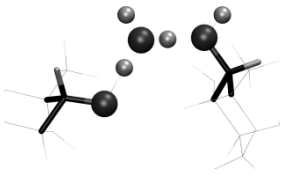

The cluster and periodic calculations resulted in PES profiles where the deprotonation reaction for OH_4 has a local minimum after deprotonation, after crossing an energy barrier. In the case of the cluster calculations, the stable structure occurs after only one proton transfer, whereas in the periodic calculations the stable structure corresponds to two proton transfers. There is also a very large difference in the heights of the energy barriers resulting from the two approaches. The energy barrier from the cluster calculations is 0.02 eV whereas the energy barrier from the periodic calculations is 0.53 eV. This means that the cluster calculations model a system where the deprotonation reaction may almost occur spontaneously from the ground state, which is not the case for the periodic calculations.

As mentioned above, the differences between the results from the cluster- and periodic calculations cannot be assigned solely to differences in the model systems, since other parameters in the calculations also differed. However, it appears that the size of the model system plays an important role in the calculations. Also, the need for a proton acceptor to be present seems evident from the SM calculations. As for the comparison of the two energy profiles attained from the cluster- and the periodic calculations for OH_4 deprotonation reaction; it is not clear from these calculations alone which one is the most reliable one. Calculated hyperfine coupling tensors indicate that the results from the periodic calculations are more reliable.

6.3 Comparison of ground state calculations with literature

As previously described (section 1.4) Pauwels and co-workers performed periodical calculations similar to those presented here for the OH_4 bond elongation (Pauwels *et al.* 2008). These calculations were, however, performed using a different computer program (and also at a different LOT). The results obtained in the periodic approach in this thesis are similar to the results of Pauwels *et al.* in that a quite high energy barrier (0.4 eV *versus* 0.5 eV in the present work) must be surpassed in order to reach a local minimum on the PES.

The main difference between the two studies is that Pauwels *et al.* had a description of three proton transfers after the barrier was surpassed in a *<2a2b2c>*[13] supercell, and as much as five proton transfers if the cell was elongated to *<a3bc>*, whereas only two proton

[13] *a*, *b* and *c* are the crystallographic axes.

transfers were observed in the simulations in this thesis (in a *<2a2b2c>* supercell). In fact the cluster calculations in this study showed only one proton transfer.

The results of Pauwels *et al.* appear to be reliable, as these authors also performed *g*- and hyperfine coupling tensor calculations of their resulting species which compared relatively well with experimental data. Also, the many proton transfers observed allowed for asking whether, in a real crystalline system, the proton would be able to move sufficiently far away from the radical to be absorbed in a another molecule. This is an important issue because the energy barrier for returning to the original cation radical from the deprotonated species is much lower than the barrier for the deprotonation. Even though only two proton transfers were observed in this thesis (for the periodic approach), the findings are in line with the suggestion by Pauwels *et al.* that the excess proton travels throughout the crystal along the "infinite" hydrogen bond chain and is trapped at a distance from the radical.

6.4 Desired properties of the calculated excited states

The periodic ground state calculations resulted in three energy profiles (OH_1, OH_2 and OH_4) showing the possibilities for stable structures after two proton transfers. The three energy profiles all have quite high energy barriers (0.5 – 0.9 eV), implying that the proton transfers are unlikely to occur from the ground state. The thermodynamical analysis given in ***Table 3*** in section 5.1.1 suggests an explanation for the experimental observation of only one of the radicals (centered on O_4). However, this analysis is only valid if there is some driving force present that mediates the reactions, along with a mechanism for stabilizing the local minima so that the relatively small energy barrier for back transfer cannot be overcome. Otherwise the occurrence of any of the three oxygen centered radicals at such low temperatures as 4 K cannot be explained. The driving force necessary to overcome the energy barriers may be present since the cation radical is in an *excited state* immediately after irradiation.

6.4.1 Excited states resulting from ionization

In an ionization process, an electron is abruptly removed from the molecule. The molecule is left in the geometrical state of the intact electronic structure, which is no longer the equilibrium geometry. The potential energy will be higher than the potential energy of the equilibrium geometry; this excess energy will become kinetic energy of the nuclei as the cation radical approaches equilibrium. This means that there is excess energy available for

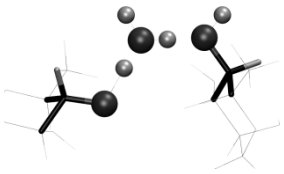

surpassing small barriers on the PES even if the cation radical should be in its electronic ground state. ***Table 1*** in section 5.1.1 indicates that the magnitude of this energy excess is 0.01 eV in the case of rhamnose, which is nowhere near enough to surpass the barrier for the proton transfer.

This energy excess is actually within the computational error margin, which can be seen from comparing the energy of the cation in the freely optimized structure and the first points in the ground state PES scans (given in tables in Appendix D). This comparison shows that the energy calculated in the first points in the PES scans (with the presence of a harmonic restraint) is actually *lower* than the energy of the freely optimized structure, which is an unphysical situation. This error is most likely due to a better convergence in the restrained calculations, as these started from the already converged wave functions of the freely optimized structure. The energy difference is about 0.01 - 0.02 eV.

The excited states resulting from ionization are described as single excitations from a doubly occupied orbital into the singly occupied orbital (SOMO) of the radical electronic structure. This type of excitation is illustrated in ***Figure 27***. It is the abrupt way in which the electron is removed in an ionization process that leads to a state of the above described character. Therefore, in examining the calculated excited states for the system, only such states are interesting in the description of the deprotonation process[14]. There is a random nature to which orbital the electron will be ejected from, but it seems fair to assume that different types of interactions will lead to a preference for outer or inner shell electrons.

[14] This is a truth with limited validity, but provides a usable starting point for the analyses.

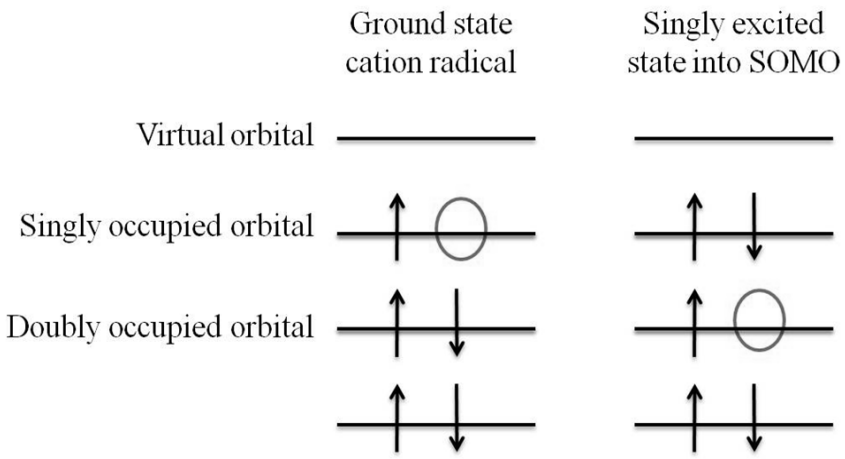

Figure 27: Diagram showing an electronically excited state resulting from an ionization process of a neutral molecule. The electron is knocked out of an originally doubly occupied orbital that is not the highest in energy, resulting in a state corresponding to an excitation from a doubly occupied orbital in the radical cation ground state into the singly occupied molecular orbital (SOMO).

The radiation to which the rhamnose crystals have been exposed prior to the experimental observation of the oxygen centered radical on O_4 (Samskog and Lund 1980; Budzinski and Box 1985) is X-rays with keV photon energies. Thus, photoelectric effect is the most important photon interaction process, and the secondary electrons released in the photon interaction processes will interact with the material through collision processes. These types of interactions may ionize deep or high, or even just excite the molecule in question. As mentioned in section 1.2.2, ejection of a tightly bound electron will lead to Auger-electron production in materials with low effective atomic number (Attix 1986). Auger-electron production would also lead to multiply charged molecules, and do therefore not correspond to the system that is studied in this work.

There is a possibility that the oxygen centered radical is a product of a multiply charged molecule/radical which has deprotonated before absorbing electrons arising from radiation interactions with other molecules, so as to re-establish charge balance. But as mentioned, this is not what is studied here. The excited states of the cation radical under investigation in the present study are those resulting from an excitation from an energetically high (occupied) orbital into the SOMO.

A state that would be likely to lead to a deprotonation (by lowering the energy barrier) would be a state in which the spin and positive charge of the radical cation are located on the oxygen from which the proton transfer occurs. This argument has been used to suggest from

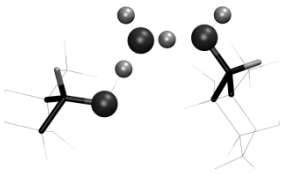

theoretical calculations, the occurrence of a certain deprotonation reaction from deoxyribose in a guanine nucleoside radical cation without explicitly modeling the proton transfer reaction (Adhikary *et al.* 2005). In the work of Adhikary *et al.* the nature of the excited state was determined by comparing the shape of the molecular orbital from which the electron was excited with that of the SOMO.

6.4.2 Reaction mediating states

If there is excited state that is aiding the reaction, it is most likely an electronically excited state considering the height of the energy barriers. In a scenario where the deprotonation reaction occurs while the molecule is in the electronically excited state, this state should possess some of the following features: First of all, the oscillator strength of the state should be small in the region of the PES corresponding to the cation radical, so that de-excitation is unlikely to occur before the deprotonation. Secondly, the possibility for deprotonation should be better in this excited state than in the ground state, either by exhibiting a lower energy barrier or no energy barrier at all. Thirdly, there should be some route for de-excitation into the ground state after the deprotonation has occurred, leaving the molecule in the local energy minimum for the ground state.

De-excitation from an electronically excited state can occur by several different routes. Radiative de-excitation, with the emission of one or more photons, is more probable when the oscillator strength of the state is high. Non-radiative de-excitation can occur in a conical intersection, where the two states are degenerate, or through internal conversion if the vibrationally excited states of the two electronic states overlap. Some of these ideas are illustrated in ***Figure 28***.

A second scenario for the de-excitation is one where non-radiative de-excitation from an electronically excited state occurs before deprotonation, for instance by internal conversion. This de-excitation might free enough energy (transfer it to kinetic energy of the nuclei) to surpass the energy barrier.

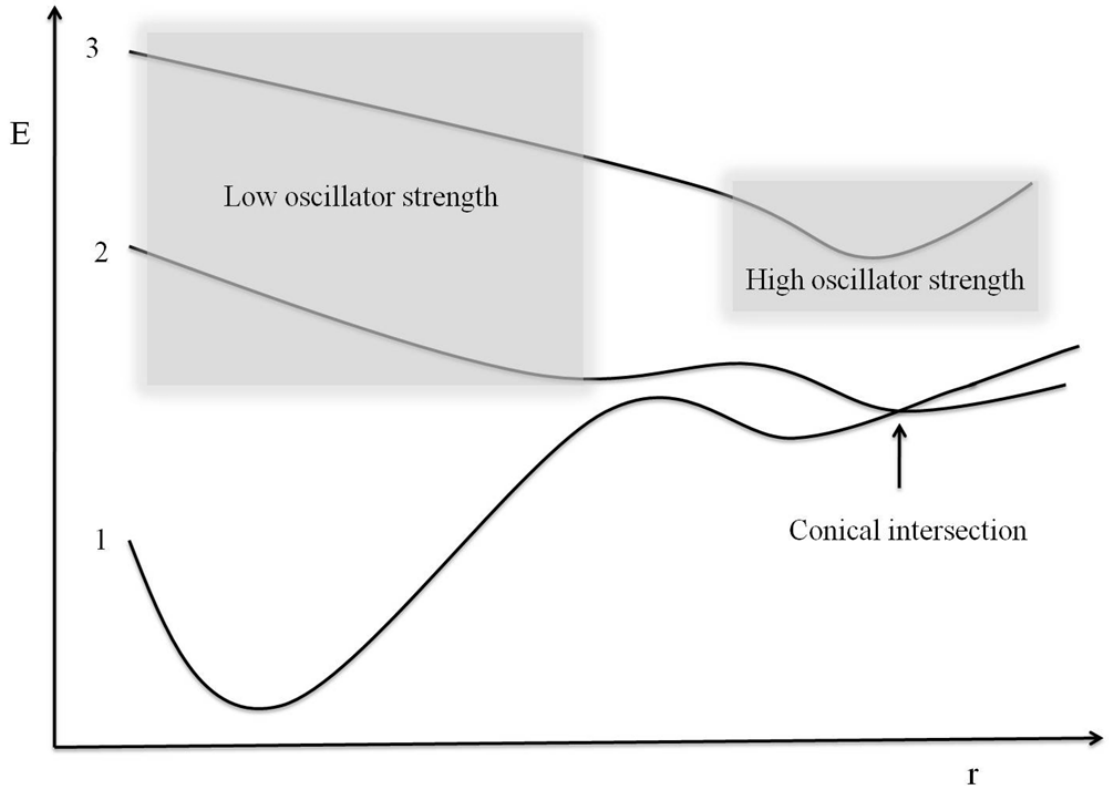

Figure 28: Two ways in which electronically excited states might contribute to the deprotonation reaction. State 1 is the ground state which has a local minimum for a long OH bond length (here represented by r) corresponding two proton transfers.

State 2 is an electronically excited state which has a different PES than the ground state. Two interesting features are shown in this state: First of all it has a lower energy barrier for the deprotonation reaction than the ground state. Secondly it has a conical intersection with the ground state after the energy barrier of the ground state is passed, making a non-radiative de-excitation at this geometry a possible way of reaching the local minimum in the ground state.

State 3 is one where the deprotonation reaction is spontaneous, and a radiative de-excitation afterwards might bring the molecule back to the stable geometry of the ground state. States 2 and 3 have in common that de-excitation into the ground state is improbable before the proton transfer has occurred.

6.5 Observed excited state properties

As was mentioned in section 5.2.2, analyses made in the present work have shown that using the MOs for analysis of the charge and spin localization of a given state is a very unreliable method. The KS orbitals can only be considered as aids in the calculations, as they do not correspond to eigenstates of the Hamiltonian of the system.

Furthermore, the calculations on the radical structure have been performed in the unrestricted KS procedure, which means that the α- and β electron orbitals need not have the same spatial distribution. This is illustrated in ***Figure 29***. In fact, it was found that the KS α-

HOMO and the β-LUMO, which in a spin restricted picture would be the same orbital referred to as the SOMO, in some cases have completely different spatial distributions. It would therefore be misleading to say that the "electron hole" is localized in the β-LUMO orbital, the "hole" may be (and usually is) distributed over several orbitals. In the present work, the implication of this has been that no charge- or spin analyses of the excited states have been made.

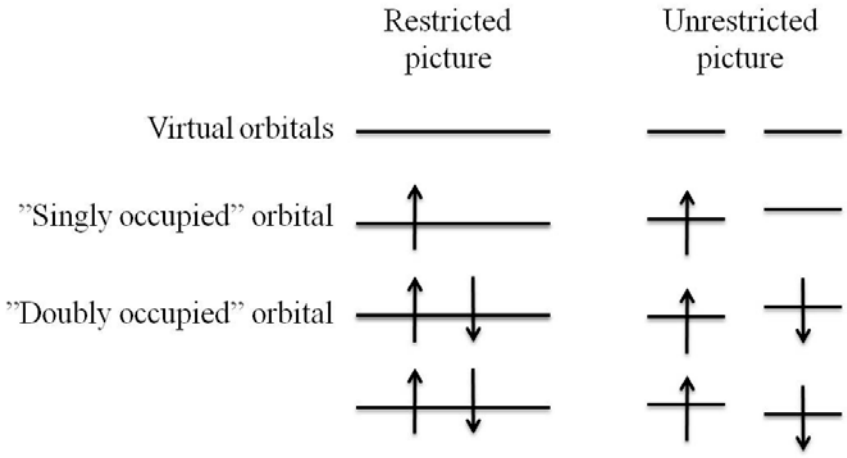

Figure 29: The picture of the orbitals as singly and doubly occupied is ruined when considering an unrestricted KS calculation. The α and β orbitals of the same level need not have exactly the same energy. The spatial distribution of the α- and β orbitals might also be different.

The tools that are left for analysis of the excited states are therefore the occupation numbers of the orbitals, the excitation energy, the oscillator strengths and the dipole transition moments between the excited state and the ground state.

The energies of the excited states along the proton transfer trajectories examined in this work (section 5.2.2), do not seem to suggest the possibility for a deprotonation reaction from any of the electronically excited states of the molecular system. Since there is no electronically excited state with an appropriate shape (***Figure 28***) for the deprotonation reaction, examinations of the oscillator strengths are of secondary interest, as they would only indicate if an excited state may de-excite more or less rapidly.

The occupation numbers have been used in the analysis to determine whether the excited state under investigation, is one that could be formed as a direct consequence of an ionization process (***Figure 27***). It is found that all the states examined are of this kind.

The dipole transition moments have been employed to determine if conical intersections in the PES profiles for the proton transfer process from OH_4 occur. No conical intersections between the excited state and the ground state have been observed.

It is concluded that the excited state calculations provide no evidence for the first scenario described in section 6.4.2. Based on that conclusion, it is most probable that the energy necessary to drive the deprotonation processes arise from immediate de-excitation from a vibrationally excited state of the ground state or from an electronically excited state.

6.6 TDDFT benchmark calculations

Section 5.2.1 holds the results from the TDDFT test calculations on H_2O, CH_3 and CO^+. The results demonstrate by comparison with experimental results that the TDDFT results are off in the excitation energies by about 1 eV.

Different functionals were used to test their individual performances, and it was found that functionals tested performed differently for different molecules. In particular PBE0 appeared to work better for water whereas B3LYP worked better for CO^+. It is therefore not possible to decide upon a functional (out of the ones tested) to be the best TDDFT functional from this limited study. It is interesting to notice that for CH_3 no functional was found to perform equally well for both states where experimental results were available. Rather, different functionals provided good approximations for the two different states. This is in line with the discussion of section 3.2.2 where it is pointed out that different functionals perform better for different types of excitations.

When it comes to basis sets, the presence of diffuse- and polarization functions showed a noticeable impact on the results, both with regard to excitation energies and to which excited states appear as well as to their ordering. Whether it was polarization functions or diffuse functions that were more important varied with the system studied, but the differences in excitation energies could be as great as 1 eV. It was also shown that the difference between using double- or triple-ζ valence was relatively small, only about 0.1 eV. This compares well with reported results for the guanine nucleoside where going from the 6-31G+ basis set to 6-311++G** in the B3LYP functional gave energy differences for the excited states of about 0.05 eV on average (Adhikary *et al.* 2005).

From the results for the small molecules, it was decided that the B3LYP functional along with a double-ζ basis set including both diffuse and polarization functions on all atoms should be appropriate to get a reasonable description of the excited states of the rhamnose cation radical.

Worth noting is the magnitude of the excitation energies attained for rhamnose, see ***Table 23*** in Appendix D. The excitation energies were as small as 0.1 eV. It is expected that

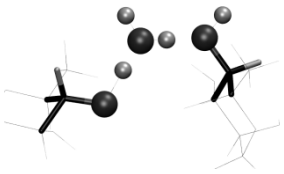

excitation energies are smaller for larger molecules. However, energies of the order of tenths of an eV are much smaller than the deviations relative to the experimental data for the small molecules. With this in mind, the TDDFT results cannot be lent much weight with respect to absolute energies, even if the ordering of the levels (and their dependence on the molecular geometries) still may be more reliable. The ordering of the states may be expected to be preserved, at least for valence excited states (Dreuw 2006), but other than that, there is little benchmark that implies that this conservation of the ordering is necessarily be the case.

6.7 Reliability of the calculations

Can any of the model systems presented in this thesis, with the appropriate computational results, be considered reliable? Starting with the ground state results, comparison to another work is possible for the OH_4 deprotonation reaction, the periodic calculations in the present work agree fairly well with the reference work (Pauwels *et al.* 2008). The presence of an energy barrier of a comparable height indicates that the present periodic results are quite reliable, if those of Pauwels *et al.* are. In addition, Pauwels *et al.* have obtained data providing for an explanation for how the neutral radical can stabilize (by indicating that the proton carrying the excess positive charge, is allowed to move far away from the radical site). No such explanation can be offered from the results of this thesis, though the attempts at doing corresponding calculations were limited.

Even though the periodic calculations offer a relatively good agreement with the results of Pauwels and co-workers, which again are in fair agreement with experimental data (Samskog and Lund 1980; Budzinski and Box 1985), Pauwels *et al.* do not put forward any explanation for the formation of the O_4-centered radical, an explanation which is necessary due to the high energy barrier that must be surpassed. This high energy barrier was as outlined in chapter 1, one of the motivating factors for the TDDFT calculations in the present work, since such calculations may allow us to investigate whether an electronically excited state can mediate the deprotonation reaction.

With respect to the energy barrier, the present cluster calculations offer a better situation, since this calculated energy barrier is much smaller than what is the case in the periodic calculations. The difference in the height of the energy barriers found in the cluster calculations and the periodic calculations might arise from the fact that the PES profiles are scanned in opposite directions in the two cases. The stable structure obtained by the cluster

approach, however, differs significantly from that obtained by the periodic approach and also from that of Pauwels *et al.*. Calculations of EPR parameters for the stable structures of both the cluster calculations and the periodic calculations imply that the results of the periodic calculations are the more reliable ones.

As for the rhamnose excited state calculations no experimental evidence is present for comparison. The additional fact that the calculations were performed in the single molecule approximation further reduces the credibility of the results. It should also be noted that all of these calculations are performed as SP calculations at different levels of theory and in a model system different from that used for the geometry optimizations as well as in a different computer program. The calculations on water presented in section 5.2.1 show that a small difference in geometry does not affect the excited states severely. However, the geometrical differences for H_2O were rather small as compared to what was observed for the rhamnose calculations (see for instance ***Figure 21*** in section 5.1.2).

The lack of charge and spin analysis of the excited states makes it impossible to determine whether there were charge-transfer states present, in the results. If there where such states, appropriate functionals (e.g. CAM-B3LYP) should be applied in order to get a fair description of these states. The calculations for the OH_4 deprotonation reaction were performed with three different functionals (PBE, BLYP and B3LYP). Still no high-level functionals including more HF exchange were tried, tough the use of at least one such functional would add to the reliability of the results.

6.8 Conclusive remarks

The major result from the periodic ground state calculations is that deprotonation reactions from the rhamnose cation radical are possible from three out of four oxygen sites (O_1, O_2 and O_4) and that the energy barriers for each of these reactions are different even if their magnitudes are not necessarily accurate. This calculational result may explain the selectivity in the radical formation in this molecule leading to a preferred structure (O_4-centered radical) in agreement with experimental data.

According to the ideas presented above on the possible role of excited states for overcoming the energy barriers, the excited state calculations performed in this study did not turn out to be sufficiently conclusive for confirming or excluding the possibility of excited states mediating the proton transfer reactions.

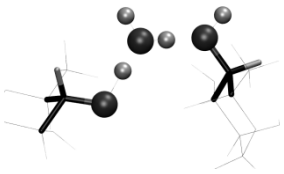

An energy barrier of about 0.5 eV should in principle not be difficult to overcome since the radiation to which the crystal is subjected, contains photons with energy of the order of keV (X-rays), and deposition of only a small part of this energy should yield sufficient energy for overcoming the energy barrier. In that case the selective stabilization of only one radical type (O_4-centered) may be understood by the thermodynamics presented in ***Table 3*** in section 5.1.1. It is however, necessary to devise a mechanism avoiding back-transfer of the proton.

6.9 What now?

Considering the results presented in this thesis, it is apparent that more work is required in order to draw full conclusions. This includes more comprehensive and detailed calculations of EPR parameters, including the *g*-tensor of the deprotonated structures, in order to compare this with experimental data. In addition, it should be considered whether it is possible to obtain a new set of experimental data for the O_4-centered radical formed in rhamnose crystals in the temperature interval 10-77 K so as to resolve the ambiguity of the presently available experimental results.

Further analyses of the excited state energies are also of interest, but such large computational and laborious tasks require more time.

It would also be of interest to compare the results from the exited state calculations with calculations using a higher LOT; both HF-based calculations and TDDFT calculations using triple-ζ basis sets and different XC functionals (such as CAM-B3LYP). One particular feature worth investigating closer is the first excited state during the OH_4 deprotonation reaction. This state is close to the ground state in energy, and it is important to determine whether this is a real state, or just a computational artifact of the LOT that is being used in the calculations.

In addition to this, the excited state calculations should be extended to systems including more surroundings. The star-shaped model with hydrogen bonded water molecules proved to be very computationally expensive, however, the similarity of the results from the star-shaped model and the single chain models could be exploited to add hydrogen bonding partners surrounding these single chains, making the cluster significantly smaller.

Finally, devising a convenient method for determining the spin and charge distribution of the excited states would be very desirable.

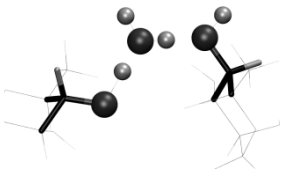

Bibliography

Adamo, C. and Barone, V. (1999). "Toward reliable density functional methods without adjustable parameters: The PBE0 model." Journal of Chemical Physics **110**(13): 6158.

Adamo, C., Scuseria, G. E. and Barone, V. (1999). "Accurate excitation energies from time-dependent density functional theory: Assessing the PBE0 model." Journal of Chemical Physics **111**(7): 2889.

Adhikary, A., Becker, D., Collins, S., Koppen, J. and Sevilla, M. D. (2006). "C5 '- and C3 '-sugar radicals produced via photo-excitation of one-electron oxidized adenine in 2 '-deoxyadenosine and its derivatives." Nucleic Acids Research **34**(5): 1501.

Adhikary, A., Khanduri, D., Kumar, A. and Sevilla, M. D. (2008). "Photoexcitation of Adenine Cation Radical A(center dot+) in the near UV-vis Region Produces Sugar Radicals in Adenosine and in Its Nucleotides." Journal of Physical Chemistry B **112**(49): 15844.

Adhikary, A., Kumar, A. and Sevilla, M. D. (2006). "Photo-induced hole transfer from base to sugar in DNA: Relationship to primary radiation damage." Radiation Research **165**(4): 479.

Adhikary, A., Malkhasian, A. Y. S., Collins, S., Koppen, J., Becker, D. and Sevilla, M. D. (2005). "UVA-visible photo-excitation of guanine radical cations produces sugar radicals in DNA and model structures." Nucleic Acids Research **33**(17): 5553.

Atherton, N. M. (1993). Principles of electron spin resonance. New York, Ellis Horwood/PTR Prentice Hall.

Atkins, P. W. and Friedman, R. S. (2005). Molecular quantum mechanics. Oxford, Oxford University Press.

Attix, F. H. (1986). Introduction to radiological physics and radiation dosimetry. New York, John Wiley.

Bauernschmitt, R. and Ahlrichs, R. (1996). "Treatment of electronic excitations within the adiabatic approximation of time dependent density functional theory." Chemical Physics Letters **256**: 454.

Becke, A. D. (1988). "Density-functional exchange-energy approximation with correct asymptotic-behavior." Physical Review A **38**(6): 3098.

Becke, A. D. (1993). "Density-functional thermochemistry .3. The role of exact exchange." Journal of Chemical Physics **98**(7): 5648.

Bernhard, W. A. and Close, D. M. (2003). DNA damage dictates the biological consequences of ionizing irradiation: The chemical pathways. Charged particle and photon interactions with matter: Chemical, physicochemical, and biological consequences with applications. A. Mozumber and Y. Hatano. New York, Marcel Dekker**:** 431.

Budzinski, E. E. and Box, H. C. (1985). "Alkoxy radicals: Delta proton hyperfine couplings." Journal of Chemical Physics **82**(8): 3487.

Byrd, R. H., Lu, P., Nocedal, J. and Zhu, C. (1995). "A limited memory algorithm for bound constrained optimization." Siam Journal on Scientific Computing **16**(5): 1190.

Casida, M. E. (1995). Time-dependent density functional response theory for molecules. Recent advances in density functional methods. D. P. Chong. Singapore, World Scientific**:** 2 b.

Casida, M. E. (2005). "Propagator corrections to adiabatic time-dependent density-functional theory linear response theory." Journal of Chemical Physics **122**(5).

Casida, M. E. (2009). "Time-dependent density-functional theory for molecules and molecular solids." Journal of Molecular Structure-Theochem **914**: 3.

Clark, T., Chandrasekhar, J., Spitznagel, G. W. and Schleyer, P. V. (1983). "Efficient diffuse function-augmented basis sets for anion calculations. III. The 3-21+G basis set for first-row elements, Li-F." Journal of Computational Chemistry **4**(3): 294.

Close, D. M. (1997). "Where are the sugar radicals in irradiated DNA?" Radiation Research **147**(6): 663.

Cramer, C. J. (2004). Essentials of computational chemistry: theories and models. Chichester, Wiley.

Dreuw, A. (2006). "Quantum chemical methods for the investigation of photoinitiated processes in biological systems: Theory and applications." Chemphyschem **7**(11): 2259.

Dreuw, A. and Head-Gordon, M. (2005). "Single-reference ab initio methods for the calculation of excited states of large molecules." Chemical Reviews **105**(11): 4009.

Dreuw, A., Weisman, J. L. and Head-Gordon, M. (2003). "Long-range charge-transfer excited states in time-dependent density functional theory require non-local exchange." Journal of Chemical Physics **119**(6): 2943.

Evans, R. D. (1955). The Atomic Nucleus, McGraw-Hill Inc.

Gaussian 03, Revision D.02, Frisch, M. J., Trucks, G. W., Schlegel, H. B., Scuseria, G. E., Robb, M. A., Cheeseman, J. R., Montgomery, J., J. A., Vreven, T., Kudin, K. N., Burant, J. C., Millam, J. M., Iyengar, S. S., Tomasi, J., Barone, V., Mennucci, B., Cossi, M., Scalmani, G., Rega, N., Petersson, G. A., Nakatsuji, H., Hada, M., Ehara, M., Toyota, K., Fukuda, R., Hasegawa, J., Ishida, M., Nakajima, T., Honda, Y., Kitao, O., Nakai, H., Klene, M., Li, X., Knox, J. E., Hratchian, H. P., Cross, J. B., Bakken, V., Adamo, C., Jaramillo, J., Gomperts, R., Stratmann, R. E., Yazyev, O., Austin, A. J., Cammi, R., Pomelli, C., Ochterski, J. W., Ayala, P. Y., Morokuma, K., Voth, G. A., Salvador, P., Dannenberg, J. J., Zakrzewski, V. G., Dapprich, S., Daniels, A. D., Strain, M. C., Farkas, O., Malick, D. K., Rabuck, A. D., Raghavachari, K., Foresman, J. B., Ortiz, J. V., Cui, Q., Baboul, A. G., Clifford, S., Cioslowski, J., Stefanov, B. B., Liu, G., Liashenko, A., Piskorz, P., Komaromi, I., Martin, R. L., Fox, D. J., Keith, T., Al-Laham, M. A., Peng, C. Y., Nanayakkara, A., Challacombe, M., Gill, P. M. W., Johnson, B., Chen, W., Wong, M. W., Gonzalez, C. and Pople, J. A. Gaussian, Inc., Wallingford CT, 2004,

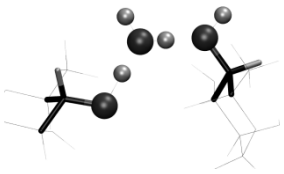

Goedecker, S., Teter, M. and Hutter, J. (1996). "Separable dual-space Gaussian pseudopotentials." Physical Review B **54**(3): 1703.

Hall, E. J. and Giaccia, A. J. (2006). Radiobiology for the radiologist. Philadelphia, Pa., Lippincott Williams & Wilkins.

Hariharan, P. C. and Pople, J. A. (1973). "The influence of polarization functions on molecular orbital hydrogenation energies." Theoretica Chimica Acta **28**(3): 213.

Hartwigsen, C., Goedecker, S. and Hutter, J. (1998). "Relativistic separable dual-space Gaussian pseudopotentials from H to Rn." Physical Review B **58**(7): 3641.

Hehre, W. J., Ditchfie. R and Pople, J. A. (1972). "Self-consistent molecular-orbtal methods 12 Further Extensions of Gaussian-type basis sets for use in molecular-orbital sudies of organic molecules." Journal of Chemical Physics **56**(5): 2257.

Henriksen, E. K. and Henriksen, T. (1998). Vår strålende verden: radioaktivitet, røntgenstråling og helse. Oslo, Fysisk institutt, Universitetet i Oslo.

Hirata, S. and Head-Gordon, M. (1999). "Time-dependent density functional theory within the Tamm-Dancoff approximation." Chemical Physics Letters **314**(3-4): 291.

Hohenberg, P. and Kohn, W. (1964). "Inhomogeneous electron gas." Physical Review B **136**(3B): B864.

Hutter, J. (2009). "Google groups, cp2k." Retrieved 04.05. 2010, from http://groups.google.com/group/cp2k/browse_thread/thread/e9094dca5701338c/a056db8a2381dc5f?lnk=gst&.

Ipatov, A., Cordova, F., Doriol, L. J. and Casida, M. E. (2009). "Excited-state spin-contamination in time-dependent density-functional theory for molecules with open-shell ground states." Journal of Molecular Structure-Theochem **914**(1-3): 60.

Kohn, W. and Sham, L. J. (1965). "Self-consistent equations including exchange and correlation effects." Physical Review **140**(4A): 1133.

Krack, M. (2005). "Pseudopotentials for H to Kr optimized for gradient-corrected exchange-correlation functionals." Theoretical Chemistry Accounts **114**: 145.

Krishnan, R., Binkley, J. S., Seeger, R. and Pople, J. A. (1980). "Self-consistent molecular orbital methods. XX. A basis set for correlated wave functions." Journal of Chemical Physics **72**(1): 650.

Kumar, A. and Sevilla, M. D. (2006). "Photoexcitation of dinucleoside radical cations: A time-dependent density functional study." Journal of Physical Chemistry B **110**(47): 24181.

Kumar, A. and Sevilla, M. D. (2008). Radiation Effects on DNA: Theoretical Investigations of Electron, Hole and Excitation Pathways to DNA Damage. Radiation Induced Molecular Phenomena in Nucleic Acids: A Comprehensive Theoretical and Experimental Analysis. M. K. Shukla and J. Leszczynski. Dordrecht, Springer Science+Business Media B.V.

Lee, C. T., Yang, W. T. and Parr, R. G. (1988). "Development of the Colle-Salvetti correlation-energy formula into a functional of the electron-density." Physical Review B **37**(2): 785.

Lippert, G., Hutter, J. and Parrinello, M. (1997). "A hybrid Gaussian and plane wave density functional scheme." Molecular Physics **92**(3): 477.

Meng, S. and Kaxiras, E. (2008). "Real-time, local basis-set implementation of time-dependent density functional theory for excited state dynamics simulations." Journal of Chemical Physics **129**(5).

Mulliken, R. S. (1955). "Electronic population analysis on LCAO-MO molecular wave functions .1." Journal of Chemical Physics **23**(10): 1833.

Pauwels, E., Declerck, R., Van Speybroeck, V. and Waroquier, M. (2008). "Evidence for a Grotthuss-like mechanism in the formation of the rhamnose alkoxy radical based on periodic DFT calculations." Radiation Research **169**(1): 8.

Pauwels, E., Van Speybroeck, V. and Waroquier, M. (2006). "Study of rhamnose radicals in the solid state adopting a density functional theory cluster approach." Journal of Physical Chemistry A **110**(20): 6504.

Peng, C. Y., Ayala, P. Y., Schlegel, H. B. and Frisch, M. J. (1996). "Using redundant internal coordinates to optimize equilibrium geometries and transition states." Journal of Computational Chemistry **17**(1): 49.

Peng, C. Y. and Schlegel, H. B. (1993). "Combining synchronous transit and quasi-newton methods to find transition states." Israel Journal of Chemistry **33**(4): 449.

Perdew, J. P., Burke, K. and Ernzerhof, M. (1996). "Generalized gradient approximation made simple." Physical Review Letters **77**(18): 3865.

Perdew, J. P., Burke, K. and Ernzerhof, M. (1997). "Generalized gradient approximation made simple (vol 77, pg 3865, 1996)." Physical Review Letters **78**(7): 1396.

Pople, J. A. and Beveridge, D. L. (1970). Approximate molecular orbital theory. New York, McGraw-Hill.

Runge, E. and Gross, E. K. U. (1984). "Density-functional theory for time-dependent systems." Physical Review Letters **52**(12): 997.

Sagstuen, E. and Hole, E. O. (2009). Radiation Produced Radicals. Electron Paramagnetic Resonance: A Practitioner's Toolkit M. Brustolon and G. Giamello. Hoboken, New Jersey, John Wiley & Sons, Inc.

Samskog, P. O. and Lund, A. (1980). "The alkoxy radical RCHO formed in irradiated single crystals of rhamnose." Chemical Physics Letters **75**(3): 525.

Shukla, M. K. and Leszczynski, J. (2005). "Excited state proton transfer in guanine in the gas phase and in water solution: A theoretical study." Journal of Physical Chemistry A **109**(34): 7775.

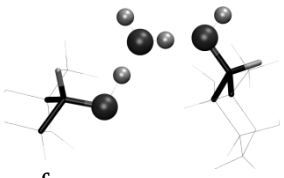

Sobolewski, A. L. and Domcke, W. (2002). "On the mechanism of nonradiative decay of DNA bases: ab initio and TDDFT results for the excited states of 9H-adenine." European Physical Journal D **20**(3): 369.

Stewart, J. J. P. (1989). "Optimization of parameters for semiempirical methods .1. Method." Journal of Computational Chemistry **10**(2): 209.

Svensson, M., Humbel, S., Froese, R. D. J., Matsubara, T., Sieber, S. and Morokuma, K. (1996). "ONIOM: A multilayered integrated MO+MM method for geometry optimizations and single point energy predictions. A test for Diels-Alder reactions and Pt(P(t-Bu)(3))(2)+H-2 oxidative addition." Journal of Physical Chemistry **100**(50): 19357.

Takagi, S. and Jeffrey, G. A. (1978). "Neutron-diffraction refinement of crystal-structure of α-L-rhamnose monohydrate." Acta Crystallographica Section B-Structural Science **34**(AUG): 2551.

CP2K version 2.0.1 (Development Version), the CP2K developers group. 2009, http://cp2k.berlios.de/

VandeVondele, J. and Hutter, J. (2007). "Gaussian basis sets for accurate calculations on molecular systems in gas and condensed phases." Journal of Chemical Physics **127**(11).

VandeVondele, J., Krack, M., Mohamed, F., Parrinello, M., Chassaing, T. and Hutter, J. (2005). "QUICKSTEP: Fast and accurate density functional calculations using a mixed Gaussian and plane waves approach." Computer Physics Communications **167**(2): 103.

Vosko, S. H., Wilk, L. and Nusair, M. (1980). "Accurate spin-dependent electron liquid correlation energies for local spin-density calculation - a critical analysis." Canadian Journal of Physics **58**(8): 1200.

Wikipedia. "DNA." Retrieved 06.08.2010 from http://en.wikipedia.org/wiki/Dna.

Yanai, T., Tew, D. P. and Handy, N. C. (2004). "A new hybrid exchange-correlation functional using the Coulomb-attenuating method (CAM-B3LYP)." Chemical Physics Letters **393**: 51.

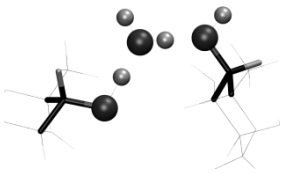

Appendix A: List of units

Units

c	$2.997\,924\,58 \times 10^{8}$ m/s	Speed of light in vacuum
eV	$1.602\,176\,5 \times 10^{-19}$ J	
g_e	-2.002 319 304	g-factor of free electron
$\hbar$	$1.05457160 \times 10^{-34}$ Js	
Hartree	4.359×10^{-18} J	Atomic unit for energy
	=2 Ry	
	=27.211 eV	
K	0° C = 273.15 K	Absolute temperature
m_e	$9.109\,389\,7 \times 10^{-31}$ kg	Electronic rest mass
Ry	2.1799×10^{-18} J	
Å	10^{-10} m	
μ_B	$\frac{e\hbar}{2m_e} = 9.274\,009\,0 \times 10^{24}$ J/T	Bohr magneton

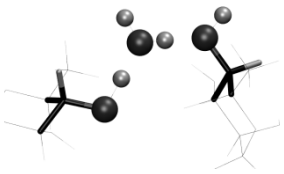

Appendix B: List of acronyms and abbreviations

A	Adenine, DNA base
ALDA	Adiabatic local density approximation
B3LYP	Hybrid exchange correlation functional
BLYP	Exchange-correlation functional
BO approx.	Born Oppenheimer approximation
C	Cytosine, DNA base
CAM-B3LYP	Exchange-correlation functional
CC	Coupled cluster
CI	Configuration interaction
CIS	Configuration interaction singles
CP2K	Computer program
CT	Charge-transfer
DFT	Density functional theory
DNA	Deoxyribonucleic acid
EPR	Electron paramagnetic resonance
G	Guanine, DNA base
G03	Gausian03, computer program
GGA	Generalized gradient approximation
GPW	Gaussian and plane wave
GTO	Gaussian type orbital
HF	Hartree-Fock
HOMO	Highest occupied molecular orbital
hν	Photon energy
KS	Kohn-Sham
LBFGS	Geometry optimization method
LDA	Local density approximation
LOT	Level of theory
LR-TDDFT	Linear response time-dependent density functional theory
LSDA	Local spin density approximation
LUMO	Lowest unoccupied molecular orbital
MCSCF	Multiconfiguration self-consistent field
MGGA	Meta-generalized gradient approximation

MO	Molecular orbital
MP1/2/4	Møller Plesset perturbation theory of 1st, 2nd or 4th order
N	Number of basis functions
ONIOM	Multilayered method for geometry optimizations
P	Phosphate (on the DNA backbone)
PBE	Exchange-correlation functional
PBE0	Exchange-correlation functional
PES	Potential energy surface
PM3	Parameterized model 3 (semiempirical model)
RHF	Restricted Hartree-Fock
ROHF	Restricted open-shell Hartree-Fock
RPA	Random phase approximation
S	Sugar (on the DNA backbone)
SCF	Self-consistent field
SE	Schrödinger equation
SM	Single molecule
SOMO	Singly occupied molecular orbital
SP	Single point
STO	Slater type orbital
T	Thymine, DNA base
TDDFRT	Time-dependent density functional response theory
TDDFT	Time-dependent density functional theory
TZVP	Triple-ζ valence basis set with polarization functions
UHF	Unrestricted Hartree-Fock
XC	Exchange-correlation
α	Spin-up (electron)
β	Spin-down (electron)

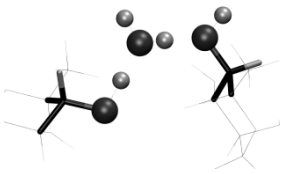

Appendix C: Programs most used

- **ChemBioDraw Ultra 12.0**

  Program used for drawing molecular structures.

  www.cambridgesoft.com

- **ChemCraft 1.5**

  Program used for visualization of output from CP2K and Gaussian03.

  www.chemcraftprog.com

- **CP2K 2.0.1 (Development version)**

  Freely available program used for performing DFT calculations with periodic boundary conditions.

  http://cp2k.berlios.de/

- **Gaussian03**

  Program for used for performing DFT and TDDFT calculations.
  www.gaussian.com

- **Gaussview 4.1**

  Program used for making input and visualizing data from Gaussian03.
  www.gaussian.com

- **MATLAB R2009b**

  Program used for making plots of results.
  www.mathworks.com

- **Paint**

  Simple drawing program used for editing illustrations, comes with Windows operating system.

- **Microsoft Office 2007**

  This thesis is written in MS Word, and some illustrations are made using MS PowerPoint. MS Excel was also used for analyzing data.

- **VMD for WIN32 1.8.7**

  Program used for visualization and making illustrations of chemical structures resulting from calculations in CP2K and Gaussian03

  http://www.ks.uiuc.edu/Research/vmd

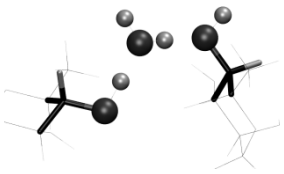

Appendix D: Results

Ground state calculations on the rhamnose radical

Table 11: Table of energies for the PES profile of the OH_1 deprotonation reaction, corresponding to the plot in ***Figure 12*** (section 5.1.1). The results are from restrained geometry optimizations using CP2K, periodical boundary conditions, BLYP/TZVP-GTH. The structure under the bar was optimized without constraints.

Bond length / Å	Energy / Hartree	Normalized energy/ eV	
1.000	-2214.286440	0	
1.080	-2214.283199	0.0882	
1.174	-2214.275538	0.2967	
1.278	-2214.266530	0.5418	
1.386	-2214.262268	0.6577	
1.487	-2214.257819	0.7788	
1.593	-2214.254218	0.8768	
1.694	-2214.252116	0.9340	
1.799	-2214.253806	0.8880	
1.897	-2214.252777	0.9160	
1.994	-2214.251021	0.9638	
1.713	-2214.255672	0.8372	(structure optimized from 1.8 Å)

Table 12: Table of energies for the PES profile of the OH_2 deprotonation reaction, corresponding to the plot in ***Figure 12*** (section 5.1.1). The results are from restrained geometry optimizations using CP2K, periodical boundary conditions, BLYP/TZVP-GTH. The structure under the bar was optimized without constraints.

Bond length / Å	Energy / Hartree	Normalized energy/ eV	
1.000	-2214.286444	0	
1.080	-2214.283044	0.0925	
1.176	-2214.275564	0.2961	
1.285	-2214.268256	0.4949	
1.393	-2214.264579	0.5950	
1.497	-2214.263697	0.6190	
1.597	-2214.262577	0.6494	
1.697	-2214.262080	0.6630	
1.797	-2214.261601	0.6760	
1.897	-2214.266181	0.5514	
1.996	-2214.265124	0.5801	
1.731	-2214.267319	0.5204	(structure optimized from 1.9 Å)

Table 13: Table of energies for the PES profile of the OH_3 deprotonation reaction, corresponding to the plot in ***Figure 12*** (section 5.1.1). The results are from restrained geometry optimizations using CP2K, periodical boundary conditions, BLYP/TZVP-GTH.

Bond length / Å	Energy / Hartree	Normalized energy/ eV
0.997	-2214.286353	0
1.075	-2214.282089	0.1160
1.168	-2214.272263	0.3834
1.285	-2214.264964	0.5820
1.393	-2214.261066	0.6881
1.496	-2214.259846	0.7213
1.594	-2214.258303	0.7633
1.694	-2214.256725	0.8062
1.794	-2214.254865	0.8568
1.892	-2214.252235	0.9284
1.992	-2214.251068	0.9601

Table 14: Table of energies for the PES profile of the OH_4 deprotonation reaction, corresponding to the plot in ***Figure 12*** (section 5.1.1). The results are from restrained geometry optimizations using CP2K, periodical boundary conditions, BLYP/TZVP-GTH. The structure under the bar was optimized without constraints.

Bond length / Å	Energy / Hartree	Normalized energy/ eV	
1.000	-2214.286438	0	
1.081	-2214.283374	0.0834	
1.176	-2214.275647	0.2936	
1.290	-2214.271024	0.4194	
1.396	-2214.268228	0.4955	
1.498	-2214.267017	0.5285	
1.599	-2214.266816	0.5339	
1.700	-2214.269694	0.4556	
1.798	-2214.269202	0.4690	
1.898	-2214.268600	0.4854	
1.997	-2214.267447	0.5168	
1.700	-2214.269704	0.4553	(structure optimized from 1.7 Å)

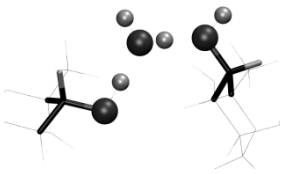

Table 15: Table of energies for the PES profile of the OH_4 deprotonation reaction, corresponding to the plot in ***Figure 22*** (section 5.1.2). The results are from restrained geometry optimizations using Gaussian03, ONOIM(PM3: B3LYP/6-311G**). The last structure in the table was optimized without constraints.

Bond length / Å	Energy / Hartree	Normalized energy/ eV	
0.98	-1304.353141	0.0722	
1.08	-1304.355796	0	
1.18	-1304.355293	0.0137	
1.28	-1304.355203	0.0161	
1.38	-1304.355555	0.0066	
1.48	-1304.355756	0.0011	(structure optimized from the 2.0 Å geometry optimized in CP2K)

H_2O

The tables all show SP TDDFT calculations of the first five singlet excited states of H_2O. Geometries can be found in ***Table 4*** (section 5.2.1). The first tables show results from calculations performed using the B3LYP-optimized geometry with different functionals and basis sets, and the last table shows results using PBE/6-311++G** for both geometries.

Table 16: See explanation on the next page.

B3LYP				
6-311G	**6-311G****	**6-311++G**	**6-311++G****	**6-31++G****
Excited State 1 7.1014 eV f=0.0212 5 -> 6 0.69193	Excited State 1 7.3500 eV f=0.0263 5 -> 6 0.69329	Excited State 1 6.6941 eV f=0.0339 5 -> 6 0.69586	Excited State 1 6.8807 eV f=0.0415 5 -> 6 0.69714	Excited State 1 6.8286 eV f=0.0443 5 -> 6 0.69736
Excited State 2 9.1252 eV f=0.0885 4 -> 6 0.68862	Excited State 2 9.2414 eV f=0.0000 5 -> 7 0.70111	Excited State 2 8.3394 eV f=0.0000 5 -> 7 0.69896	Excited State 2 8.4204 eV f=0.0000 5 -> 7 0.70006	Excited State 2 8.3608 eV f=0.0000 5 -> 7 0.70171
Excited State 3 9.1267 eV f=0.0000 5 -> 7 0.70045	Excited State 3 9.6792 eV f=0.0848 4 -> 6 0.69011	Excited State 3 8.6061 eV f=0.0927 4 -> 6 0.69366	Excited State 3 9.0637 eV f=0.0894 4 -> 6 0.69499	Excited State 3 9.0238 eV f=0.0889 4 -> 6 0.69519
Excited State 4 11.2767 eV f=0.0590 4 -> 7 0.69196	Excited State 4 11.6110 eV f=0.0510 4 -> 7 0.69552	Excited State 4 10.2400 eV f=0.0283 4 -> 7 0.70157	Excited State 4 10.5836 eV f=0.0227 4 -> 7 0.70222	Excited State 4 10.5393 eV f=0.0222 4 -> 7 0.70244
Excited State 5 13.6590 eV f=0.2387 3 -> 6 0.69035	Excited State 5 13.5921 eV f=0.2322 3 -> 6 0.69197	Excited State 5 10.9471 eV f=0.0150 5 -> 8 0.68758 5 -> 11 0.13293	Excited State 5 11.0812 eV f=0.0126 5 -> 8 0.67953 5 -> 11 0.17488	Excited State 5 11.1699 eV f=0.0008 5 -> 8 0.70161

Table 17: See explanation on the next page.

BLYP		**B3LYP**	
6-311++G**	**6-31++G****	**6-311++G****	**6-31++G****
Excited State 1 6.2450 eV f=0.0407 5 -> 6 0.69908	Excited State 1 6.1829 eV f=0.0432 5 -> 6 0.69896	Excited State 1 6.8807 eV f=0.0415 5 -> 6 0.69714	Excited State 1 6.8286 eV f=0.0443 5 -> 6 0.69736
Excited State 2 7.6648 eV f=0.0000 5 -> 7 0.70717	Excited State 2 7.5943 eV f=0.0000 5 -> 7 0.70727	Excited State 2 8.4204 eV f=0.0000 5 -> 7 0.70006	Excited State 2 8.3608 eV f=0.0000 5 -> 7 0.70171
Excited State 3 8.3890 eV f=0.0833 4 -> 6 0.69393	Excited State 3 8.3375 eV f=0.0832 4 -> 6 0.69439	Excited State 3 9.0637 eV f=0.0894 4 -> 6 0.69499	Excited State 3 9.0238 eV f=0.0889 4 -> 6 0.69519
Excited State 4 9.7901 eV f=0.0192 4 -> 7 0.70322	Excited State 4 9.7379 eV f=0.0187 4 -> 7 0.70347	Excited State 4 10.5836 eV f=0.0227 4 -> 7 0.70222	Excited State 4 10.5393 eV f=0.0222 4 -> 7 0.70244
Excited State 5 10.4829 eV f=0.0103 5 -> 8 0.69706 5 -> 11 0.10098	Excited State 5 10.5951 eV f=0.0000 5 -> 8 0.70270	Excited State 5 11.0812 eV f=0.0126 5 -> 8 0.67953 5 -> 11 0.17488	Excited State 5 11.1699 eV f=0.0008 5 -> 8 0.70161

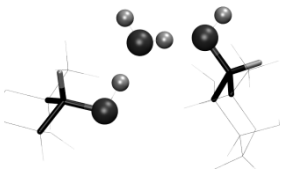

Table 16: Results from SP TDDFT calculation on H_2O using the B3LYP functional and different basis sets. All calculations were performed using geometries optimized at the B3LYP/6-311G** LOT. The results shown are excitation energies, oscillator strengths and numbers of the orbitals taking part in the excitation. The results are discussed in section 5.2.1.

Table 17: Results from SP TDDFT calculation on H_2O using the different functionals and the 6-311++G** and 6-31++G** basis sets. All calculations were performed using geometries optimized at the B3LYP/6-311G** LOT. The results shown are excitation energies, oscillator strengths and numbers of the orbitals taking part in the excitation. The results are discussed in section 5.2.1.

Table 18: Results from SP TDDFT calculation on H_2O using the PB3 functional and the 6-311++G** basis set for geometries optimized at the B3LYP/6-311G** and PBE/6-311G** LOT. The results shown are excitation energies, oscillator strengths and numbers of the orbitals taking part in the excitation. The results are discussed in section 5.2.1.

PBE		**PBE0**	
6-311++G**	**6-31++G****	**6-311++G****	**6-31++G****
Excited State 1 6.2450 eV f=0.0407 5 -> 6 0.69908	Excited State 1 6.1829 eV f=0.0432 5 -> 6 0.69896	Excited State 1 6.3970 eV f=0.0419 5 -> 6 0.70030	Excited State 1 6.3329 eV f=0.0436 5 -> 6 0.70021
Excited State 2 7.6648 eV f=0.0000 5 -> 7 0.70717	Excited State 2 7.5943 eV f=0.0000 5 -> 7 0.70727	Excited State 2 7.8538 eV f=0.0000 5 -> 7 0.70721	Excited State 2 7.7799 eV f=0.0000 5 -> 7 0.70729
Excited State 3 8.3890 eV f=0.0833 4 -> 6 0.69393	Excited State 3 8.3375 eV f=0.0832 4 -> 6 0.69439	Excited State 3 8.5654 eV f=0.0835 4 -> 6 0.69527	Excited State 3 8.5139 eV f=0.0831 4 -> 6 0.69568
Excited State 4 9.7901 eV f=0.0192 4 -> 7 0.70322	Excited State 4 9.7379 eV f=0.0187 4 -> 7 0.70347	Excited State 4 10.0007 eV f=0.0188 4 -> 7 0.70362	Excited State 4 9.9493 eV f=0.0189 4 -> 7 0.70371
Excited State 5 10.4829 eV f=0.0103 5 -> 8 0.69706 5 -> 11 0.10098	Excited State 5 10.5951 eV f=0.0000 5 -> 8 0.70270	Excited State 5 10.6478 eV f=0.0094 5 -> 8 0.69770	Excited State 5 10.7564 eV f=0.0000 5 -> 8 0.70346

Table 18: See explanation on the previous page.

B3LYP GEO	**PBE GEO**
Excited State 1 6.3970 eV f=0.0419 5 -> 6 0.70030	Excited State 1 6.3559 eV f=0.0411 5 -> 6 0.69998
Excited State 2 7.8538 eV f=0.0000 5 -> 7 0.70721	Excited State 2 7.8150 eV f=0.0000 5 -> 7 0.70706
Excited State 3 8.5654 eV f=0.0835 4 -> 6 0.69527	Excited State 3 8.5183 eV f=0.0845 4 -> 6 0.69454
Excited State 4 10.0007 eV f=0.0188 4 -> 7 0.70362	Excited State 4 9.9523 eV f=0.0202 4 -> 7 0.70322
Excited State 5: 10.6478 eV f=0.0094 5 -> 8 0.69770	Excited State 5: 10.5876 eV 117. f=0.0105 5 -> 8 0.69814

CH_3

The tables show SP TDDFT calculations of the first ten excited states of CH3 using different basis sets and functionals. Geometries can be found in ***Table 4*** (section 5.2.1). The first two states with oscillator strengths different from zero are highlighted.

Table 19: Results from SP TDDFT calculation on CH_3 using the B3LYP functional and different basis sets. All calculations were performed for geometries optimized at the B3LYP/6-311G** LOT. The results shown are excitation energies, oscillator strengths and numbers of the orbitals taking part in the excitation. The results are discussed in section 5.2.1.

Table 20: Results from SP TDDFT calculation on CH_3 using the different functionals and the 6-311++G** and 6-31++G** basis sets. All calculations were performed for geometries optimized at the B3LYP/6-311G** LOT. The results shown are excitation energies, oscillator strengths and numbers of the orbitals taking part in the excitation. The results are discussed in section 5.2.1.

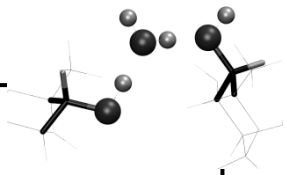

Table 19: See explanation on the previous page.

B3LYP 6-311G	**6-311++G**	**6-311G****	**6-311++G****	**6-31++G****
Excited State 1 6.3359 eV f=0.0162 5A -> 6A 0.99739 2B -> 5B -0.10678	**Excited State 1 5.2552 eV f=0.0320 5A -> 6A 0.99641**	**Excited State 1 6.3379 eV f=0.0181 5A -> 6A 0.99876**	**Excited State 1 5.2540 eV f=0.0344 5A -> 6A 0.99695**	**Excited State 1 5.1853 eV f=0.0391 5A -> 6A 0.99813**
Excited State 2 7.0866 eV f=0.0000 5A -> 7A 0.19524 5A -> 8A -0.10013 4B -> 5B 0.98742	Excited State 2 6.4347 eV f=0.0000 5A -> 7A 0.90526 5A -> 8A 0.38094 3B -> 5B -0.13496 4B -> 5B -0.12966	Excited State 2 6.9712 eV f=0.0000 5A -> 7A 0.17368 4B -> 5B 0.99428	Excited State 2 6.4309 eV f=0.0000 5A -> 7A 0.90514 5A -> 8A 0.34860 3B -> 5B 0.18256 4B -> 5B -0.16642	Excited State 2 6.3649 eV f=0.0000 5A -> 7A 0.98102 3B -> 5B -0.19522
Excited State 3 7.0879 eV f=0.0000 5A -> 7A 0.10026 5A -> 8A 0.19536 3B -> 5B 0.98739	Excited State 3 6.4348 eV f=0.0000 5A -> 7A -0.38102 5A -> 8A 0.90522 3B -> 5B 0.12933 4B -> 5B -0.13533	Excited State 3 6.9725 eV f=0.0000 5A -> 8A -0.17377 3B -> 5B 0.99426	Excited State 3 6.4310 eV f=0.0000 5A -> 7A -0.34877 5A -> 8A 0.90504 3B -> 5B -0.16594 4B -> 5B -0.18317	Excited State 3 6.3653 eV f=0.0000 5A -> 8A 0.98087 4B -> 5B 0.19583
Excited State 4 8.0612 eV f=0.0000 5A -> 7A 0.96378 5A -> 8A -0.17383 4B -> 5B -0.18801	Excited State 4 6.9993 eV f=0.0000 5A -> 8A 0.16731 4B -> 5B 0.98083 4B -> 9B -0.10589	Excited State 4 8.0513 eV f=0.0000 5A -> 7A 0.96843 5A -> 8A -0.17661 4B -> 5B -0.16585	Excited State 4 6.8740 eV f=0.0000 5A -> 8A 0.22209 4B -> 5B 0.97046 4B -> 9B -0.10738	Excited State 4 6.9266 eV f=0.0000 5A -> 8A -0.18792 4B -> 5B 0.97975 4B -> 9B -0.11586
Excited State 5 8.0617 eV f=0.0000 5A -> 7A 0.17379 5A -> 8A 0.96376 3B -> 5B -0.18816	Excited State 5 7.0006 eV f=0.0000 5A -> 7A 0.16685 3B -> 5B 0.98092 3B -> 9B -0.10592	Excited State 5 8.0518 eV f=0.0000 5A -> 7A 0.17658 5A -> 8A 0.96842 3B -> 5B 0.16596	Excited State 5 6.8752 eV f=0.0000 5A -> 7A -0.22135 3B -> 5B 0.97066 3B -> 9B -0.10741	Excited State 5 6.9278 eV f=0.0000 5A -> 7A 0.18732 3B -> 5B 0.97990 3B -> 9B -0.11580
Excited State 6 11.0738 eV f=0.0002 4A -> 6A -0.68902 3B -> 8B 0.10796 4B -> 6B 0.71148 4B -> 7B -0.10829	Excited State 6 7.3079 eV f=0.0000 5A -> 9A 0.99481	**Excited State 6 10.9781 eV f=0.0002 3A -> 8A -0.10449 4A -> 6A -0.68720 4A -> 7A 0.10486 3B -> 8B -0.11422 4B -> 6B 0.71078 4B -> 7B -0.11454**	Excited State 6 7.3121 eV f=0.0000 5A -> 9A 0.99490	Excited State 6 7.3244 eV f=0.0000 5A -> 9A -0.99355
Excited State 7 11.0753 eV f=0.0002 3A -> 6A 0.68900 3B -> 6B -0.71146 3B -> 7B -0.10819 4B -> 8B -0.10818	Excited State 7 7.9054 eV f=0.0000 5A -> 10A 0.99833	Excited State 7 10.9796 eV f=0.0002 3A -> 6A 0.68717 3A -> 7A 0.10491 4A -> 8A 0.10454 3B -> 6B 0.71076 3B -> 7B 0.11448 4B -> 8B -0.11440	Excited State 7 7.8435 eV f=0.0000 5A -> 10A 0.99890	Excited State 7 8.1308 eV f=0.0000 5A -> 10A 0.99501 5A -> 11A -0.10058
Excited State 8 11.9249 eV f=0.2204 4A -> 6A 0.70477 4B -> 6B 0.68649	Excited State 7.9060 eV f=0.0000 5A -> 11A 0.99833	**Excited State 8 11.8411 eV f=0.2237 4A -> 6A 0.70541 4B -> 6B 0.68627**	Excited State 8 7.8440 eV f=0.0000 5A -> 11A 0.99889	Excited State 8 8.1312 eV f=0.0000 5A -> 10A 0.10057 5A -> 11A 0.99504
Excited State 9 11.9264 eV f=0.2204 3A -> 6A 0.70476 3B -> 6B 0.68650	**Excited State 9 8.7634 eV f=0.1400 5A -> 12A 0.99856**	Excited State 9 11.8425 eV f=0.2234 3A -> 6A 0.70540 3B -> 6B -0.68624	**Excited State 9 8.7295 eV f=0.1453 5A -> 12A 0.99379 5A -> 13A 0.11425**	**Excited State 9 9.0023 eV f=0.0455 5A -> 12A 0.99237 5A -> 13A -0.10130**
Excited State 10 12.2108 eV f=0.0000 3A -> 7A -0.21295 3A -> 8A -0.41665 4A -> 7A -0.41782 4A -> 8A 0.21346 2B -> 6B -0.11624 3B -> 7B 0.27726 3B -> 8B 0.46237 4B -> 7B 0.46372 4B -> 8B -0.27795	Excited State 10 9.1486 eV f=0.0346 5A -> 13A 0.98258 2B -> 5B -0.19874	Excited State 10 12.5401 eV f=0.0000 5A -> 9A 1.00451	Excited State 10 9.1381 eV f=0.0184 5A -> 12A -0.11411 5A -> 13A 0.98017 2B -> 5B -0.18213	Excited State 10 10.0144 eV f=0.1187 5A -> 12A -0.10989 5A -> 13A -0.96871 2B -> 5B 0.26684 5A -> 13A -0.96871 2B -> 5B 0.26684

Table 20: See explanation on previous page.

BLYP		**B3LYP**	
6-311++G**	**6-31++G****	**6-311++G****	**6-31++G****
Excited State 1 **4.7928 eV f=0.0329** **5A -> 6A 1.00310**	**Excited State 1** **4.7147 eV f=0.0381** **5A -> 6A 1.00384**	**Excited State 1** **5.2540 eV f=0.0344** **5A -> 6A 0.99695**	**Excited State 1** **5.1853 eV f=0.0391** **5A -> 6A 0.99813**
Excited State 2 5.8979 eV f=0.0000 5A -> 7A 1.00018 3B -> 5B 0.11567	Excited State 2 5.8237 eV f=0.0000 5A -> 7A 1.00147 3B -> 5B -0.11482	Excited State 2 6.4309 eV f=0.0000 5A -> 7A 0.90514 5A -> 8A 0.34860 3B -> 5B 0.18256 4B -> 5B -0.16642	Excited State 2 6.3649 eV f=0.0000 5A -> 7A 0.98102 3B -> 5B -0.19522
Excited State 3 5.8981 eV f=0.0000 5A -> 8A 1.00016 4B -> 5B -0.11588	Excited State 3 5.8247 eV f=0.0000 5A -> 8A 1.00138 4B -> 5B 0.11511	Excited State 3 6.4310 eV f=0.0000 5A -> 7A -0.34877 5A -> 8A 0.90504 3B -> 5B -0.16594 4B -> 5B -0.18317	Excited State 3 6.3653 eV f=0.0000 5A -> 8A 0.98087 4B -> 5B 0.19583
Excited State 4 6.7024 eV f=0.0000 5A -> 8A 0.10042 4B -> 5B 1.00451	Excited State 4 6.7534 eV f=0.0000 4B -> 5B 1.00648	Excited State 4 6.8740 eV f=0.0000 5A -> 8A 0.22209 4B -> 5B 0.97046 4B -> 9B -0.10738	Excited State 4 6.9266 eV f=0.0000 5A -> 8A -0.18792 4B -> 5B 0.97975 4B -> 9B -0.11586
Excited State 5 6.7036 eV f=0.0000 5A -> 7A -0.10021 3B -> 5B 1.00454	Excited State 5 6.7545 eV f=0.0000 3B -> 5B 1.00653	Excited State 5: 6.8752 eV f=0.0000 5A -> 7A -0.22135 3B -> 5B 0.97066 3B -> 9B -0.10741	Excited State 5 6.9278 eV f=0.0000 5A -> 7A 0.18732 3B -> 5B 0.97990 3B -> 9B -0.11580
Excited State 6 6.9023 eV f=0.0000 5A -> 9A 0.98901	Excited State 6 6.9298 eV f=0.0000 5A -> 9A 0.98645	Excited State 6 7.3121 eV f=0.0000 5A -> 9A 0.99490	Excited State 6 7.3244 eV f=0.0000 5A -> 9A -0.99355
Excited State 7 7.3804 eV f=0.0000 5A -> 10A 1.00565	Excited State 7 7.6633 eV f=0.0000 5A -> 10A 0.70537 5A -> 11A -0.71945	Excited State 7 7.8435 eV f=0.0000 5A -> 10A 0.99890	Excited State 7 8.1308 eV f=0.0000 5A -> 10A 0.99501 5A -> 11A -0.10058
Excited State 8 7.3809 eV f=0.0000 5A -> 11A 1.00565	Excited State 8 7.6636 eV f=0.0000 5A -> 10A 0.71941 5A -> 11A 0.70538	Excited State 8 7.8440 eV f=0.0000 5A -> 11A 0.99889	Excited State 8 8.1312 eV f=0.0000 5A -> 10A 0.10057 5A -> 11A 0.99504
Excited State 9 **8.2307 eV f=0.1370** **5A -> 12A 1.00336**	**Excited State 9** **8.5132 eV f=0.0508** **5A -> 12A 1.00312**	**Excited State 9** **8.7295 eV f=0.1453** **5A -> 12A 0.99379** **5A -> 13A 0.11425**	**Excited State 9** **9.0023 eV f=0.0455** **5A -> 12A 0.99237** **5A -> 13A -0.10130**
Excited State 10 8.7598 eV f=0.0277 5A -> 13A 0.98928 2B -> 5B -0.19334	Excited State 10 9.4921 eV f=0.0075 4A -> 6A -0.48855 4B -> 6B 0.87649	Excited State 10 9.1381 eV f=0.0184 5A -> 12A -0.11411 5A -> 13A 0.98017 2B -> 5B -0.18213	Excited State 10 10.0144 eV f=0.1187 5A -> 12A -0.10989 5A -> 13A -0.96871 2B -> 5B 0.26684 5A -> 13A -0.96871 2B -> 5B 0.26684

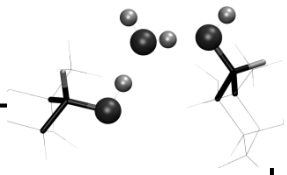

PBE		**PBE0**	
6-311++G**	**6-31++G****	**6-311++G****	**6-31++G****
Excited State 1 **4.9954 eV f=0.0358** **5A -> 6A 1.00585**	**Excited State 1** **4.9127 eV f=0.0392** **5A -> 6A 1.00624**	**Excited State 1** **5.5412 eV f=0.0369** **5A -> 6A 0.99614**	**Excited State 1** **5.4769 eV f=0.0400** **5A -> 6A 0.99737** **5A -> 12A -0.11187**
Excited State 2 6.1467 eV f=0.0000 5A -> 7A 0.96841 5A -> 8A 0.23079 3B -> 5B 0.11051 4B -> 5B -0.13012	Excited State 2 6.0665 eV f=0.0000 5A -> 7A 0.97622 5A -> 8A 0.21464 3B -> 5B -0.10720 4B -> 5B -0.10350	Excited State 2 6.7378 eV f=0.0000 5A -> 7A 0.55604 5A -> 8A 0.73189 5A -> 14A 0.13912 4B -> 5B -0.38459	Excited State 2 6.6831 eV f=0.0000 5A -> 7A 0.64550 5A -> 8A 0.70276 5A -> 14A 0.11454 3B -> 5B -0.11543 4B -> 5B -0.27857
Excited State 3 6.1468 eV f=0.0000 5A -> 7A -0.23085 5A -> 8A 0.96841 3B -> 5B -0.12985 4B -> 5B -0.11073	Excited State 3 6.0666 eV f=0.0000 5A -> 7A -0.21467 5A -> 8A 0.97621 3B -> 5B 0.10331 4B -> 5B -0.10737	Excited State 3 6.7380 eV f=0.0000 5A -> 7A 0.73249 5A -> 8A -0.55612 5A -> 15A 0.13905 3B -> 5B 0.38319	Excited State 3 6.6832 eV f=0.0000 5A -> 7A 0.70304 5A -> 8A -0.64547 5A -> 15A -0.11446 3B -> 5B -0.27775 4B -> 5B 0.11582
Excited State 4 6.7901 eV f=0.0000 5A -> 8A 0.12204 4B -> 5B 1.00135	Excited State 4 6.8483 eV f=0.0000 5A -> 8A 0.11071 4B -> 5B 1.00554	Excited State 4 7.0560 eV f=0.0000 5A -> 7A 0.15729 5A -> 8A 0.35201 4B -> 5B 0.92119 4B -> 11B -0.11763	Excited State 4 7.1051 eV f=0.0000 5A -> 8A 0.27468 4B -> 5B 0.95520 4B -> 9B -0.12960
Excited State 5 6.7914 eV f=0.0000 5A -> 7A -0.12177 3B -> 5B 1.00141	Excited State 5 6.8495 eV f=0.0000 5A -> 7A 0.11050 3B -> 5B 1.00558	Excited State 5 7.0571 eV f=0.0000 5A -> 7A -0.35064 5A -> 8A 0.15677 3B -> 5B 0.92182 3B -> 11B -0.11775	Excited State 5 7.1063 eV f=0.0000 5A -> 7A 0.27381 3B -> 5B 0.95548 3B -> 9B -0.12969
Excited State 6 7.0044 eV f=0.0000 5A -> 9A -0.99026	Excited State 6 7.0424 eV f=0.0000 5A -> 9A 0.98683	Excited State 6 7.4989 eV f=0.0000 5A -> 9A 0.99668	Excited State 6 7.5173 eV f=0.0000 5A -> 9A 0.99531
Excited State 7 7.5903 eV f=0.0000 5A -> 10A 1.00502	Excited State 7 7.8793 eV f=0.0000 5A -> 10A 1.00676	Excited State 7 8.1404 eV f=0.0000 5A -> 10A 0.99524 5A -> 14A -0.10910	Excited State 7 8.4345 eV f=0.0000 5A -> 10A 0.99673 5A -> 14A -0.10599
Excited State 8 7.5909 eV f=0.0000 5A -> 11A 1.00501	Excited State 8 7.8801 eV f=0.0000 5A -> 11A 1.00675	Excited State 8 8.1411 eV f=0.0000 5A -> 11A 0.99525 5A -> 15A 0.10903	Excited State 8 8.4353 eV f=0.0000 5A -> 11A 0.99673 5A -> 15A -0.10591
Excited State 9 **8.4266 eV f=0.1449** **5A -> 12A 1.00268**	**Excited State 9** **8.7538 eV f=0.0571** **5A -> 12A 1.00451**	**Excited State 9** **8.9781 eV f=0.1506** **5A -> 12A 0.98412** **5A -> 13A 0.17498**	**Excited State 9** **9.2959 eV f=0.0525** **5A -> 6A 0.11811** **5A -> 12A 0.99008** **5A -> 13A -0.11171**
Excited State 10 8.9486 eV f=0.0128 5A -> 13A 0.98921 2B -> 5B -0.20401	Excited State 10 9.6234 eV f=0.0005 4A -> 6A 0.67288 4B -> 6B -0.74615	Excited State 10 9.3999 eV f=0.0075 5A -> 6A -0.11467 5A -> 12A -0.17469 5A -> 13A 0.96860 2B -> 5B -0.18768	Excited State 10 10.2148 eV f=0.1076 5A -> 12A 0.12287 5A -> 13A 0.96604 2B -> 5B -0.28089

CO^+

The tables show SP TDDFT calculations of the first ten excited states of CO^+ using different basis sets and functionals. Geometries can be found in ***Table 4*** (section 5.2.1). The first two states with oscillator strengths different from zero are highlighted. Note that states 1 and 2 are practically degenerate, and correspond to the same excitations with opposite signs of the excitation coefficients.

Table 21: Results from SP TDDFT calculation on CO^+ using the B3LYP functional and different basis sets. All calculations were performed for geometries optimized at the B3LYP/6-311G** LOT. The results shown are excitation energies, oscillator strengths and numbers of the orbitals taking part in the excitation. The results are discussed in section 5.2.1.

Table 22: Results from SP TDDFT calculation on CO^+ using the different functionals and the 6-311++G** and 6-31++G** basis sets. All calculations were performed for geometries optimized at the B3LYP/6-311G** LOT. The results shown are excitation energies, oscillator strengths and numbers of the orbitals taking part in the excitation. The results are discussed in section 5.2.1.

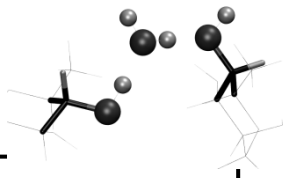

Table 21: See explanation on the previous page.

B3LYP

6-311G	**6-311++G**	**6-311G****	**6-311++G****	**6-31++G****
Excited State 1	**Excited State 1**	**Excited State 1**	**Excited State 1**	**Excited State 1**
3.6850 eV f=0.0071	**3.6768 eV f=0.0070**	**3.3756 f=0.0049**	**3.3789 eV f=0.0048**	**3.3466 eV f=0.0049**
4A -> 8A -0.12554	**4A -> 8A -0.12433**	**4A -> 8A -0.11250**	**4A -> 8A -0.11210**	**4A -> 8A -0.11391**
5B -> 7B 0.97514	**5B -> 7B 0.96646**	**5B -> 7B 1.02513**	**5B -> 7B 1.02539**	**5B -> 7B 1.02938**
6B -> 7B 0.31749	**6B -> 7B 0.34337**	**6B -> 7B 0.10682**	**6B -> 7B 0.10384**	
Excited State 2	**Excited State 2**	**Excited State 2**	**Excited State 2**	**Excited State 2**
3.6867 eV f=0.0071	**3.6785 eV f=0.0070**	**3.3759 eV f=0.0049**	**3.3793 eV f=0.0048**	**3.3468 eV f=0.0049**
4A -> 9A -0.12551	**4A -> 9A -0.12429**	**4A -> 9A -0.11249**	**4A -> 9A -0.11209**	**4A -> 9A -0.11390**
5B -> 7B -0.31741	**5B -> 7B -0.34329**	**5B -> 7B -0.10681**	**5B -> 7B -0.10383**	**6B -> 7B 1.02933**
6B -> 7B 0.97492	**6B -> 7B 0.96623**	**6B -> 7B 1.02508**	**6B -> 7B 1.02534**	
Excited State 3	**Excited State**	**Excited State 3**	**Excited State 3**	**Excited State 3**
5.5185 eV f=0.0129	**5.5262 eV f=0.0128**	**5.6220 eV f=0.0132**	**5.6354 eV f=0.0130**	**5.5647 eV f=0.0136**
5A -> 8A 0.28884	**5A -> 8A 0.28969**	**5A -> 8A 0.28786**	**5A -> 8A 0.28869**	**5A -> 8A 0.28200**
6A -> 9A 0.28883	**6A -> 9A 0.28968**	**6A -> 9A 0.28786**	**6A -> 9A 0.28869**	**6A -> 9A 0.28200**
4B -> 7B 0.97259	**4B -> 7B 0.97190**	**4B -> 7B 0.97259**	**4B -> 7B 0.97173**	**4B -> 7B 0.97353**
Excited State 4	Excited State 4	Excited State 4	Excited State 4	Excited State 4
7.6358 eV f=0.0042	7.6274 eV f=0.0042	7.6769 eV f=0.0049	7.6667 eV f=0.0050	7.6722 eV f=0.0049
5A -> 8A 0.52906	5A -> 8A 0.52668	5A -> 8A 0.53376	5A -> 8A 0.53187	5A -> 8A 0.51917
6A -> 9A 0.52911	6A -> 9A 0.52673	6A -> 9A 0.53379	6A -> 9A 0.53189	5A -> 9A 0.12295
4B -> 7B -0.24438	4B -> 7B -0.24828	4B -> 7B -0.24799	4B -> 7B -0.25199	6A -> 8A -0.12296
5B -> 8B -0.19125	5B -> 8B -0.20988	5B -> 8B -0.27454	5B -> 8B -0.26278	6A -> 9A 0.51920
5B -> 9B -0.54804	5B -> 9B -0.53927	5B -> 9B -0.50195	5B -> 9B -0.50578	4B -> 7B -0.24588
6B -> 8B 0.54812	6B -> 8B 0.53935	6B -> 8B 0.50198	6B -> 8B 0.50582	5B -> 9B -0.56524
6B -> 9B -0.19123	6B -> 9B -0.20986	6B -> 9B -0.27455	6B -> 9B -0.26278	6B -> 8B 0.56528
Excited State 5	Excited State 5	Excited State 5	Excited State 5	Excited State 5
8.3184 eV f=0.0000	8.3035 eV f=0.0000	8.2533 eV f=0.0000	8.2354 eV f=0.0000	8.2446 eV f=0.0000
5A -> 8A 0.65092	5A -> 8A 0.64883	5A -> 8A 0.66053	5A -> 8A 0.66002	5A -> 8A 0.66756
5A -> 9A 0.12727	5A -> 9A 0.13936	5A -> 9A 0.12839	5A -> 9A 0.13251	6A -> 9A -0.66753
6A -> 8A 0.12727	6A -> 8A 0.13936	6A -> 8A 0.12839	6A -> 8A 0.13251	5B -> 8B -0.11989
6A -> 9A -0.65087	6A -> 9A -0.64878	6A -> 9A -0.66050	6A -> 9A -0.66000	5B -> 9B -0.37348
5B -> 9B -0.41171	5B -> 9B -0.40968	5B -> 8B -0.15537	5B -> 8B -0.15118	6B -> 8B -0.37345
6B -> 8B -0.41165	6B -> 8B -0.40962	5B -> 9B -0.36111	5B -> 9B -0.36022	6B -> 9B 0.11989
		6B -> 8B -0.36109	6B -> 8B -0.36019	
		6B -> 9B 0.15536	6B -> 9B 0.15116	

Table 22: See explanation on previous page.

BLYP		**B3LYP**	
6-311++G**	**6-31++G****	**6-311++G****	**6-31++G****
Excited State 1 **3.1427 eV f=0.0046** **4A -> 8A -0.11554** **5B -> 7B 1.03673**	**Excited State 1** **3.1101 eV f=0.0046** **4A -> 8A 0.11823** **5B -> 7B 1.01058** **6B -> 7B -0.25537**	**Excited State 1** **3.3789 eV f=0.0048** **4A -> 8A -0.11210** **5B -> 7B 1.02539** **6B -> 7B 0.10384**	**Excited State 1** **3.3466 eV f=0.0049** **4A -> 8A -0.11391** **5B -> 7B 1.02938**
Excited State 2 **3.1429 eV f=0.0046** **4A -> 9A -0.11552** **6B -> 7B 1.03669**	**Excited State 2** **3.1102 eV f=0.0046** **4A -> 9A 0.11823** **5B -> 7B 0.25537** **6B -> 7B 1.01055**	**Excited State 2** **3.3793 eV f=0.0048** **4A -> 9A -0.11209** **5B -> 7B -0.10383** **6B -> 7B 1.02534**	**Excited State 2** **3.3468 eV f=0.0049** **4A -> 9A -0.11390** **6B -> 7B 1.02933**
Excited State 3 **5.0838 eV f=0.0181** **5A -> 8A 0.22613** **6A -> 9A 0.22613** **4B -> 7B 0.97542**	**Excited State 3** **5.0436 eV f=0.0184** **5A -> 8A 0.22554** **6A -> 9A 0.22554** **4B -> 7B 0.97423**	**Excited State 3** **5.6354 eV f=0.0130** **5A -> 8A 0.28869** **6A -> 9A 0.28869** **4B -> 7B 0.97173**	**Excited State 3** **5.5647 eV f=0.0136** **5A -> 8A 0.28200** **6A -> 9A 0.28200** **4B -> 7B 0.97353**
Excited State 4 7.9001 eV f=0.0024 5A -> 8A 0.53827 6A -> 9A 0.53824 4B -> 7B -0.14245 5B -> 8B -0.50270 5B -> 9B -0.25208 6B -> 8B 0.25207 6B -> 9B -0.50269	Excited State 4 7.8973 eV f=0.0023 5A -> 8A 0.52553 5A -> 9A 0.11515 6A -> 8A -0.11516 6A -> 9A 0.52556 4B -> 7B -0.14292 5B -> 9B -0.55921 6B -> 8B 0.55924	Excited State 4 7.6667 eV f=0.0050 5A -> 8A 0.53187 6A -> 9A 0.53189 4B -> 7B -0.25199 5B -> 8B -0.26278 5B -> 9B -0.50578 6B -> 8B 0.50582 6B -> 9B -0.26278	Excited State 4 7.6722 eV f=0.0049 5A -> 8A 0.51917 5A -> 9A 0.12295 6A -> 8A -0.12296 6A -> 9A 0.51920 4B -> 7B -0.24588 5B -> 9B -0.56524 6B -> 8B 0.56528
Excited State 5 8.4806 eV f=0.0000 5A -> 8A -0.61952 5A -> 9A -0.12408 6A -> 8A -0.12408 6A -> 9A 0.61953 5B -> 8B 0.35901 5B -> 9B 0.21474 6B -> 8B 0.21476 6B -> 9B -0.35905	Excited State 5 8.4812 eV f=0.0000 5A -> 8A 0.62669 6A -> 9A -0.62667 5B -> 8B -0.12335 5B -> 9B -0.40210 6B -> 8B -0.40207 6B -> 9B 0.12335	Excited State 5 8.2354 eV f=0.0000 5A -> 8A 0.66002 5A -> 9A 0.13251 6A -> 8A 0.13251 6A -> 9A -0.66000 5B -> 8B -0.15118 5B -> 9B -0.36022 6B -> 8B -0.36019 6B -> 9B 0.15116	Excited State 5 8.2446 eV f=0.0000 5A -> 8A 0.66756 6A -> 9A -0.66753 5B -> 8B -0.11989 5B -> 9B -0.37348 6B -> 8B -0.37345 6B -> 9B 0.11989

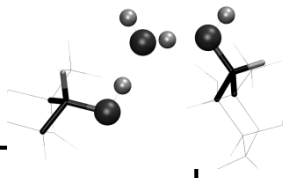

PBE		PBE0	
6-311++G**	6-31++G**	6-311++G**	6-31++G**
Excited State 1 3.4331 eV f=0.0048 4A -> 8A -0.12481 7A -> 8A -0.10083 5B -> 7B 1.03822	Excited State 1 3.3998 eV f=0.0049 4A -> 8A 0.12621 5B -> 7B 1.04140	Excited State 1 3.8111 eV f=0.0052 4A -> 8A -0.11787 5B -> 7B 0.98885 6B -> 7B 0.28853	Excited State 1 3.7673 eV f=0.0053 4A -> 8A -0.11867 5B -> 7B 1.01829 6B -> 7B 0.16222
Excited State 2 3.4334 eV f=0.0048 4A -> 9A -0.12480 7A -> 9A -0.10083 6B -> 7B 1.03817	Excited State 2 3.4000 eV f=0.0049 4A -> 9A 0.12620 6B -> 7B 1.04137	Excited State 2 3.8116 eV f=0.0052 4A -> 9A -0.11786 5B -> 7B -0.28851 6B -> 7B 0.98877	Excited State 2 3.7677 eV f=0.0053 4A -> 9A -0.11867 5B -> 7B -0.16221 6B -> 7B 1.01823
Excited State 3 5.3845 eV f=0.0171 5A -> 8A 0.26192 6A -> 9A 0.26192 4B -> 7B 0.96362	Excited State 3 5.3359 eV f=0.0175 5A -> 8A 0.26063 6A -> 9A 0.26063 4B -> 7B 0.96304	Excited State 3 6.0240 eV f=0.0086 6A -> 8A 0.39266 7A -> 9A 0.39266 4B -> 7B 0.91024 5B -> 8B -0.10425 5B -> 9B -0.17272 6B -> 8B 0.17270 6B -> 9B -0.10426	Excited State 3 5.9548 eV f=0.0093 6A -> 8A 0.38181 7A -> 9A 0.38181 4B -> 7B 0.91886 5B -> 9B -0.17836 6B -> 8B 0.17835
Excited State 4 7.9319 eV f=0.0040 5A -> 8A 0.52728 6A -> 9A 0.52726 4B -> 7B -0.19907 5B -> 8B -0.37638 5B -> 9B -0.41874 6B -> 8B 0.41874 6B -> 9B -0.37637	Excited State 4 7.9322 eV f=0.0037 5A -> 8A 0.51926 6A -> 9A 0.51929 4B -> 7B -0.19673 5B -> 8B -0.18597 5B -> 9B -0.53267 6B -> 8B 0.53270 6B -> 9B -0.18597	Excited State 4 7.6904 eV f=0.0101 6A -> 8A -0.47976 7A -> 9A -0.47979 4B -> 7B 0.42728 5B -> 8B 0.28386 5B -> 9B 0.47019 6B -> 8B -0.47024 6B -> 9B 0.28385	Excited State 4 7.6900 eV f=0.0096 6A -> 8A -0.48058 7A -> 9A -0.48062 4B -> 7B 0.40889 5B -> 8B 0.18916 5B -> 9B 0.52086 6B -> 8B -0.52091 6B -> 9B 0.18916
Excited State 5 8.5330 eV f=0.0000 5A -> 8A -0.62508 5A -> 9A -0.11577 6A -> 8A -0.11577 6A -> 9A 0.62509 5B -> 8B 0.23230 5B -> 9B 0.34066 6B -> 8B 0.34068 6B -> 9B -0.23232	Excited State 5 8.5373 eV f=0.0000 5A -> 8A 0.62847 6A -> 9A -0.62844 5B -> 8B -0.17418 5B -> 9B -0.37777 6B -> 8B -0.37775 6B -> 9B 0.17417	Excited State 5 8.1424 eV f=0.0000 6A -> 8A 0.67641 6A -> 9A 0.12965 7A -> 8A 0.12965 7A -> 9A -0.67638 5B -> 8B -0.15273 5B -> 9B -0.34785 6B -> 8B -0.34782 6B -> 9B 0.15271	Excited State 5 8.1577 eV f=0.0000 6A -> 8A 0.68074 7A -> 9A -0.68070 5B -> 8B -0.15626 5B -> 9B -0.34905 6B -> 8B -0.34902 6B -> 9B 0.15625

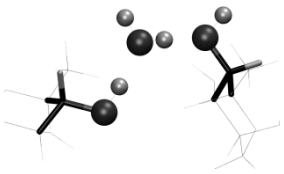

Table 23: Excitation energies (in eV) for the first nine excited states through the OH_4 bond elongation corresponding to the plots in ***Figure 25*** and ***Figure 26*** in section 5.2.2. Calculations were performed in G03 using the geometries from the optimizations in CP2K. The first point in the bond elongation is missing because of convergence failure of the excited state calculation.

Bond length / Å	**1.081**	**1.176**	**1.290**	**1.396**	**1.498**	**1.599**	**1.700**	**1.798**	**1.898**	**1.997**
Excited state 1	0.07	0.11	0.56	1.09	1.56	1.93	2.76	2.90	3.01	3.09
Excited state 2	0.12	0.12	0.45	0.98	1.45	1.82	2.67	2.80	2.92	3.00
Excited state 3	0.36	0.47	0.71	0.70	0.67	0.63	0.57	0.56	0.55	0.54
Excited state 4	0.58	0.58	1.01	1.52	2.00	2.36	3.18	3.31	3.42	3.50
Excited state 5	0.82	0.84	1.28	1.80	2.27	2.63	3.48	3.62	3.74	3.81
Excited state 6	0.94	1.06	1.41	1.56	1.75	1.91	2.10	2.15	2.19	2.22
Excited state 7	1.10	1.20	1.51	1.76	1.99	2.15	2.40	2.46	2.51	2.54
Excited state 8	1.38	1.39	1.82	2.32	2.78	3.13	3.91	4.04	4.15	4.22
Excited state 9	1.45	1.50	1.83	2.08	2.33	2.55	2.79	2.86	2.92	2.96

The plots below show the energy of the first 10 excited states found through SP calculations for geometries from optimizations using CP2K for OH_1 and OH_2 and both CP2K and G03 for OH_4. The excitation energies are added to the ground state energies from the geometry optimizations.

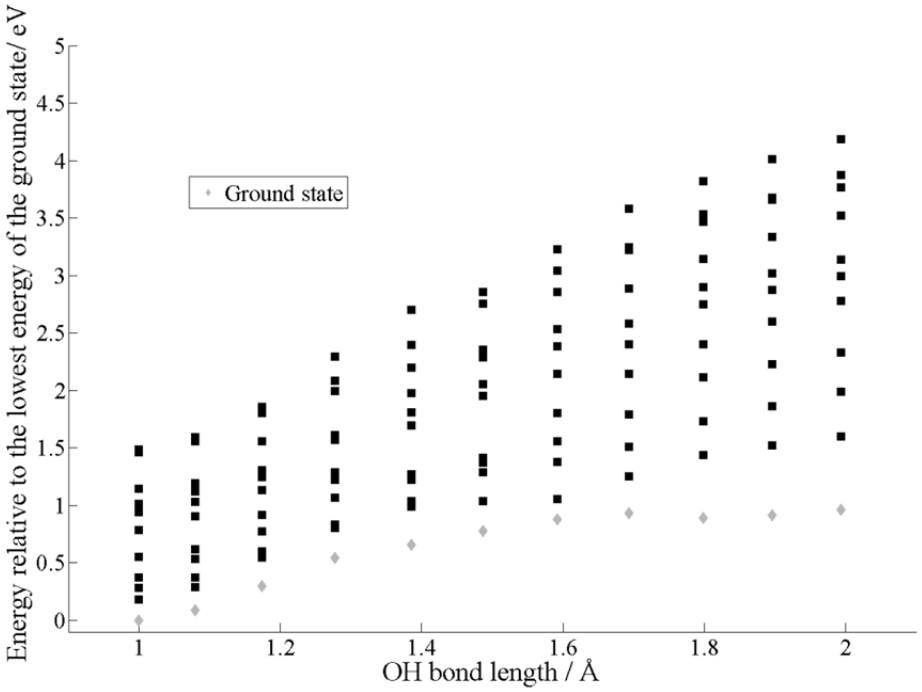

Figure 30: First ten excited states for the OH_1 deprotonation reaction. The single chain model was used, and the excited states were calculated at the B3LYP/6-31++G** LOT. The calculations were performed as SP calculations for geometries optimized in CP2K and the ground state energy from the geometry optimizations are used as the basis energy.

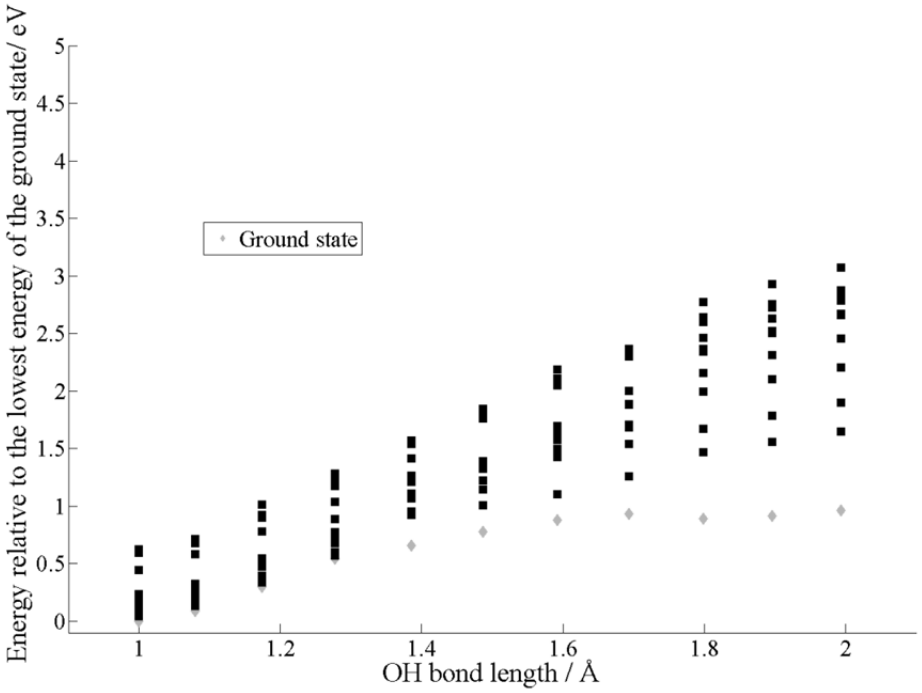

Figure 31: First ten excited states for the OH_1 deprotonation reaction. The star shaped model was used, and the excited states were calculated at the B3LYP/6-31++G** LOT. The calculations were performed as SP calculations for geometries optimized in CP2K and the ground state energy from the geometry optimizations are used as the basis energy.

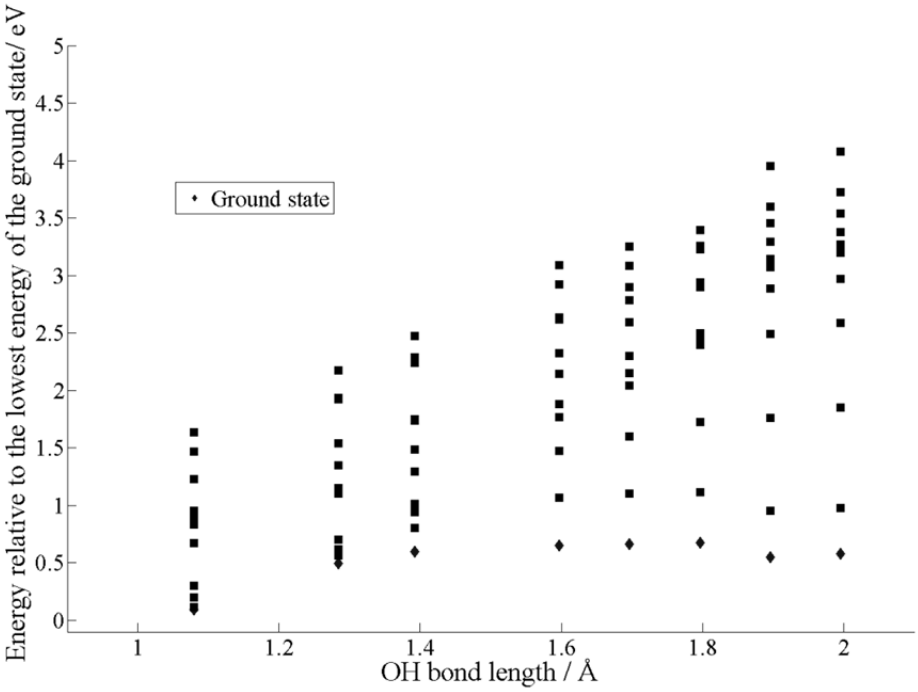

Figure 32: First ten excited states for the OH_2 deprotonation reaction. The single chain model was used, and the excited states were calculated at the B3LYP/6-31++G** LOT. The calculations were performed as SP calculations for geometries optimized in CP2K and the ground state energy from the geometry optimizations are used as the basis energy.

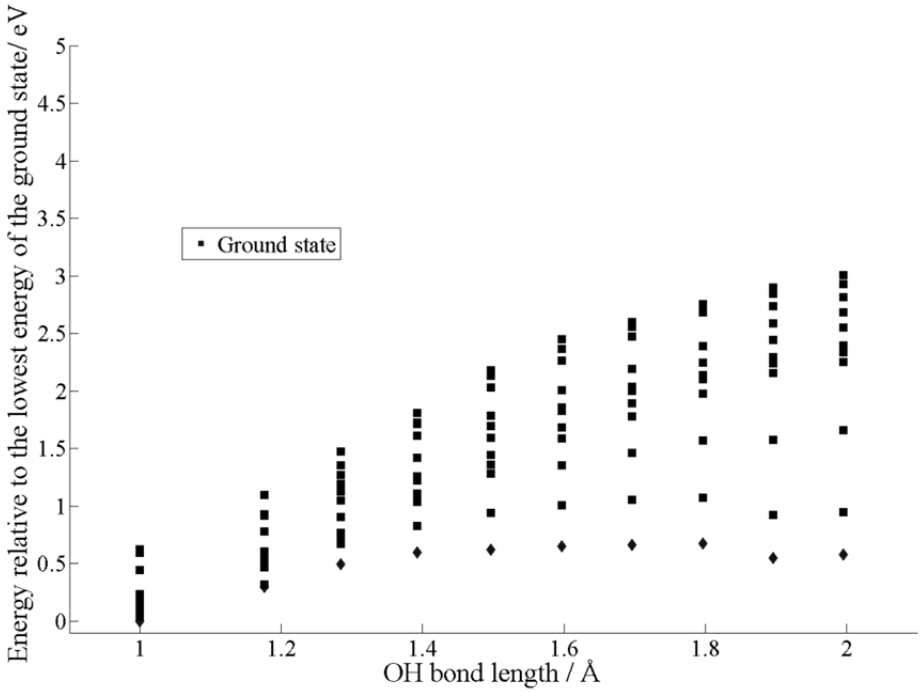

Figure 33: First ten excited states for the OH_2 deprotonation reaction. The star shaped model was used, and the excited states were calculated at the B3LYP/6-31++G** LOT. The calculations were performed as SP calculations for geometries optimized in CP2K and the ground state energy from the geometry optimizations are used as the basis energy.

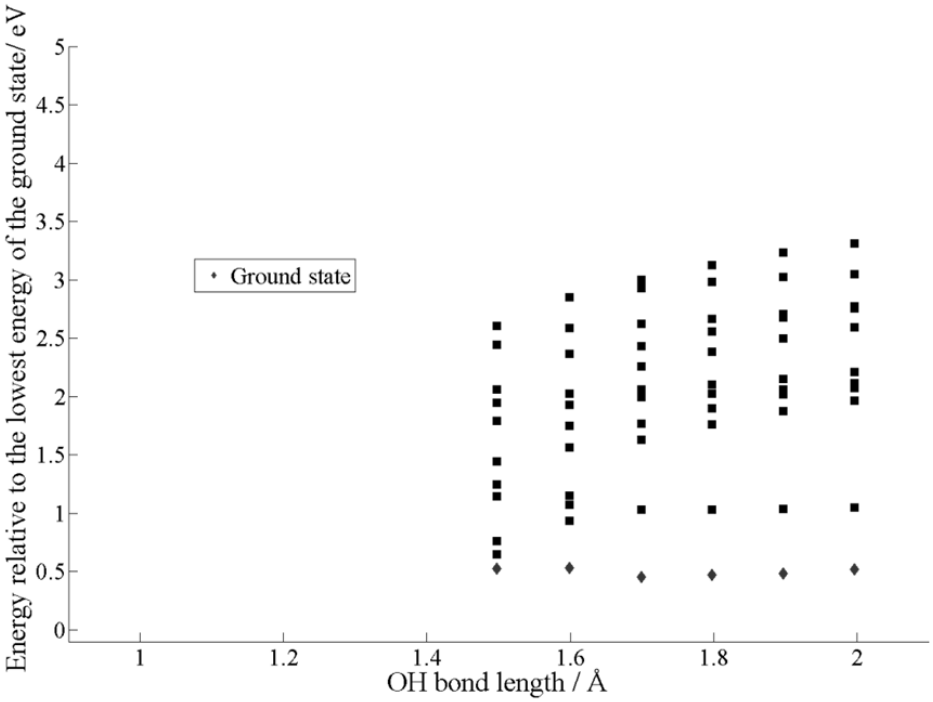

Figure 34: First ten excited states for the OH_4 deprotonation reaction. The single chain model was used, and the excited states were calculated at the PBE/6-31++G** LOT. The calculations were performed as SP calculations for geometries optimized in CP2K and the ground state energy from the geometry optimizations are used as the basis energy.

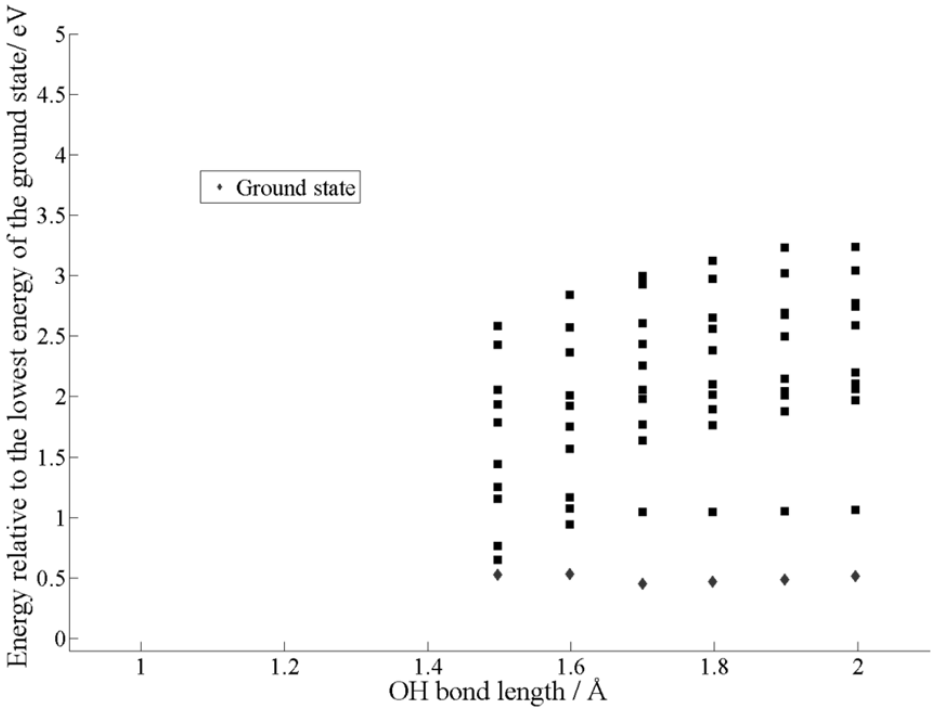

Figure 35: First ten excited states for the OH_4 deprotonation reaction. The single chain model was used, and the excited states were calculated at the BLYP/6-31++G** LOT. The calculations were performed as SP calculations for geometries optimized in CP2K and the ground state energy from the geometry optimizations are used as the basis energy.

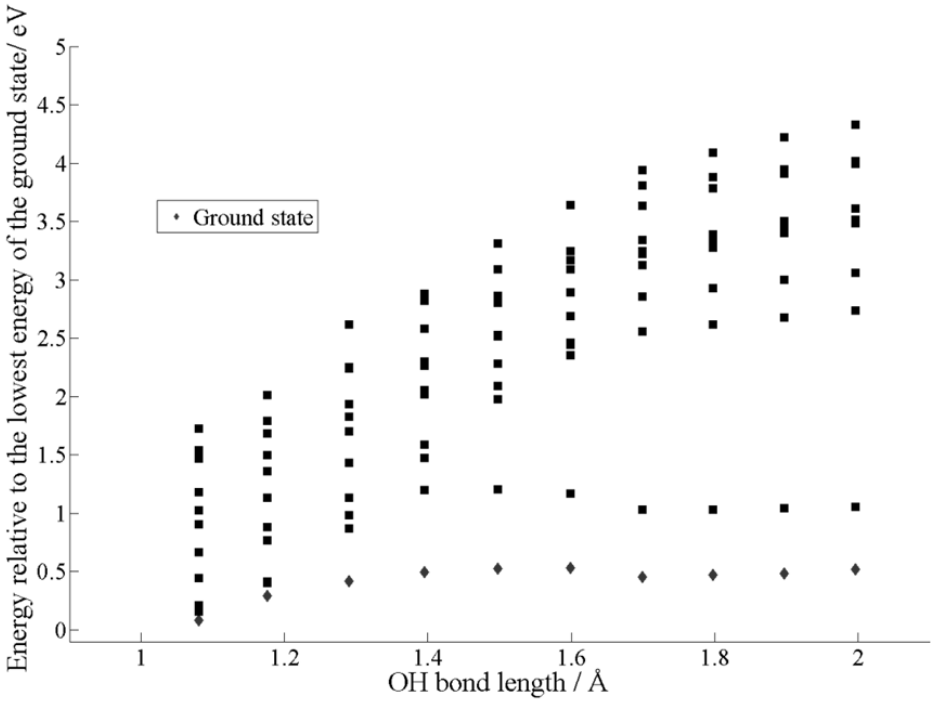

Figure 36: First ten excited states for the OH_4 deprotonation reaction. The single chain model was used, and the excited states were calculated at the B3LYP/6-31++G** LOT. The calculations were performed as SP calculations for geometries optimized in CP2K and the ground state energy from the geometry optimizations are used as the basis energy.

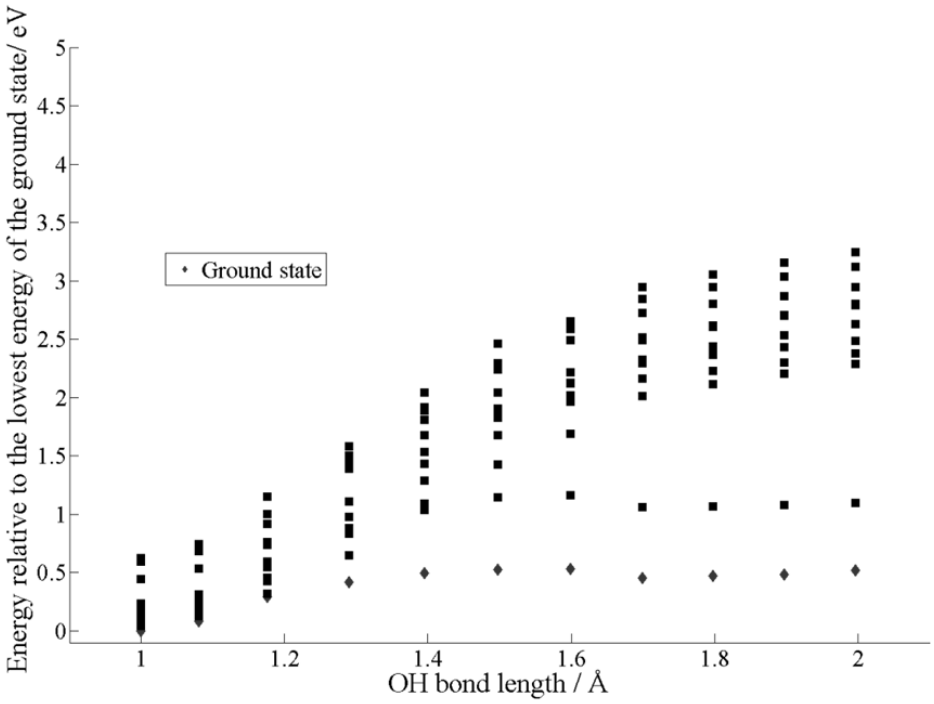

Figure 37: First ten excited states for the OH_4 deprotonation reaction. The star shaped model was used, and the excited states were calculated at the B3LYP/6-31++G** LOT. The calculations were performed as SP calculations for geometries optimized in CP2K and the ground state energy from the geometry optimizations are used as the basis energy.

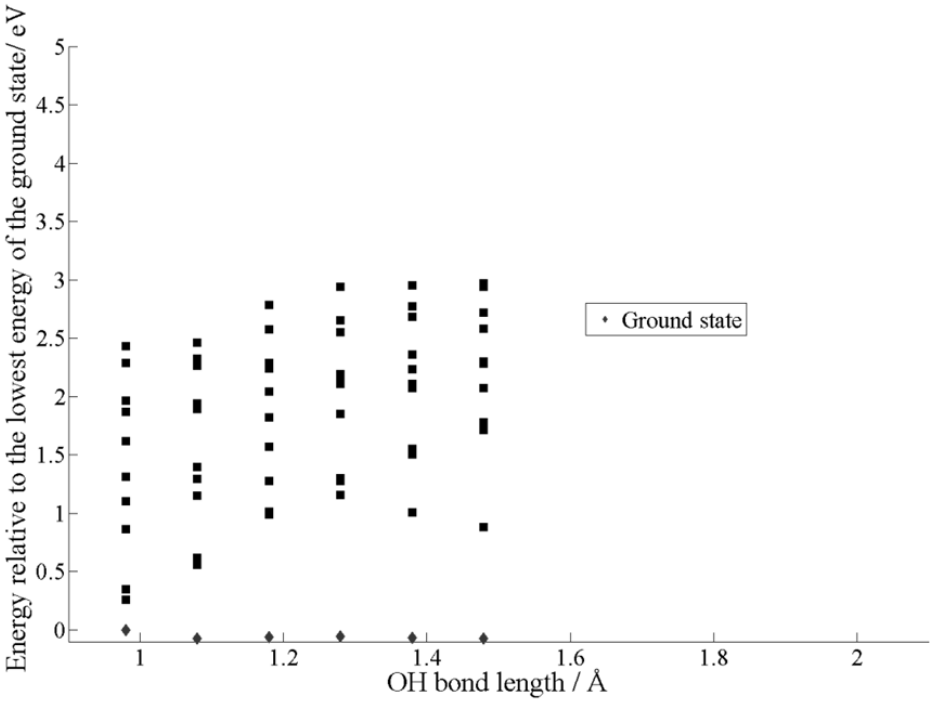

Figure 38: First ten excited states for the OH_4 deprotonation reaction. The single chain model was used, and the excited states were calculated at the B3LYP/6-31++G** LOT. The calculations were performed as SP calculations on geometries optimized in a cluster in Gaussian03 and the ground state energy from the geometry optimizations are used as the basis energy.

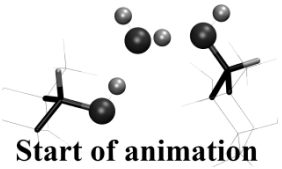

Appendix E: Animation

For those who wish to flip quickly through this thesis, the advice is to start in the back, and keep an eye on the upper right corner. Here is shown an animation of the most thorougly studied deprotonation reaction of this thesis, the OH_4 deprotonation. The geometries used in the animation are those of the linear interpolations used for the analysis of the excited states for the geometries calculated in the periodic code.